Università degli Studi di Padova

Dipartimento di Geoscienze

SCUOLA DI DOTTORATO DI RICERCA IN: SCIENZE DELLA TERRA

CICLO XXVII

CHARACTERIZATION OF ARCHAEOLOGICAL BONES FROM THE AL KHIDAY CEMETERY (CENTRAL SUDAN): STRUCTURE AND MICROSTRUCTURE OF DIAGENETICALLY ALTERED BIOAPATITE

Direttore della Scuola: Ch.mo Prof. Massimiliano Zattin

Supervisore: Ch.mo Prof. Gilberto Artioli

Co-supervisore: Dr. Lara Maritan, Dr. Ivana Angelini

Dottorando: Gregorio Dal Sasso

RIASSUNTO

Il tessuto osseo è composto principalmente da una frazione organica e una minerale, detta bioapatite. Lo studio di ossa umane, frequentemente rinvenute durante scavi archeologici, forniscono importanti informazioni sulla salute, demografia, antichità, dieta e mobilità di popolazioni vissute nel passato, nonché informazioni riguardo alle condizioni paleo-ambientali. Tuttavia, l'affidabilità di queste informazioni dipende molto dallo stato di conservazione delle ossa stesse, ed in particolare dalla conservazione della loro originale composizione chimica e isotopica. L'alterazione delle ossa è dovuta a processi tafonomici e diagenetici, principalmente influenzati dalle condizioni climatico-ambientali, che interessano le ossa dalla morte dell'individuo e durante il seppellimento. Di conseguenza, lo studio della diagenesi di ossa archeologiche, che mira a determinarne lo stato di conservazione, tenendo in considerazione il relativo contesto archeologico e paleo-ambientale, è di fondamentale importanza nell'interpretazione di risultati ottenuti da analisi chimiche e isotopiche. Sulla base di queste considerazioni si inserisce il presente progetto di ricerca, finalizzato alla datazione al radiocarbonio della bioapatite di ossa umane provenienti dal sito archeologico 16D4 – Al Khiday 2 (Sudan) e a determinarne l'affidabilità. Lo scavo del sito 16D4 ha portato alla luce un cimitero caratterizzato da diverse fasi di sepoltura, appartenenti a differenti periodi di uso cimiteriale dell'area cronologicamente distribuiti durante l'Olocene. Questo particolare contesto archeologico fornisce un interessante caso studio che permette di valutare l'affidabilità della datazione sulla bioapatite e allo stesso tempo di studiare l'influenza dei cambiamenti climatici, avvenuti in Sudan centrale durante l'Olocene, sulla diagenesi delle ossa. Prima di procedere con la datazione al radiocarbonio, campioni di ossa e di suoli (campionati sul sito) sono stati esaminati con approccio multidisciplinare al fine di determinare lo stato di conservazione delle ossa e caratterizzare la diagenesi delle ossa tenendo in considerazioni processi pedogenetici cambiamenti delle condizioni climatico–ambientali e di seppellimento. Successivamente alcuni campioni di bioapatite sono stati datati al radiocarbonio e l'affidabilità dei risultati è stata discussa.

I campioni di ossa sono stati analizzati mediante microscopia ottica ed elettronica a scansione, diffrazioni a raggi X su polvere, micro-tomografia a raggi X, spettroscopia IR a trasformata di Fourier e micro-Raman. I campioni di un orizzonte carbonatico, campionati sul sito archeologico, sono stati analizzati mediante microscopia ottica, in catodoluminescenza e elettronica a scansione. Le datazione al radiocarbonio mediante spettrometria si massa con acceleratore sono state ottenute su campioni di bioapatite e di carbonati pedogenetici.

I risultati ottenuti su questo caso studio dimostrano che la datazione di bioapatite di campioni molto alterati non è affidabile. Lo studio di ossa e suoli ha fornito importanti informazioni sull' alterazione diagenetica delle ossa e sulla sua dipendenza dai cambiamenti climatici e ambientali avvenuti nella regione durante l'Olocene abbiano. Inoltre, i risultati ottenuti in questo lavoro evidenziano l'importanza di un approccio multidisciplinare allo studio di contesti archeologici e paleo-ambientali.

ABSTRACT

Bone is a composite material constituted by the association of an organic matrix and bioapatite nano-crystals. Human bones, frequently recovered from archaeological contexts, represent a valuable source of information on health, demography, age, diet and mobility of ancient populations as well as on environmental conditions experienced. However the reliability of such information depends on the preservation state of bone material and its constituents, i.e. the preservation of the in vivo chemical and isotopic composition. Bone alteration is caused by taphonomic and diagenetic processes, mainly driven by environmental conditions, affecting bones since the death of the individual and during burial. Therefore, a diagenetic study on archaeological bones, aiming to accurately determine their preservation state, taking into account the archaeological and palaeoenvironmental contexts, is a fundamental step when retrieving information by chemical or isotopic analyses.

Based on this perspective, this research project is mainly addressing the radiocarbon dating of the bioapatite fraction of human bones, coming from the archaeological site 16D4 – Al Khiday 2 (Sudan) and the assessment of the reliability of results. At 16D4, a multi-stratified cemetery was excavated and several burial phases were recovered. In fact, the site was used as a burial ground at different periods along almost the entire Holocene. The well-defined archaeological context provided a set of samples suitable to investigate the reliability of the radiocarbon dating of bioapatite as well as the influence of environmental/climatic changes, occurring in Central Sudan along the Holocene, on bone diagenesis. Firstly a multi-disciplinary study on bones and associated soil sediments has been carried out, in order to define the preservation state of bones as well as to provide a model for diagenetic processes taking into account pedogenic processes and changes in environmental, climatic and local burial conditions.

Based in the established model for diagenetic alteration of these bones, radiocarbon dating on selected bioapatite samples was performed and reliability of results discussed.

Characterization of bone samples was carried out by optical and scanning electron microscopy, X-ray computed micro-tomography, X-ray powder diffraction, Fourier transform infrared spectroscopy and micro-Raman spectroscopy. Samples of pedogenic calcrete horizon, found at the 16D4 site, were analysed by optical, cathodoluminescence, and scanning electron microscopy. Bone and calcrete samples were prepared for ^{14}C-AMS dating.

Results from this case study prove that the radiocarbon dating of bioapatite for heavily altered bone samples may not be reliable. Characterization of bones and associated soil sediments provided valuable information on the diagenetic history of bones and on the influence of changes in environmental and local burial conditions on bone preservation. Moreover, results highlight the relevance of a multi-disciplinary approach to the study of the archaeological and palaeoenvironmental contexts.

This essay is organised in six main chapters, treating different aspects of this research project. Each chapter is formatted as a paper ready to be submitted to an international journal or already published.

TABLE OF CONTENTS

INTRODUCTION

Human bones recovered from archaeological contexts represent a valuable source of information about the past. Bioarchaeological, anthropological, chemical and isotopic analyses can be carried out in order to retrieve information on health, demography, age, diet, mobility of ancient populations as well as on environmental conditions experienced. The large amount of data resulted from these studies enables scientists to investigate the social, economic and cultural transformations within human groups over time. However, the reliability of retrieved information depends on the preservation state of bone material and its constituents. Bone diagenesis is, in fact, a complex phenomenon involving taphonomic and alteration processes, affecting bones from the death of the individual onwards. Diagenetic processes, mainly driven by local burial and environmental conditions, may severely alter the macro- and micro-structures of bones as well as the chemical and isotopic composition of its constituents. Therefore, a diagenetic study on archaeological bones, aiming to accurately determine their preservation state, is essential in order to assess the reliability of information retrieved by chemical or isotopic analyses. Moreover, the study of alteration processes provides a better understanding of the diagenetic history of bones, of the mechanisms involved in bone alteration as well as of the archaeological and palaeoenvironmental context.

Based on this perspective, the study of archaeological human bones recovered at the multi-stratified cemetery of Al Khiday 2 (16D4 site), near Khartoum (Sudan) was carried out. Here, several burial phases belonging to different periods along almost the entire Holocene were identified. Under an archaeological viewpoint, the great relevance of archaeological the sites excavated in the Al Khiday area (El Salha archaeological project) lies in the fact that they revealed the first and, so far, unique case of well-preserved stratigraphy referring to the Mesolithic (7^{th} millennium BC) period in Central Sudan. Moreover well-contextualized evidence of the Neolithic (second half of the 5^{th} millennium BC), Meroitic and post Meroitic (1^{st}century BC-6^{th} century AD) periods were also recovered. The study of this well-defined archaeological context provided an indirect chronological attribution for the several burial phases found at the Al Khiday cemetery. However, the oldest burial phase, characterized by numerous skeletons buried in a prone and elongated position, an unusual burial ritual, was only chronologically constrained by the chronological sequence established at Al Khiday. A *terminus ante quem* for this burial phase was established at the first quarter of the 7^{th} millennium BC, on the basis of the stratigraphic relationship with radiometrically dated archaeological features; however a more precise age determination was not achieved. In fact, difficulties in direct and indirect dating of graves were encountered, given the poor preservation of bones, in particular the lack of collagen, and the lack of associated material (goods) suitable for

dating within the burial pit. An alternative source of ^{14}C for direct dating of bones can be found in the structural carbonate contained in bioapatite, the mineral fraction of bone. However, given the poor preservation of these bones, assessing the reliability of radiocarbon ages obtained on bioapatite is necessary. In order to answer important archaeological questions about the burial phases chronology, a diagenetic study on bones has been carried out in this research. The well-defined archaeological and palaeoenvironmental context of this case study provided a set of samples suitable to investigate the effects of diagenetic alteration on radiocarbon ages determination. Moreover, given the wide span of time covered by different burial phases, during which profound climate changes occurred in the region, this case study provide also the chance to study the effects of different environmental conditions on bone diagenesis.

This research project is mainly addressing the radiocarbon dating of the bioapatite fraction of bones and the assessment of the reliability of results. In order to achieve this purposes, a multi-disciplinary approach to the study of bones and associated soil sediments was carried out, aiming to: i) define type and extent of diagenetic alteration; ii) assess the preservation state of bones, in particular the preservation of the biogenic composition of bioapatite; iii) define the interaction between bones and the burial environment, by the study of pedogenic processes occurring within soil sediments; iv) provide a model for the alteration process taking into account the wide chronological period covered by burial phases (almost the entire Holocene) as well as environmental and climatic changes occurring in Central Sudan along this wide span of time.

This research has been developed along subsequent steps in order to characterize bone preservation state, under a microstructural, mineralogical and geochemical viewpoint, as well as soil sediments and pedogenetic processes involved. Based in the established model for diagenetic alteration of these bones, radiocarbon dating on selected bioapatite samples was performed and reliability of results discussed.

The first chapter deals with the histological and microstructural characterization of bone specimens. This part of the work was addressed to define, at the micro-scale, the variability of diagenetic alteration, in terms of types and extent, among different burial phases, in relation to the climate and environmental changes occurring during Holocene.

The second chapter is addressed to the study of bone samples by Fourier transform infrared spectroscopy. Preservation state of collagen and of bioapatite was investigated by means of several parameters calculated from the infrared spectra. In particular, the extent of diagenetic alteration of bioapatite among burial phases was monitored and related to changes in climate conditions.

The third chapter is focused on the determination of crystallinity index, a widely used parameter related to bioapatite crystallinity, by Fourier transform infrared spectroscopy. Issues concerning the approach to data acquisition and the influence of sample preparation on results have been considered. In addition, the values obtained for the IR crystallinity index, were compared to the mean size of bioapatite crystallite measured by X-ray powder diffraction data, in order to investigate the consistency of results.

The fourth chapter deals with micro-Raman imaging of bone sections. Information on diagenetic alteration processes of the bioapatite structure were retrieved from parameters calculated from the Raman spectra. Moreover, acquisition of multispectral maps provided valuable spatially-resolved information on the preservation state of archaeological bone as well as the heterogeneous spatial distribution of the diagenetic features.

The fifth chapter shows the results obtained on the micromorphological, mineralogical and geochemical study of the calcrete horizon sampled at Al Khiday 2. Archaeological and geomorphological investigations revealed strong interaction between pedogenetic processes, leading to calcrete formation, and the archaeological record. The Results provide a clearer understanding of calcrete formation and development over time and the interaction between pedogenetic processes and bone diagenesis was investigated.

Finally, the sixth chapter is focused on the radiocarbon dating of selected bioapatite samples. Results are discussed in terms of reliability of radiocarbon ages, taking into account information on bone alteration and burial environment acquired in this study as well as information provided by archaeological, geomorphological and palaeoenvironmental investigations. A reasonable interpretation of the chronological sequence of burial phases is also provided.

CHAPTER 1

Palaeogeography, Palaeoclimatology, Palaeoecology 416 (2014) 30–42

Contents lists available at ScienceDirect

Palaeogeography, Palaeoclimatology, Palaeoecology

journal homepage: www.elsevier.com/locate/palaeo

Bone diagenesis at the micro-scale: Bone alteration patterns during multiple burial phases at Al Khiday (Khartoum, Sudan) between the Early Holocene and the II century AD

Gregorio Dal Sasso [a,*], Lara Maritan [a], Donatella Usai [b], Ivana Angelini [a], Gilberto Artioli [a]

[a] Department of Geosciences, University of Padova, Via G. Gradenigo 6, 35131 Padova, Italy
[b] Centro Studi Sudanesi e Sub-Sahariani (CSSeS), Strada Canizzano 128/d, 31100 Treviso, Italy

ARTICLE INFO

Article history:
Received 20 February 2014
Received in revised form 23 June 2014
Accepted 25 June 2014
Available online 12 July 2014

Keywords:
Bone diagenesis
Scanning electron microscopy
X-ray computed micro-tomography
Taphonomy
Early Holocene palaeoenvironmental conditions
Sudan

ABSTRACT

Histological analysis is widely applied to archaeological and fossil bones in order to identify diagenetic changes in bone microstructure. Diagenetic processes, affecting bones from the body deposition to the discovery, strongly depend on environmental conditions; therefore the study of diagenetic alterations provides valuable information on the taphonomic history of bones and on their burial environment. Histological analysis was performed on 58 samples of human compact bone found at Al Khiday (Khartoum, Sudan), a multi-stratified archaeological site that revealed a cemetery with distinct burial phases dating from the Early Holocene to the II century AD. The well-defined archaeological context provides a set of bone samples belonging to the same site but buried in different phases and under different environmental conditions: Central Sudan was characterised by a humid environment with seasonal swamps and palaeo-lakes in the Early Holocene, while in the II century AD the environmental conditions were more similar to the current arid climate of the Sub-Saharan belt.
Scanning electron microscopy (SEM) and high-resolution X-ray computed micro-tomography (μ-CT) analysis revealed extensive bacterial and fungal attack, and secondary phases precipitation and dissolution in the samples. The analysis of textural relationships between each diagenetic feature enabled to establish a relative chronological sequence of events acting during burial. Moreover, different patterns of diagenetic alterations were observed for burial phases of different ages, proving a strong relationship between diagenesis and environmental conditions.

1. Introduction

Archaeological human bones, from the death of the individual onwards, undergo different diagenetic processes, which are site-dependent and strongly related to burial and environmental conditions (Child, 1995; Hedges et al., 1995; Nielsen-Marsh and Hedges, 2000; Hedges, 2002; Reiche et al., 2003; Smith et al., 2007). Considering the complex structure of bones, a composite material constituted by an intimate association of organic matrix and inorganic crystallites, and described in terms of hierarchical levels of organisation (Weiner and Traub, 1992; Weiner and Wagner, 1998), diagenetic processes affect bones at different scale. Therefore, the length scale of structural hierarchy of bones, investigated when studying diagenetic alterations, depends on the analytical technique applied and the purposes of the research.

This study aims to contribute towards the understanding of bone diagenesis at the micro-scale by applying high resolution X-ray computed micro-tomography (μ-CT) and scanning electron microscopy (SEM) to bone samples from the multi-stratified cemetery discovered at Al Khiday (Khartoum, Sudan). The well-defined archaeological context provided a set of bone samples belonging to different burial phases, covering a wide span of time from the early Holocene to the I millennium AD, thus encompassing a period of profound climatic changes. Analyses were carried out on bones from the same site but buried during different periods and experiencing different environmental conditions. Funeral practise of burying the dead in pits, preventing bone weathering from sub-aerial exposure and scavenging, is recorded for all burial phases at Al Khiday. Therefore, the variability of diagenetic alterations, in terms of abundance and type, is due to environmental conditions during burial.

On this basis, the main aim of this research is to evaluate the preservation state of bone microstructure in relation to environmental conditions and the climatic changes occurred in the region. Moreover, microscopic analysis on bone microstructure and detection of diagenetic alterations among samples is a valuable procedure in order to select suitable and less altered samples before proceeding with further analyses, such as dating.

* Corresponding author.
E-mail address: gregorio.dalsasso@studenti.unipd.it (G. Dal Sasso).

http://dx.doi.org/10.1016/j.palaeo.2014.06.034
0031-0182/

Fig. 1. Location of archaeological sites 16D4, 16D4-b and 16D5 at Al Khiday, Khartoum, Sudan (from Google Earth, version 7.1.2.2041; 15°25′27.80″N, 32°22′11.55″E, alt 106.82 km, Image Landsat, [11/02/2014]; 15°27′11.64″N, 32°24′24.81″E, alt 2.20 km, 2014 Digital Globe, [11/02/2014]).

2. Archaeological and palaeoenvironmental background

Archaeological survey carried out within the "El Salha Archaeological Project" (Usai and Salvatori, 2005) located about 200 sites along the White Nile, between Omdurman (Sudan) and Jebel Aulia dam. Extensive excavation was conducted on a group of archaeological sites (named 16D5, 16D4 and 16D4b) located near Al Khiday village (Omdurman, Khartoum, Sudan), on the western bank of the White Nile, at 3.5 km from the present-day river course, about 22 km south of the confluence with the Blue Nile (Fig. 1), revealing Mesolithic settlements and a cemetery (Usai and Salvatori, 2007; Salvatori and Usai, 2009; Usai et al., 2010; Salvatori et al., 2011; Zerboni, 2011). Since 2005, archaeological excavations carried out at 16D4 (or Al Khiday 2) site (almost 1400 m^2 have been excavated) revealed a multi-stratified cemetery (Fig. 2.1) with distinct burial phases and evidences of a Mesolithic occupation of the site (Usai et al., 2010; Salvatori et al., 2011).

A hundred and ninety graves were excavated and at least three different burial phases (pre-Mesolithic, Neolithic and Meroitic) were identified on the bases of direct and indirect dating. The most ancient phase, counting 90 graves and defined as pre-Mesolithic (Fig. 2.2), is characterised by bodies buried in a prone and elongated position, a rarely documented burial ritual (Usai et al., 2010), without grave goods (with the exception of an individual with an ivory bracelet). Attribution to pre-Mesolithic is due to the stratigraphic relationship observed between these graves and pits belonging to the Mesolithic occupation of the site. Archaeological excavations revealed, until now, 104 Mesolithic pits (0.5–1.2 m wide and 0.5–1 m deep), characterised by different fillings and related to different functions, radiometrically dated to the 6700–6300 cal years BC (Usai et al., 2010; Salvatori et al., 2011; Salvatori, 2012). The clear evidence of 16 of these pits cutting individuals buried in a prone position (Fig. 2.7) shows that graves are older than the Mesolithic pits and provides a *terminus ante quem* for this burial phase.

The site was subsequently used as a cemetery during the Neolithic period: 38 Neolithic graves (4550–4250 cal years BC) have been excavated (Usai et al., 2010; Salvatori et al., 2011); bodies were buried in flexed position with pottery vessels and personal adornments (Fig. 2.4). Meroitic is the third burial phase identified at 16D4 site, dated between the I century BC and the II century AD (Usai et al., 2010). The skeletons (43) are in a flexed position and some grave goods have been recovered (Fig. 2.5). The Meroitic grave structure is more monumental than in the prehistoric case and is composed of a rectangular shaft leading to a smaller chamber. Due to the large size of the shaft, up to 3 m by 2 m, these graves heavily affected the preservation of the most ancient burial phases at 16D4 site.

Bone samples belonging to these burial phases were studied in this research; however, a fourth group of samples was also considered. In fact, a possible fourth burial phase (19 individuals), showing funeral ritual similar to that observed for the Neolithic phase, but without grave goods and a macroscopic bone preservation state more similar

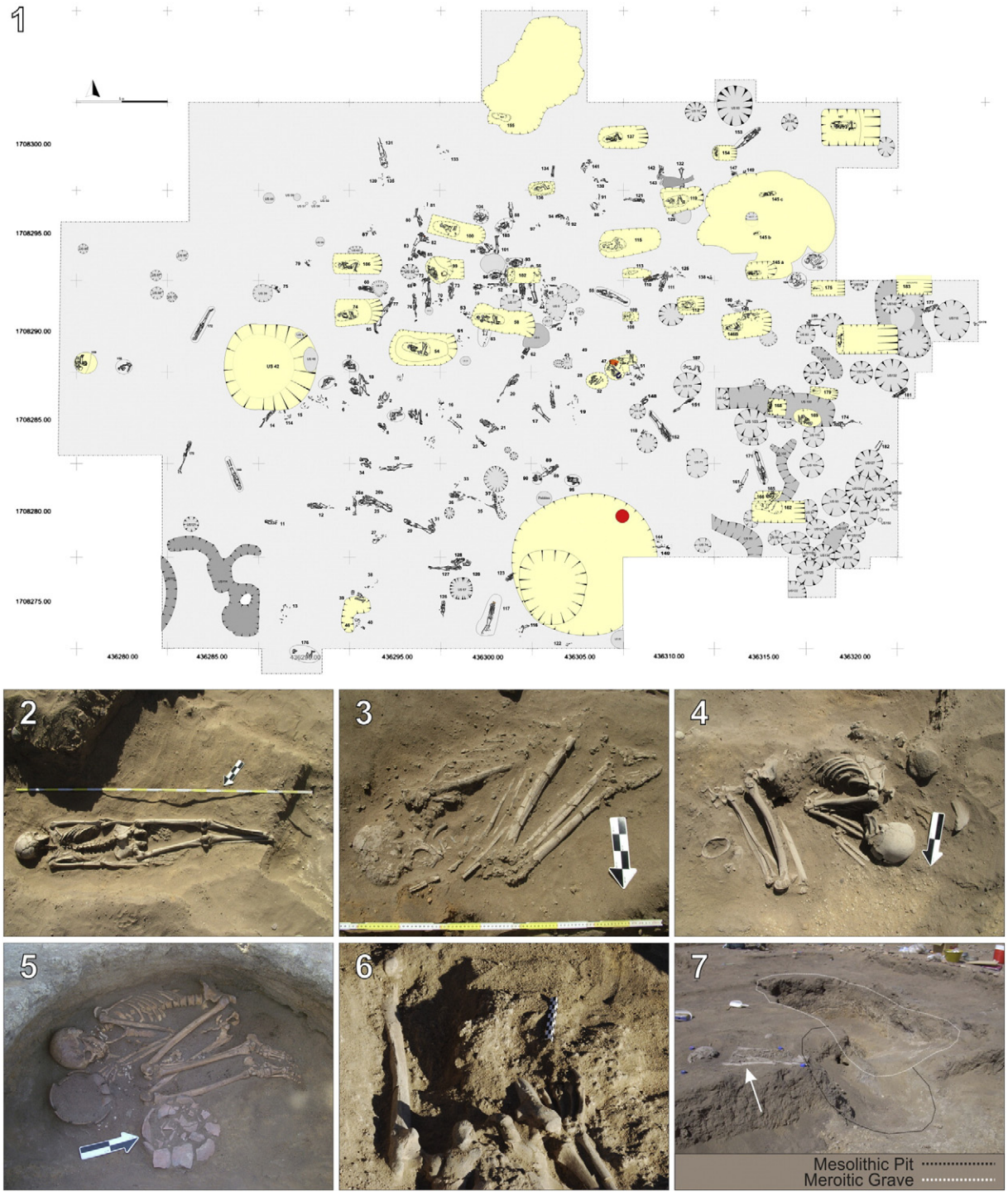

Fig. 2. (©CSSeS). 2.1. Plan of 16D4 archaeological site updated to 2012 field season; location of graves and Mesolithic pits is displayed. 2.2–5. A representative example of each burial phase: 2.2. Pre-Mesolithic (Grave 153); 2.3. Mesolithic (Grave 128); 2.4. Neolithic (Grave 98); 2.5. Meroitic (Grave 159). 2.6. Carbonate concretions partially embed pre-Mesolithic bones (Grave 152). 2.7. Mesolithic pit cuts through a prone and elongated individual belonging to the pre-Mesolithic burial phase.

to that observed for the pre-Mesolithic phase, was identified (Fig. 2.3); graves belonging to this phase were tentatively labelled Mesolithic, as possibly related to the first phase of settlement area located at nearby site 16D5 (or Al Khiday 1) and less probably to the settlement phase identified at the same cemetery.

During the wide chronological period considered in this research, between the early Holocene and the beginning of the I millennium AD, deep environmental and climatic changes occurred in the region (Gasse, 2000; Nicoll, 2004; Williams, 2009; Williams and Jacobsen, 2011; Zerboni, 2011; Macklin et al., 2013; Zerboni, 2013). In the early Holocene, North Africa was characterised by wetter climatic conditions, due to stronger monsoonal activity and increased rainfall. Greater water availability was proved by palaeo-hydrological records, showing a higher flooding level for the Nile, formation of lakes and wadis draining into the Nile. Numerous short dry periods occurred during the early Holocene Optimum Climaticum due to global climatic changes, leading to precipitation decrease in areas close to the tropics; the most intense, dated at the end of the VII millennium cal BC, probably constituted an arid period for a wide area in North Africa, causing the desiccation of former lakes. By the middle Holocene gradual changes in the

Table 1
Histological Index (HI) values and different types of diagenetic alteration observed for each sample. HI (ranges from 0 to 5; 0 stands for "no original features identifiable, other than Haversian canals" and 5 stands for "very well preserved, virtually indistinguishable from fresh bone" (Hedges et al., 1995)); relative amount/extent of non-Wedl and Wedl MFD, secondary calcite (Calcite) and manganese oxides (Mn oxides), if present, was estimated by comparison among samples and assigned to a categorical class, on a scale ranging from 1 (low amount) to 5 (high amount).

Burial phase	Grave number	Bone type	HI	Secondary mineral phases		Non-Wedl MFD	Wedl MFD
				Calcite	Mn oxides		
Pre-Mesolithic	24	Right humerus	3	2	–	3	–
		Left Femur	2	3	–	4	–
	55	Right humerus	3	2	–	2	–
		Right femur	1	2	1	5	–
	69	Left humerus	3	3	–	2	1
		Left femur	2	3	–	2	1
	88	Right humerus	2	3	–	4	–
		Right femur	0	4	–	5	–
	132	Right radius	3	2	1	3	–
		Left femur	4	2	1	2	–
	156	Left humerus	1	1	–	5	–
		Left femur	2	2	–	4	–
	157	Left humerus	1	3	–	4	–
		Right femur	0	3	–	5	–
	160	Right humerus	1	4	1	1	3
		Right femur	2	3	3	2	2
	170	Right humerus	2	–	2	2	1
		Right femur	1	–	–	3	3
	172	Right humerus	2	2	4	3	–
		Left femur	3	2	4	2	–
	174	Left humerus	2	1	–	3	–
		Left femur	2	1	–	4	–
	177	Right humerus	2	2	1	3	–
		Left femur	2	2	1	3	–
Mesolithic	31	Left humerus	0	4	2	5	–
		Right femur	0	4	2	5	–
	120	Left humerus	3	2	3	2	–
		Left femur	4	2	–	1	–
	128	Left humerus	3	3	3	2	1
		Right femur	3	3	4	2	2
	142	Right humerus	0	5	2	4	–
		Right femur	1	4	2	4	–
	163	Left humerus	5	1	–	–	–
		Right femur	4	1	–	–	2
	164	Right humerus	3	2	–	–	3
		Right femur	3	2	–	–	2
Neolithic	3	Left humerus	4	1	–	–	1
		Left femur	2	4	–	–	2
	4	Right humerus	3	2	–	2	1
		Left femur	0	2	–	5	–
	103	Right humerus	1	3	–	4	1
		Right femur	0	3	–	5	–
	107	Left humerus	3	4	–	–	2
		Right femur	3	4	–	–	2
	158	Left humerus	2	4	–	3	1
		Left femur	2	3	–	3	1
Meroitic	50	Left humerus	3	–	–	–	1
		Left femur	3	–	–	–	2
	115	Left humerus	4	–	–	–	2
		Left femur	4	–	–	–	1
	136	Right humerus	4	–	–	–	1
		Left femur	4	–	–	–	1
	137	Left humerus	4	–	–	–	2
		Left femur	3	–	–	–	4
	159	Right humerus	5	–	–	–	1
		Left femur	4	–	–	–	2
	166	Right humerus	4	–	–	–	3
		Right femur	4	–	–	–	2

environmental conditions and weaker monsoonal activity lead to a progressive decrease in rainfall and water availability towards desert climatic conditions; the end of the African humid period dated at about the beginning of the IV millennium cal BC.

Geomorphological survey carried out at Al Khiday and the surrounding area, combined with micro-morphological study of the soil, archaeological evidences and radiocarbon dating (Usai et al., 2010; Salvatori et al., 2011; Zerboni, 2011), showed that Mesolithic sites are located on river sand bar (Cremaschi et al., 2007), visible at the limit of the alluvial sediments deposited by early Holocene higher White Nile floods, and rising few metres above the flooding plain. The flat area beyond the sand bar is characterised by the occurrence of dark sediments rich in organic matter, dated to 6650–6470 cal BC, deposited by a former seasonal swamp. Palaeoenvironmental records show the seasonality of these swamps, fed by the flood of the White Nile during the wet season and desiccated during the dry season, as well as the overall higher water availability than that currently registered. Williams and Adamson (1980) dated the occurrence in the area of

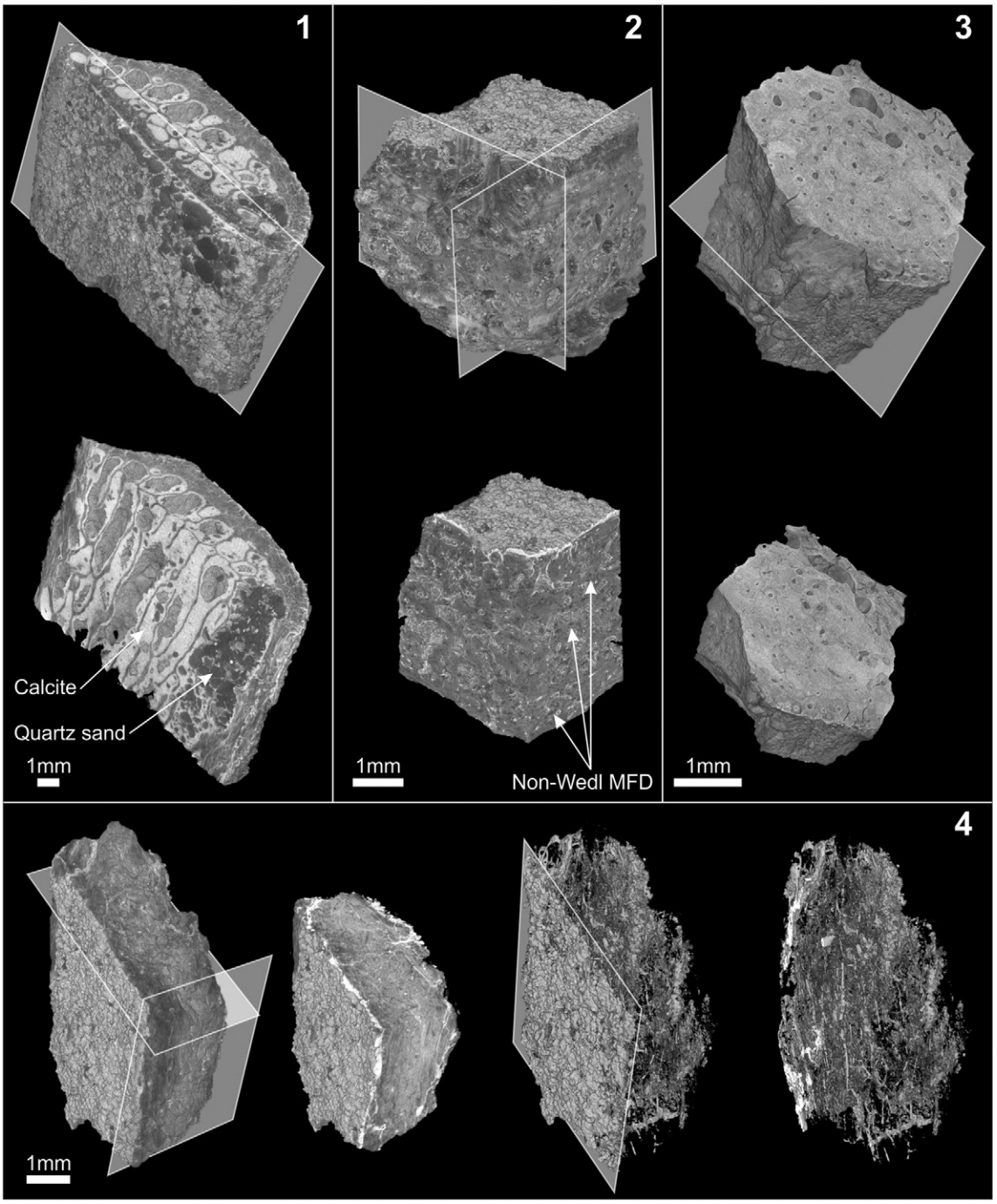

Fig. 3. μ-CT three-dimensional reconstruction of different types of bone and examples of virtual sections. 3.1. Pre-Mesolithic rib fragment (Grave 69); secondary calcite (light grey), cementing quartz sand (dark grey), covers the external surface of the sample and fills the inner porosity. 3.2. Neolithic skull fragment (Grave 103); a thin layer of secondary calcite (light grey) precipitated on external surface and in the bone porosity; arrows point to some non-Wedl foci produced by bacterial activity. 3.3. Meroitic femur fragment (Grave 159). 3.4. Pre-Mesolithic femur fragment (Grave 69); on the right isolation of secondary calcite, which covers the external surface and permeates fractures and vascular system of the bone sample.

seasonal swamps fed by the White Nile floods to 6000–5700 cal BC. Moreover, alternation of wet and dry seasons is proved by the occurrence of pedologic horizons rich in carbonate concretions, as subsequent events of calcium carbonate dissolution and re-precipitation, determined by changes in evapotranspiration conditions, led to calcium carbonate accumulation in the soil (Zerboni, 2011; Zerboni, 2013). Results obtained by archaeological and geomorphological investigations at Al Khiday proved the Mesolithic occupation of the area during higher flood of the White Nile and formation of palaeo-swamps, while during the Meroitic use of the site more arid climate conditions occurred. Neolithic use of the site occurred during the transition from the early Holocene wetter environmental conditions to drier conditions.

Conventional and AMS radiocarbon dates cited in the present paper have been calibrated BC according to INTCAL13 (Reimer et al., 2013) with OxCal 4.2 (Bronk Ramsey, 2009) software.

3. Material and methods

This research was carried out in two distinct stages. In the first one, a preliminary study on different bone types of presumed different

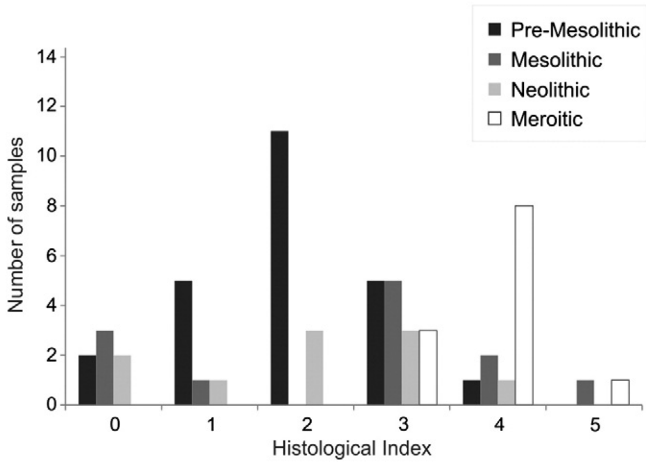

Fig. 4. Frequency distribution of analysed bone samples on the bases of HI and burial phase.

chronology was performed to assess the degree of alteration by characterising the nature and distribution of the mineral phases: 9 bone fragments, a skull, a rib and a femur from a pre-Mesolithic, a Neolithic and a Meroitic individual were analysed by high-resolution X-ray computed micro-tomography (μ-CT), X-ray diffraction (XRD), and scanning electron microscopy (SEM). These preliminary analyses helped to define the most suitable type of samples to be analysed in the second stage, on the basis of the preservation state of the bone microstructure. μ-CT analysis was performed using a Skyscan 1172 high-resolution computed micro-tomography (Salvo et al., 2003), equipped with a Cu X-ray tube and operating at 60 kV and 167 nA, with an Al filter 0.5 mm thick. No sample preparation was required. Radiographies were acquired with an angular step of 0° 18′, a resolution of 1840 × 1336 pixels and pixel size ranging between 3 and 5 μm. Micro-CT is a non-destructive technique which enables a 3D reconstruction of the sample internal structure, allowing any number of virtual sections to be visualised and extracted. Moreover, different phases constituting the sample can be easily identified and separately analysed, based on their X-ray absorption coefficient contrast.

In the second stage, mid-shaft part of long bones, femur (F) and humerus (H), chosen as the most suitable portions to be analysed, were sampled from 29 graves (for a total of 58 bone samples), respectively from 12 pre-Mesolithic, 6 Mesolithic, 5 Neolithic and 6 Meroitic graves, representative of each burial phase (Table 1). A portion of each bone fragment was embedded under vacuum in epoxy resin (Araldite 2020) and cross sections were cut. The exposed bone sections, with an average area of about 5 × 5 mm, were polished using 1000, 2500 and 4000 grit sandpaper on a rotating stage with water as lubricant and then 5 μm and 1 μm diamond suspension on a polishing cloth. Carbon coating was applied in order to avoid charging effects. Histological analysis was performed by SEM with a CamScan MX 2500 coupled to a detector for energy dispersive X-ray spectroscopy (EDS), equipped with a LaB_6 cathode and operating at 20 kV and 160 nA. Backscattered electron images (SEM-BSE images) of bone cross sections were acquired for all samples, with a resolution of 1280 × 1024 pixels. Histological analysis focused on the presence and type of microscopic focal destruction (MFD) and secondary mineral phases. The preservation state of bone microstructure was described using the Histological Index (HI) proposed by Hedges et al. (1995): on a scale of integer numbers from 0 to 5 (0 stands for "no original features identifiable, other than Haversian canals" and 5 stands for "very well preserved, virtually indistinguishable from fresh bone" (Hedges et al., 1995)) a value was assigned to each sample on the basis of the extent of observed MFD. Since, in some cases, MFD is not homogeneously distributed among the section but it can be more intense in certain areas (i.e. periosteal or endosteal areas or in the proximity of Haversian canals) an average value for HI was assigned. According to literature data (Hackett, 1981; Bell, 1990; Jans et al., 2002; Turner-Walker and Syversen, 2002; Jans et al., 2004; Fernández-Jalvo et al., 2010; Müller et al., 2011) MFD was described as non-Wedl and Wedl foci. Non-Wedl MFD is characterised by areas of high concentration of micro-channels and pores, up to 2 μm in diameter, surrounded by a hyper-mineralised rim, due to dissolution and re-precipitation of bone apatite with a higher density (showing a lighter grey tone on SEM-BSE images) with respect to the surrounding bone, caused by bacterial activity. According to Hackett (1981) non-Wedl foci are classified as *linear longitudinal*, *budded* and *lamellate*. Wedl foci, caused by fungal activity, show a different arrangement, in which micro-tunnelling, up to 8 μm in diameter, is not characterised by hyper-mineralised rims.

Since the diagenetic alteration effects observed into this study are various and occur with different intensities, we choose to explicitly consider and provide an average estimation of the amount/extent for MFD (non-Wedl and Wedl MFD) and secondary mineral phases. For this reason, a categorical class, on a scale ranging from 1 (low amount) to 5 (high amount), was established and calibrated independently from that defined for HI, for comparison among all the analysed samples.

These data were statistically treated by principal component analysis using the software Statgraphics Centurion XVI.

The preliminary mineralogical identification of secondary phases was carried out on some samples using a DXR Thermo Scientific Raman microscope, equipped with a diode-pumped solid state 532 nm laser, operating at a power of 2 mW, with a spectral resolution in the range 2.7–4.2 cm^{-1} and a spatial resolution of 1.1 μm. Acquired spectra were

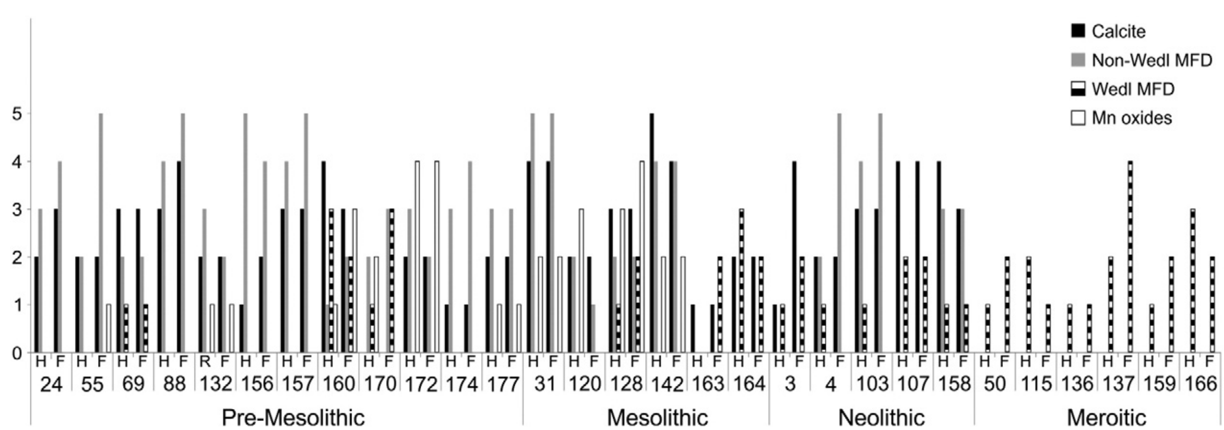

Fig. 5. Bar diagram of the relative amount/extent of non-Wedl and Wedl MFD, secondary calcite (Calcite) and manganese oxides (Mn oxides) estimated by sample comparison and assigned to a categorical class, on a scale ranging from 1 (low amount) to 5 (high amount). Femur (F) and humerus (H) samples are grouped by burial phase; grave number is also reported.

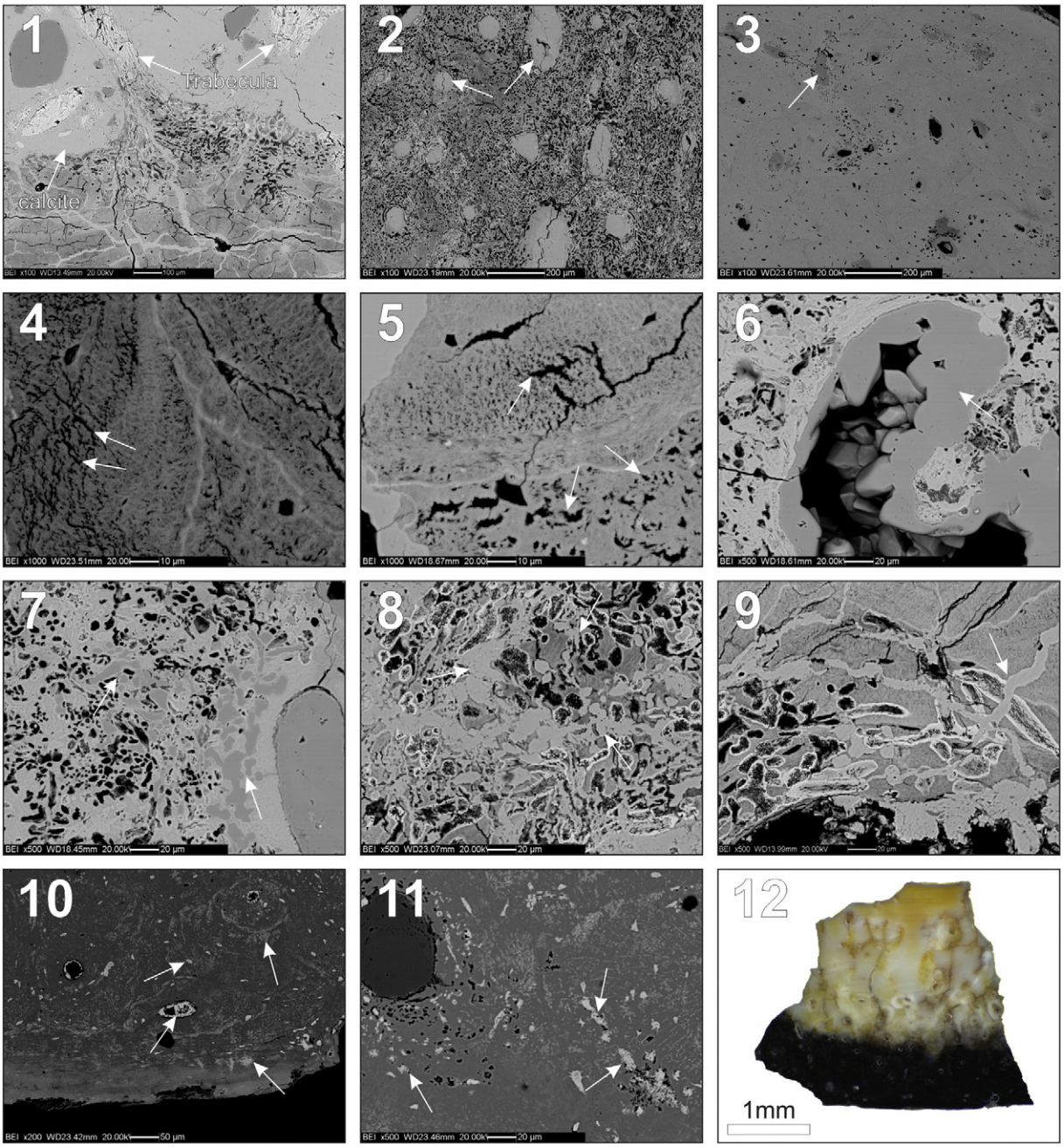

Fig. 6. 6.1–11. SEM microphotographs of pre-Mesolithic bone sections. 6.1. Trabecular bone highly altered by bacterial activity (rib, Grave 69); calcite (light grey) permeates bone porosity. 6.2, 6.3. Different extent of non-Wedl MFD affecting bone microstructure; arrows indicate secondary calcite occurring in Haversian canals (femur, Grave 88 and humerus, Grave 55, respectively). 6.4. Wedl MFD (femur, Grave 69). 6.5. Wedl MFD; arrows indicates pores with irregular shape, caused by partial dissolution of bone apatite (femur, Grave 160). 6.6. Sparry secondary calcite (arrow) precipitated in the bone vascular system (femur, Grave 157). 6.7, 6.8. Secondary calcite permeates non-Wedl foci, produced by bacterial activity (humerus, Grave 157 and femur, Grave 88, respectively). 6.9. Fracture (arrow) filled in with calcite, crosses through bacterial colonies (femur, Grave 69). 6.10. Manganese oxides permeate interlamellar porosity, *lacunae*, *canaliculi* and partially fill Haversian canals (femur, Grave 172). 6.11. Manganese oxides permeate non-Wedl foci produced by bacterial activity (femur, Grave 172). 6.12. Photograph of bone section, acquired at the stereoscopic microscope, shows a 1 mm thick dark area at the periosteal surface; in 6.10 a detail of the same area analysed by SEM (femur, Grave 172).

tentatively compared with reference database published on the RRUFF website (http://rruff.info).

4. Results

μ-CT analysis provides a 3D internal structure reconstruction of bone samples, showing the pristine bone microstructure and the distribution of diagenetic features in a three-dimensional space. The acquired tomography enables to analyse both longitudinal and cross sections, as well as sections with any orientation, which therefore can be selected without any constrain, as in the case of traditional 2-dimensional cross sections. Results obtained from μ-CT analysis for skull, rib and femur bone fragments indicate that microstructure of femurs is better preserved than that of skulls and ribs (Fig. 3). These latter types of bone, partially constituted by trabecular bone, are characterised by higher porosity, which is here often filled in by secondary calcite and occasionally quartz sand grains from the soil (Fig. 3.1). Moreover, the thin *trabeculae* are more heavily affected by MFD and the original bone microstructure is almost completely lost (Fig. 6.1). Both MFD and secondary mineral phases occurrence in each sample are

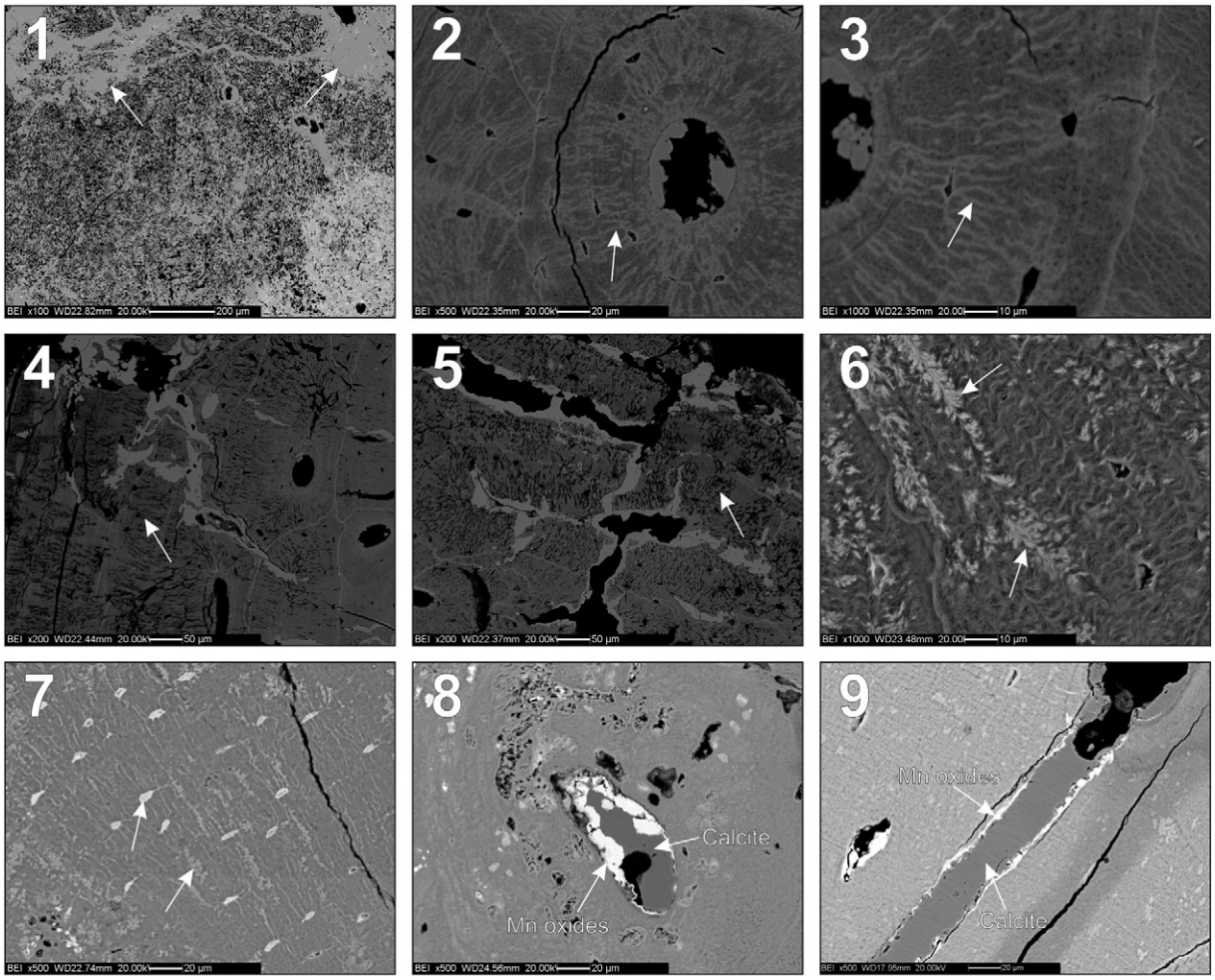

Fig. 7. SEM microphotographs of Mesolithic bone sections. 7.1. Bone microstructure heavily damaged by non-Wedl MFD (low HI value); arrows indicate calcite precipitated in Haversian canals, fractures and micro-porosity produced by bacterial activity (humerus, Grave 31). 7.2, 7.3. Wedl MFD; enhanced *canaliculi* (humerus, Grave 164). 7.4, 7.5. Wedl MFD; enlarged *canaliculi* (humerus and femur, Grave 164, respectively). 7.6, 7.7. Manganese dendrites permeate inter-lamellar porosity and *lacunae* (femur, Grave 142). 7.8, 7.9. Manganese oxides precipitated before secondary calcite in Haversian canal and fracture, respectively (femur, Grave 142 and Grave 128, respectively).

homogeneously distributed in the 3D volume, hence any cross section cut from the sample can be considered representative of the sample itself. Due to the μ-CT spatial resolution, ranging between 3 and 5 μm/pixel, single pores and thin micro-tunnelling caused by MFD, smaller than 2 μm in diameter, were not detected, while larger features, such as bacterial colonies, were easily identified (Fig. 3.2). Secondary calcite forms an external surface deposit and permeates both the bone vascular system and fractures (Fig. 3.4).

Microscopic analysis on the 58 selected bone fragments pointed out a different amount/extent of both secondary mineral phases and MFD, showing a diachronic variation of the diagenetic alteration effects (Table 1). Low HI values, ranging between 0 and 2 in a large number of pre-Mesolithic, Mesolithic and Neolithic samples (75%, 30% and 60%, respectively), reveal an average poor preservation of bone microstructure, while Meroitic bones are less affected by MFD, since HI values range between 3 and 5 (Table 1; Fig. 4).

A very good accordance of type and, with few exceptions, extent of MFD between femur and humerus from the same grave was observed (Fig. 5). Non-Wedl tunnelling, consisting of *linear longitudinal* and *budded* foci, according to Hackett (1981) classification, can be observed in samples as both few isolated (ranging between 5 and 15 μm in diameter) and large and nearly superimposed bacterial colonies (up to 100 μm wide), all showing the characteristic micro-tunnelling and hyper-mineralised rim (Figs. 6.2–3, 8.1–3). The extent of bacterial attack among the samples strongly affects bone microstructure, which is nearly unaltered in some cases (samples with high HI in Table 1; Figs. 6.3, 8.4), while almost completely lost in others (samples with low H in Table 1; Figs. 6.2, 7.1, 8.1–2). Non-Wedl tunnelling was mainly detected among pre-Mesolithic samples (Fig. 6), it also occurs in the Mesolithic (Fig. 7) and Neolithic (Fig. 8) remains, whereas it completely lacks in the Meroitics (Fig. 9).

As for Wedl MFD, destructive foci were observed for few samples among different burial phases, all characterised by diameters ranging between 2 and 6 μm, larger than those observed for the non-Wedl MFD, and lacking re-precipitated bone apatite (Figs. 6.4, 8.5, 9.1). They are often associated with larger pores having irregular shape (10–12 μm long and 4–7 μm wide), micro-tunnelling and micro-fissures, due to the partial dissolution of bone mineral (Figs. 6.5, 8.6, 9.2–3). These features were more frequently detected among Neolithic and Meroitic samples (about 60%) than in pre-Mesolithic (about 15%) and Mesolithic (about 40%) ones. In some cases thin micro-tunnelling (Fig. 9.5) and enhanced (Figs. 7.2–3, 9.6–7) or enlarged (Figs. 7.4–5, 9.2–4) *canaliculi* (connecting osteocytes to the bone vascular system) were also observed, mostly occurring in the outermost part of the bone (100–200 μm under the periosteal surface). They were rarely detected among pre-Mesolithic and Mesolithic samples (about 10% and 15%, respectively), more frequently observed among Neolithics (60% of the samples), whereas they are the main type of diagenetic alteration for the Meroitic remains, both in frequency of occurrence (90% of cases) and in extent.

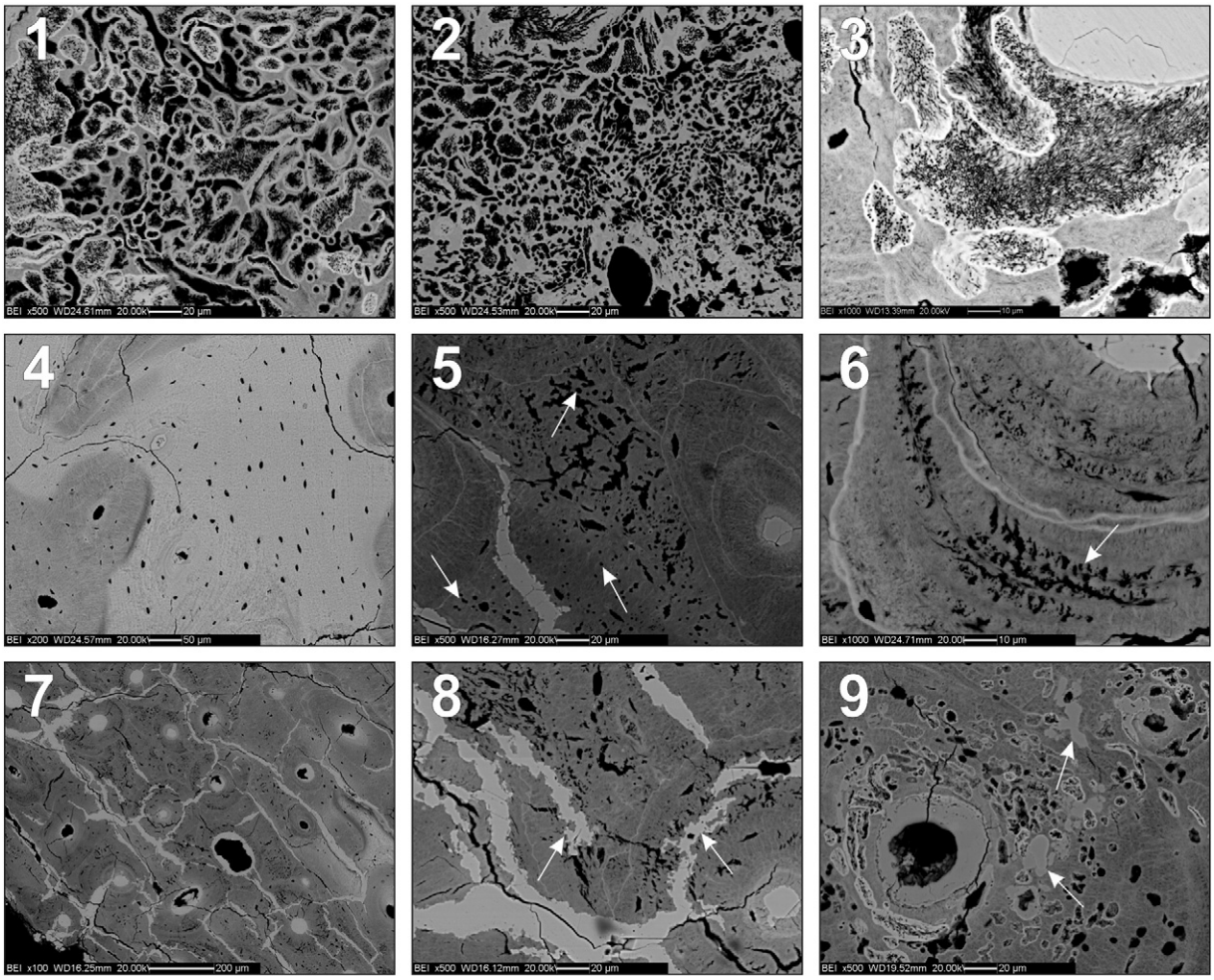

Fig. 8. SEM microphotographs of Neolithic bone sections. 8.1, 8.2, 8.3. Micro-tunnelling surrounded by hyper-mineralised rim due to bacterial colonies, characteristic for non-Wedl MFD (humerus, Grave 103; femur, Grave 4 and Grave 103, respectively). 8.4. Well-preserved bone microstructure (high HI value) (humerus, Grave 3). 8.5. Wedl MFD (femur, Grave 107). 8.6. Wedl MFD; pores with irregular shape (arrow) and associated with micro-tunnelling (femur, Grave 3). 8.7. Secondary calcite permeates fractures and bone vascular system (femur, Grave 107). 8.8. Secondary calcite precipitated in micro-porosity similar to that observed in 8.6 (femur, Grave 107). 8.9. Secondary calcite precipitated in non-Wedl foci produced by bacterial activity (femur, Grave 158).

In most of the samples, the presence of empty micro-fractures and large fractures cannot univocally be attributed to diagenetic alteration, as some of them may derive from physical stress during sample preparation or SEM analysis. This is supported by the increase in number and density of the fractures observed by SEM on a section of Meroitic femur (Fig. 9.8), previously analysed by μ-CT (Figs. 3.3, 9.9). Therefore, in such a case the fractures were not considered to be related to specific diagenetic processes. Fractures occur in all the studied bone fragments, with no specific relation, in terms of size, quantity and distribution in the bone microstructure, to the burial phase.

Besides MFD, precipitation of secondary mineral phases, in particular of calcite and manganese oxides, is the diagenetic alteration process that mostly affects bone microstructure. Archaeological excavation recovered pre-Mesolithic, Mesolithic and Neolithic bones often encrusted by a thin layer of calcium carbonate cementing quartz sand. Moreover, in few cases, some bones of pre-Mesolithic graves were found partially embedded in carbonate concretions (Fig. 2.6). Microscopic analysis revealed the intense permeation of bone microstructure by secondary calcite, occurring in almost all pre-Mesolithic, Mesolithic and Neolithic bone samples (with the exception of pre-Mesolithic Grave 170), whereas it is completely absent in Meroitic samples (Table 1). The quantity of secondary calcite is very variable sample by sample, and no diachronic trends can be observed (Fig. 5). A 100 μm–1 mm thick layer of calcite is often present on the external surfaces of bone samples (Fig. 3.1, 3.2, 3.4). Sparry calcite occurs in the bone vascular system (Fig. 6.2, 6.6), in the Haversian and Volkmann's canals, and in the micro-pores produced for bone apatite dissolution by bacterial activity (Figs. 6.7–8, 8.9). In addition, secondary calcite can partially or completely fill fractures (Fig. 8.7) of different sizes (micro-fractures 2 μm thick and 20 μm long — large fractures up to 200 μm thick and 1–2 mm long).

Manganese oxides occur only in pre-Mesolithic and Mesolithic samples (about 40% and 60%, respectively). A macroscopic observation of bone cross sections affected by manganese oxides deposition shows black areas (Fig. 6.12) about 0.5–1 mm thick, located in some cases at the periosteal surface, in others in the innermost portion of the bone section. SEM-BSE images (Figs. 6.10, 7.6–7), acquired for those black areas, revealed a high concentration of a mineral phase showing dendritic habit (Potter and Rossman, 1979) and permeating inter-lamellar porosity, lacunae, canaliculi and partially filling Haversian canals as well as micro-porosity originated by MFD (Fig. 6.11). Micro-chemical analysis indicates that these precipitations are composed of Mn, Ba and Ca; semi-quantitative estimation, expressed as weight percentage of the oxides, points out a variable composition for MnO (73–77%), BaO (15–20%) and CaO (3–6%).

Micro-Raman analysis (Fig. 10) on Mn oxides shows the occurrence of strong peaks at 580 and 618 cm^{-1} and weaker peaks at 156, 166, 198, 298, 391 and 510 cm^{-1}. Absence of characteristic H_2O Raman frequency

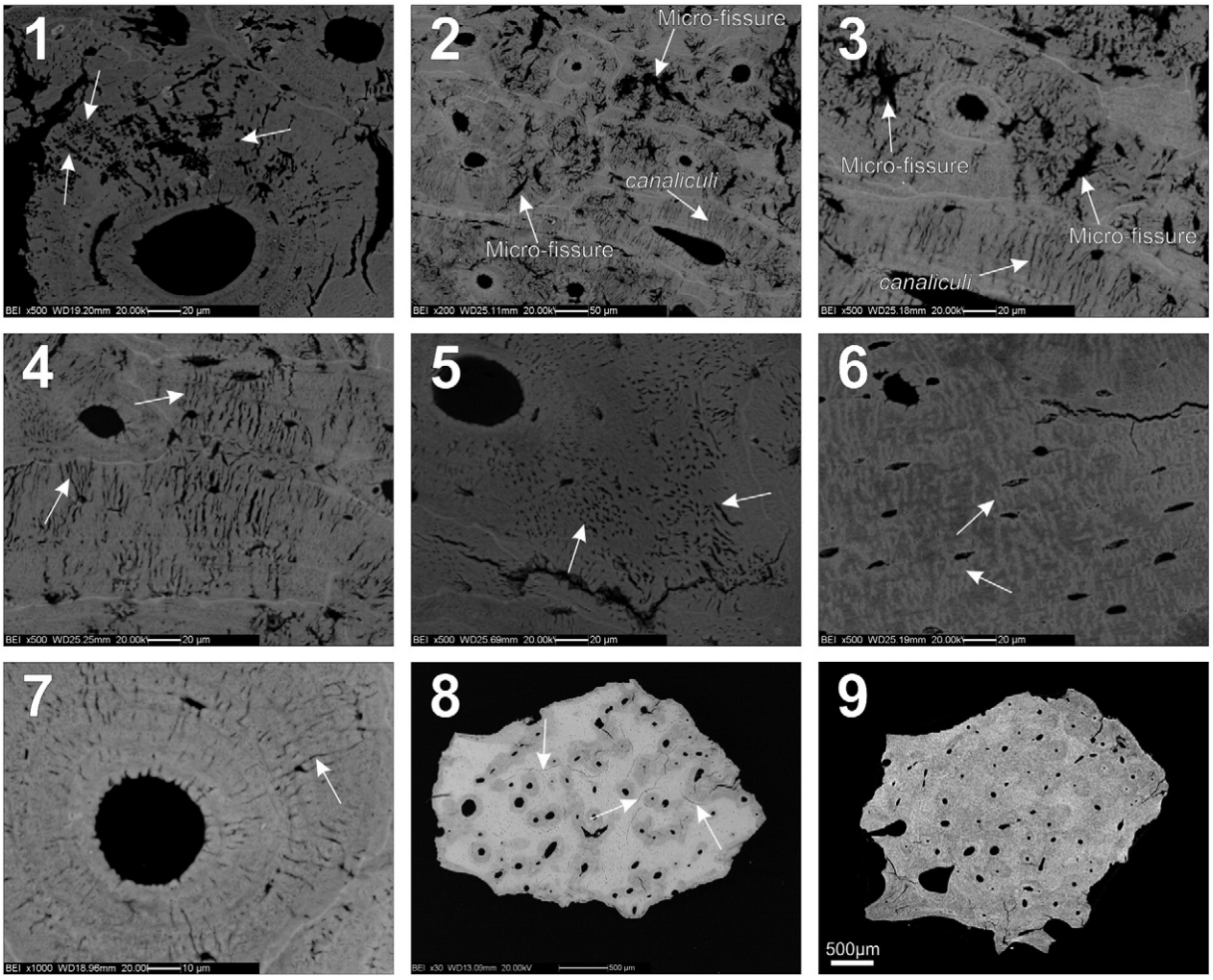

Fig. 9. 9.1–8. SEM microphotographs of Meroitic bone sections. 9.1. Wedl MFD (femur, Grave 50). 9.2–3. Wedl MFD; micro-fissures and enlarged *canaliculi* (femur, Grave 137). 9.4. Wedl MFD; enlarged *canaliculi* (femur, Grave 137). 9.5. Wedl MFD; thin micro-tunnelling (femur, Grave 159). 9.6–7. Wedl MFD; enhanced *canaliculi* (humerus, Grave 166 and Grave 115, respectively). 9.8. Arrows indicate micro-fractures caused by physical stress during sample preparation (femur, Grave 159). 9.9. Reconstruction of two-dimensional cross section of bone fragment by μ-CT; micro-fractures detected on SEM-BSE images from the same sample (9.8) here were not observed (femur, Grave 159).

indicates that this Mn oxide is an anhydrous phase. The broad band in the 400–700 cm^{-1} region may be due to Mn(III) and Mn(IV) (Julien et al., 2004). Combining this information with results from micro-chemical analysis and SEM observations may suggest the occurrence of a mixture of manganese oxides. Presence of hollandite-type phases can be tentatively hypothesised.

In order to graphically visualise the intensity/extent of different diagenetic effects on bones with respect to the age, the average estimation of secondary mineral phases, MFD (non-Wedl MFD and Wedl MFD) and HI was statistically treated by principal component analysis (Fig. 11). All the Meroitic bones cluster together at high value of PC1 and negative PC3, due to the high HI, to the occurrence of Wedl MFD and to the absence of non-Wedl MDF and of secondary mineral phases. Mesolithic bones tend to group into two distinct clusters: one at negative values of PC1 and PC2 and positive PC3, due to the high concentration of secondary calcite and bacteria micro-tunnelling (non-Wedl MFD), very poor preservation state (low HI) and the absence of Wedl MFD; another one at positive PC1 and variable PC2 and PC3, due to the better preservation state (high HI), scarce concentration of secondary calcite and bacterial micro-tunnelling. Bones from both pre-Mesolithic and Neolithic graves are spread over the diagram, possibly because they are affected by diagenetic processes of different intensities.

5. Discussion

A diachronic occurrence of diagenetic alterations was observed on the basis of their textural relationships, establishing a relative chronological sequence of events, which altered bone microstructure. Detection of manganese oxides and sparry calcite in the micro-porosity, produced by bacterial activity, proves that precipitation of these secondary phases is subsequent to non-Wedl MFD (6.7–9, 6.11, 8.9). Moreover, calcite seals fractures crossing through bacterial colonies (Fig. 6.9), indicating that non-Wedl MFD precedes fracture formation. In addition, the lack of evidences of bacterial colonies superimposed to areas affected by secondary mineral phases precipitation shows that non-Wedl MFD is the first diagenetic alteration occurring after body deposition. For the same reasons, also formation of Wedl foci irregular in shape, observed in some samples, occurred before calcite precipitation (Fig. 8.8). SEM-BSE images of bone sections showing high concentration of manganese oxides (Figs. 6.10, 7.7), macroscopically detected as black areas, show a very low occurrence of secondary calcite, despite its ubiquitous abundance, since manganese oxides already permeated the micro-porosity of bone before calcite precipitation. Moreover, some sections show Haversian canals and fractures partially filled in with manganese oxides, adhering to canal (and fracture) surface, and subsequently filled in with calcite (Fig. 7.8–9). This clearly proves that manganese oxides

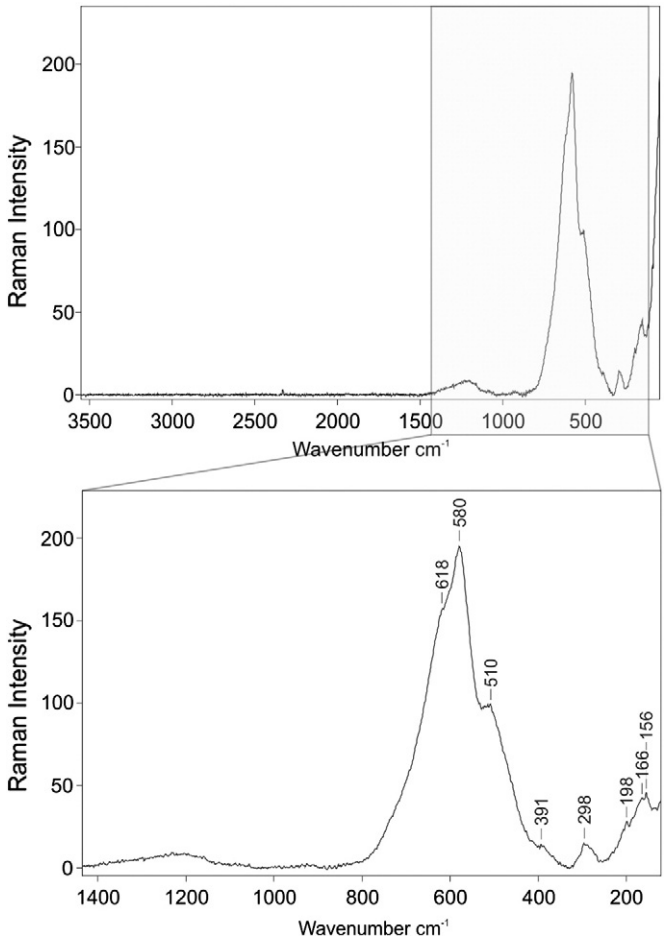

Fig. 10. Raman spectrum of manganese oxides obtained on a femur section (Grave 172).

precipitated before calcite and they both occurred as the result of two different diagenetic processes. This chronological sequence of diagenetic events concerns only pre-Mesolithic and Mesolithic graves, since only these burial phases show all diagenetic alterations previously described (Fig. 12).

A very similar model of subsequent events affecting Neolithic graves can be established with the exception of manganese oxides deposition, which did not occur for this burial phase. This sequence of events cannot be proposed for Meroitic graves, as bacterial activity, calcite and manganese oxides precipitation did not affect this burial phase (Fig. 12).

Textural relationship between MFD, in particular bacterial activity, and secondary mineral phases precipitation in pre-Mesolithic, Mesolithic and Neolithic samples indicates that non-Wedl MFD took place

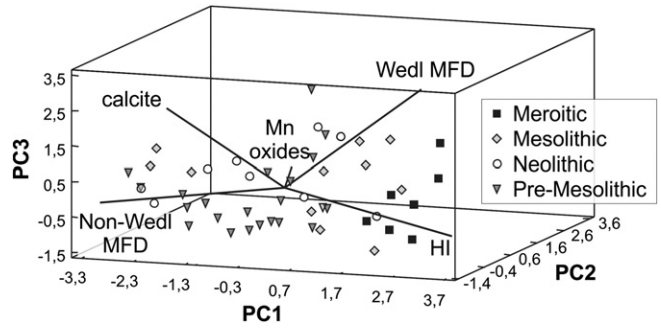

Fig. 11. Score and loading plot of principal component analysis of different diagenetic effects, with PC1, PC2 and PC3 representing 55%, 19% and 16% of the total variance, considering sample burial phases.

only in the early diagenesis of bones, affecting bone microstructure in a short-scale time after body deposition. The widespread bacterial activity observed in pre-Mesolithic, Mesolithic and Neolithic bones is commonly favoured by more humid environmental conditions with respect to those encountered by Meroitic bones, completely lacking of non-Wedl MFD. Diagenetic features attributed to Wedl MFD can be the result of fungal or other microorganisms activity as well as their combined action (Pitre et al., 2013). Similar diagenetic features were already described by Fernández-Jalvo et al. (2010), who analysed the early diagenesis of unburied animal bones after an exposure of 30 years in a temperate environment. Thin micro-tunnelling and enlarged *canaliculi*, similar to those identified in this research mainly among Meroitic samples and occasionally in the other burial phases (affecting the outermost portion of bones, about 100 μm from the periosteal surface), were related to soil acidity and biogenic corrosion due to moss, algae and lichens (Fernández-Jalvo et al., 2010). However, the different climate conditions at Al Khiday site (with respect to those at Neuadd, UK (Fernández-Jalvo et al., 2010)) and the lack of further evidence relating these features to a specific diagenetic agent increase the complexity in modelling bone diagenesis due to Wedl MFD. Nevertheless, occurrence of Wedl MFD foci in all burial phases indicates a weak dependence from environmental condition changes.

Ion mobilisation and precipitation of secondary mineral phases require groundwater circulating in the soil and, hence, through the bones (Trueman et al., 2004). Manganese oxides were detected only in pre-Mesolithic and Mesolithic bones indicating that this secondary phase precipitated during the most humid period encountered in the span period considered in this research, when seasonal swamps, fed by higher flood of the White Nile, were active. Water saturation in waterlogged soil under anoxic conditions possibly promoted the Mn(II) mobilisation. Bodies were likely buried in a humid soil in an oxic–anoxic transition zone, depending on the water table level, where Mn oxidation and precipitation in bone microstructure occurred, possibly favoured by microbial activity (Tebo et al., 2005).

Subsequently, environmental changes lead to secondary calcite precipitation: high evaporation rates at the water table level occurring during short dry periods, punctuating the early and middle Holocene, formed pedologic horizons rich in calcium carbonate concretions. Alternation of wet and dry periods leads to a series of subsequent events of calcite dissolution and precipitation, resulting in a long-lasting process of calcium carbonate accumulation in the soil and, therefore, in bones.

6. Conclusions

Analysis of diagenetic alterations of four burial phases from the same archaeological site, covering a wide span of time from the early Holocene to the beginning of the I millennium AD, proved that environmental and climatic conditions strongly influence bone diagenesis.

High variability in terms of occurrence and extent of diagenetic alterations was observed in samples belonging to the same burial phase; nevertheless, results obtained for bones belonging to the same individual show a good agreement. Hence bone diagenesis is dependent both on the regional environmental and on the local burial conditions.

Diagenetic alterations of bones belonging to the Mesolithic burial phase are more similar to those observed for the pre-Mesolithic one than for the Neolithic phase. This may confirm the correct identification of a fourth burial phase, possibly older than the Neolithic phase.

Results obtained from μ-CT and SEM analysis provide valuable information on bone preservation at the micro-scale.

Acknowledgements

We are grateful to Sandro Salvatori, co-director of "El Salha Archaeological Project" for the precious collaboration. We would like to thank Tina Jakob for her help for bone sampling and Ina Reiche for her useful advice. We thank the "National Corporation for Antiquities and

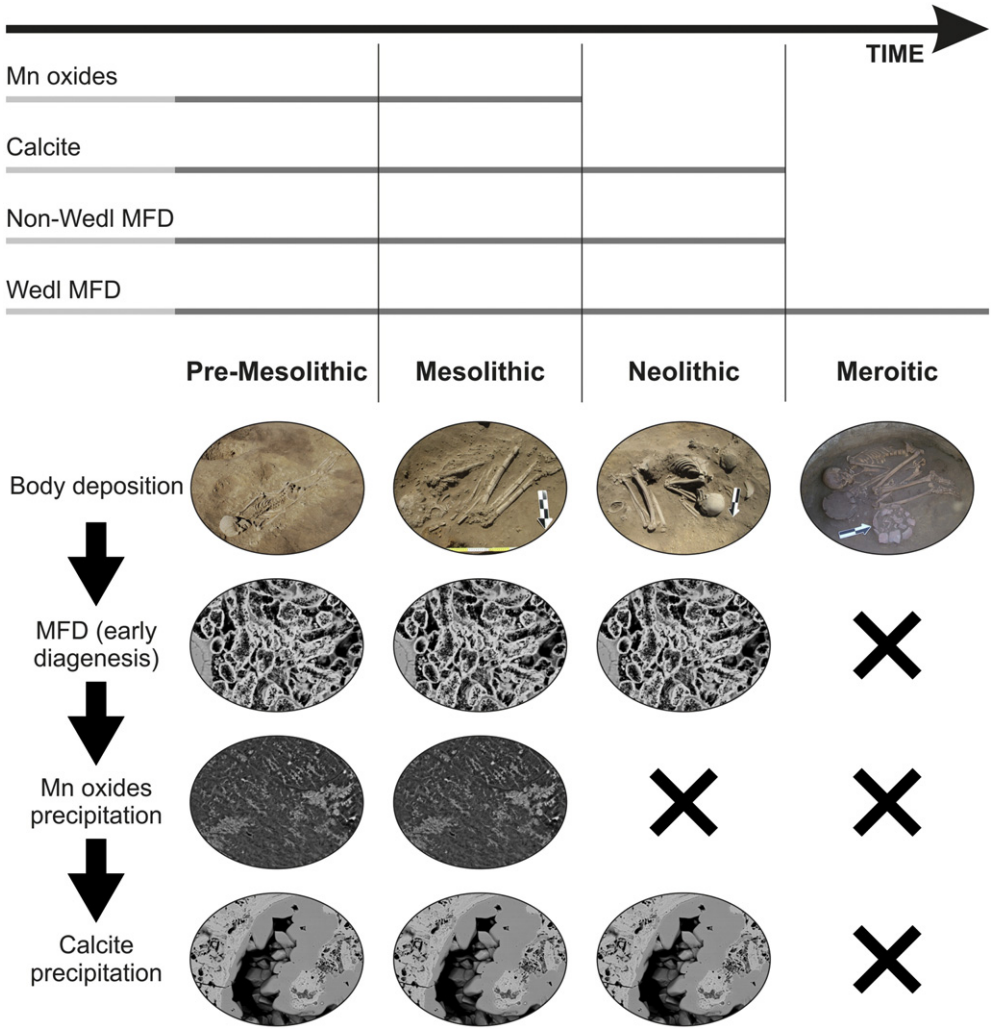

Fig. 12. Summary sketch of alterations occurrence and diagenetic sequence of events among burial phases.

Museums", Khartoum (Sudan), in particular the General Director Abdelrahman Ali Mohamed, for authorising the study of archaeological bones; "Ministero degli Affari Esteri" (MAE) of the Italian Government and "Centro Studi Sudanesi e sub-Sahariani" (CSSeS) for funding the archaeological research. We would also like to thank two anonymous reviewers for their critical reading and suggestions, which considerably improved the manuscript, and Antoine Zazzo and Vincent Balter for the efficient editorial handling.

Appendix A. Supplementary data

Supplementary data associated with this article can be found in the online version, at http://dx.doi.org/10.1016/j.palaeo.2014.06.034. These data include Google map of the most important areas described in this article.

References

Bell, L.S., 1990. Palaeopathology and diagenesis; an SEM evaluation of structural changes using backscattered electron imaging. J. Archaeol. Sci. 17, 85–102.
Bronk Ramsey, C., 2009. Dealing with outliers and offsets in radiocarbon dating. Radiocarbon 51, 1023–1045.
Child, A.M., 1995. Towards an understanding of the microbial decomposition of archaeological bone in the burial environment. J. Archaeol. Sci. 22, 165–174.
Cremaschi, M., Salvatori, S., Usai, D., Zerboni, A., 2007. A further tessera to the huge mosaic: studying the ancient settlement pattern of the El Salha region (south-west of Omdurman, Central Sudan). In: Kroeper, K., Chlodnicki, M., Kobusiewicz, M. (Eds.), Archaeology of the Earliest North-eastern Africa. Poznan Archaeological Museum, pp. 39–48.
Fernández-Jalvo, Y., Andrews, P., Pesquero, D., Smith, C., Marín-Monfort, D., Sánchez, B., Geigl, E., Alonso, A., 2010. Early bone diagenesis in temperate environments Part I: surface features and histology. Palaeogeogr. Palaeoclimatol. Palaeoecol. 288, 62–81.
Gasse, F., 2000. Hydrological changes in the African tropics since the Last Glacial Maximum. Quatern. Sci. Rev. 19, 189–211.
Hackett, C.J., 1981. Microscopical focal destruction (tunnels) in excavated human bones. Med. Sci. Law 21, 243–265.
Hedges, R.E.M., Millard, A.R., Pike, A.W.G., 1995. Measurements and relationships of diagenetic alteration of bone from three archaeological sites. J. Archaeol. Sci. 22, 201–209.
Hedges, R.E.M., 2002. Bone diagenesis: an overview of the processes. Archaeometry 44 (3), 319–328.
Jans, M.M.E., Kars, H., Nielsen-Marsh, C.M., Smith, C.I., Nord, A.G., Arthur, P., Earl, N., 2002. In situ preservation of archaeological bone: a histological study within multidisciplinary approach. Archaeometry 44 (3), 343–352.
Jans, M.M.E., Nielsen-Marsh, C.M., Smith, C.I., Collins, M.J., Kars, H., 2004. Characterisation of microbial attack on archaeological bone. J. Archaeol. Sci. 31, 87–95.
Julien, C.M., Massot, M., Poinsignon, C., 2004. Lattice vibrations of manganese oxides. Part I. Periodic structures. Spectrochim. Acta A 60, 689–700.
Macklin, M.G., Woodward, J.C., Welsby, D.A., Duller, G.A.T., Williams, F.M., Williams, M.A.J., 2013. Reach-scale river dynamics moderate the impact of rapid Holocene climate change on floodwater farming in the desert Nile. Geology 41, 695–698.
Müller, K., Chadefaux, C., Thomas, N., Reiche, I., 2011. Microbial attack of archaeological bones versus high concentrations of heavy metals in the burial environment. A case study of animal bones from a mediaeval copper workshop in Paris. Palaeogeogr. Palaeoclimatol. Palaeoecol. 310, 39–51.

Nicoll, K., 2004. Recent environmental changes and prehistoric human activity in Egypt and Northern Sudan. Quatern. Sci. Rev. 23, 564–580.
Nielsen-Marsh, C.M., Hedges, R.E.M., 2000. Patterns of diagenesis in bone I: the effects of site environments. J. Archaeol. Sci. 27, 1139–1150.
Pitre, M.C., Correia, P.M., Mankowski, P.J., Klassen, J., Day, M.J., Lovell, N.C., Currah, R., 2013. J. Archaeol. Sci. 40, 24–29.
Potter, M.R., Rossman, G.R., 1979. Mineralogy of manganese dendrites and coatings. Am. Mineral. 64, 1219–1226.
Reiche, I., Favre-Quattropani, L., Vignaud, C., Bocherens, H., Charlet, L., Menu, M., 2003. A multi-analytical study of bone diagenesis: the Neolithic site of Bercy (Paris, France). Meas. Sci. Technol. 14, 1608–1619.
Reimer, P.J., Bard, E., Bayliss, A., Beck, J.W., Blackwell, P.G., Bronk Ramsey, C., Buck, C.E., Cheng, H., Edwards, R.L., Friedrich, M., Grootes, P.M., Guilderson, T.M., Haflidason, H., Hajdas, I., Hatté, C., Heaton, T.J., Hoffmann, D.L., Hogg, A.G., Hughen, K.A., Kaiser, K.F., Kromer, B., Manning, S.W., Niu, M., Reimer, R.W., Richards, D.A., Scott, E.M., Southon, J.R., Staff, R.A., Turney, C.S.M., Van der Plicht, J., 2013. IntCal13 and Marine13 Radiocarbon Age Calibration Curves 0–50,000 Years Cal. BP. Radiocarbon 55, 1869–1887.
Salvatori, S., Usai, D., 2009. El Salha project 2005: New Khartoum Mesolithic sites from central Sudan. Kush 19, 87–96.
Salvatori, S., Usai, D., Zerboni, A., 2011. Mesolithic site formation and palaeoenvironment along the White Nile (Central Sudan). Afr. Archaeol. Rev. 28, 177–211.
Salvatori, S., 2012. Disclosing archaeological complexity of the Khartoum Mesolithic. New data at the site and regional level. Afr. Archaeol. Rev. 29, 399–472.
Salvo, L., Cloetens, P., Maire, E., Zabler, S., Blandin, J.J., Buffière, J.Y., Josserond, C., 2003. X-ray micro-tomography an attractive characterisation technique in materials science. Nucl. Instrum. Methods Phys. Res., Sect. B 200, 273–286.
Smith, C.I., Nielsen-Marsh, C.M., Jans, M.M.E., Collins, M.J., 2007. Bone diagenesis in the European Holocene I: patterns and mechanisms. J. Archaeol. Sci. 34, 1485–1493.
Tebo, B.M., Johnson, H.A., McCarthy, J.K., Templeton, A.S., 2005. Geomicrobiology of manganese(II) oxidation. Trends Microbiol. 13 (9), 421–428.
Trueman, C.N.G., Behrensmeyer, A.K., Tuross, N., Weiner, S., 2004. Mineralogical and compositional changes in bones exposed on soil surface in Amboseli National Park, Kenya: diagenetic mechanisms and the role of sediment pore fluids. J. Archaeol. Sci. 31, 721–739.
Turner-Walker, G., Syversen, U., 2002. Quantifying histological changes in archaeological bones using BSE-SEM image analysis. Archaeometry 44 (3), 461–468.
Usai, D., Salvatori, S., 2005. The IsIAO archaeological project in the El Salha area (Omdurman South, Sudan): results and perspectives. Africa 60 (3–4), 474–493.
Usai, D., Salvatori, S., 2007. The oldest representation of a Nile boat. Antiquity 81, 314.
Usai, D., Salvatori, S., Iacumin, P., Di Matteo, A., Jakob, T., Zerboni, A., 2010. Excavating a unique pre-Mesolithic cemetery in Central Sudan. Antiquity 84, 323.
Weiner, S., Traub, W., 1992. Bone structure: from Angstroms to microns. FASEB J. 6, 879–885.
Weiner, S., Wagner, H.D., 1998. The material bone: structure–mechanical function relations. Annu. Rev. Mater. Sci. 28, 271–298.
Williams, M.A.J., Adamson, D., 1980. Late Quaternary depositional history of the Blue and White Nile rivers in central Sudan. In: Williams, M.A.J., Faure, H. (Eds.), The Sahara and the Nile: Quaternary Environments and Prehistoric Occupation in Northern Africa. Balkema, Rotterdam, pp. 281–304.
Williams, M.A.J., 2009. Late Pleistocene and Holocene environments in the Nile basin. Glob. Planet. Chang. 69, 1–15.
Williams, M.A.J., Jacobsen, G.E., 2011. A wetter climate in the desert of northern Sudan 9900–7600 years ago. SAHARA 22, 7–14.
Zerboni, A., 2011. Micromorphology reveals in situ Mesolithic living floors and archaeological features in multiphase sites in Central Sudan. Geoarchaeology 26, 365–391.
Zerboni, A., 2013. Early Holocene palaeoclimate in North Africa: an overview. In: Shirai, N. (Ed.), Neolithisation of Northeastern Africa. Studies in Early Near Eastern Production, Subsistence, and Environment, Berlin, Ex Oriente, 16, pp. 65–82.

CHAPTER 2

Variability of bone diagenesis among multiple burial phases at Al Khiday (Khartoum, Sudan): a FTIR spectroscopic study in attenuated total reflection mode

1. Introduction

Human bones are frequently found within archaeological records and are studied at different levels, as valuable information for anthropological, cultural and palaeoenvironmental studies can be retrieved. Bone is a composite material with a complex structure described in terms of hierarchical levels of organization (Weiner and Wagner, 1998), constituted by the association of an organic matrix (mainly type-I collagen) and a mineral phase. The latter, is constituted by nanocrystals of bioapatite, with a composition resembling that of hydroxyapatite ($Ca_{10}(PO_4)_6(OH)_2$) but considerably departing from stoichiometry, as a number of elements enter the structure in minor and trace quantity and ionic substitutions occur (LeGeros, 1981; Elliot, 2002, Gómez-Morales, 2013). When buried, bones undergo several taphonomic and diagenetic processes, mainly influenced by environmental and local burial conditions, leading to the alteration of both the organic and mineral constituents at different extent. Collagen deterioration, microbiological alteration, ions depletion or uptake and secondary mineral phases deposition can occur (Hedges, 2002; Nielsen-Marsh and Hedges, 2000; Smith et al., 2007; Lee-Thorp, 2008; Sponheimer and Lee-Thorp, 1999; Weiner, 2010). The study of bone diagenesis for a specific site has therefore the double purpose to i) understand how, by which way and at which extent these processes have altered archaeological bones and ii) contribute to assess the reliability of retrieved information with respect to the in vivo composition or isotopic signature of bone.

This research investigates the diagenetic alteration of human bones from the archaeological site 16D4 at Al Khiday (Khartoum, Sudan), where a multi-stratified cemetery was excavated, revealing four different burial phases, covering a wide span of time, from the pre-Mesolithic to the Meroitic (Usai et al., 2010; Dal Sasso et al., 2014-a), namely from the early Holocene to the early 1st millennium AD. Since, profound climatic changes occurred during the Holocene in North Africa, from humid environment towards drier conditions more similar to the current arid climate of the Sub-Saharan belt, this case study investigates a set of bone samples that have been buried in the same site but at different periods, thus experiencing different environmental conditions. Moreover, since all burial phases share the similar ritual practise of burying the dead in pits, presumably shortly or even immediately after death, diagenetic alterations are assumed to be due to environmental and local burial conditions. In order to characterise the preservation state of these bones, a Fourier transform infrared spectroscopy (FTIR) study have been carried out. This

analytical approach is widely used in the study of bone diagenesis, as it requires a low amount of material (1 mg), and is sensitive in investigating both mineral and organic phases, with fast and nearly inexpensive analytical procedure, which enables one to investigate a large set of samples. Spectrum obtained from FTIR shows which fraction of the incident infrared radiation is absorbed by the sample at a particular wavelength, thus providing information on molecular bonds and their chemical environment. Qualitative and semi-quantitative analyses can be performed in order to investigate the nature as well as the atomic order/disorder of mineral and organic matter in analysed samples. Therefore, FTIR spectroscopy can provide valuable information on the preservation state as well as structural and chemical properties of archaeological bones (Lebon et al., 2010; Salesse et al., 2014; Weiner and Bar-Yosef,, 1990). Several analytical techniques coupled with FTIR spectroscopy are currently applied in material characterisation, requiring different sample preparation methods. While the traditional transmission FTIR mode, performed on pellets prepared with potassium bromide (KBr) is extensively used to study bone material, only recently Attenuated Total Reflection FTIR (ATR-FTIR) mode have been applied to investigate bone diagenesis (Beasley at al. 2014; Lebon et al. 2014; Hollund et al. 2012). The main advantage of measurement in ATR-FTIR with respect to transmission mode is the minimal sample preparation required, implying faster analysis and reducing the influence of sample preparation on the measurements. In fact, the use of different protocols to prepare KBr pellets and even the same preparation procedure performed by different operators can induce at least minimal differences in FTIR spectrum, which however heavily affect the determination of diagenetic parameters calculated on the basis of peak intensity ratio (Asscher et al., 2011a; 2011b; Surovell and Stiner, 2001). Moreover, KBr is hygroscopic, thus an accurate, and time consuming, sample preparation is required in order to reduce at minimum the effect of atmospheric moisture on the acquired spectra; conversely, ATR-FTIR is still sensitive to environmental humidity but its effect is more easily removed.

Taking into consideration all these aspects, this study aims to evaluate the preservation state of the archaeological bones found at Al Khiday by applying ATR-FTIR spectroscopy, and to correlate results with climatic and environmental conditions during burial. But, since FTIR spectroscopy in transmission mode is much more frequently applied to bone diagenesis study, a subset of samples were also analysed by FTIR spectroscopy and results compared with those obtained by ATR-FTIR spectroscopy, with the double aim to verify the reliability of results themselves and to monitor eventual systematic variations due to the different analytical techniques.

2. FTIR spectroscopy of bone

When analysing bone material, major absorption bands of the organic matrix are located in the region from 1700 to1300 cm^{-1}, where two peaks, at 1660 and 1550 cm^{-1} corresponding to the amide I and amide II vibrational bands, respectively, can be detected. Bioapatite shows several absorption bands relative to carbonate and phosphate groups. Among ionic substitutions in bioapatite crystal structure, carbonate substitution is the most significant (4-7 wt.%) and it is easily detectable by FTIR measurements. Carbonate ions occur in the A and B crystallographic sites, substituting hydroxyl ions and phosphate ions, respectively, and are thought to stabilize the surface of apatite nanocrystals. The presence of ionic substitutions in the bioapatite structure influence the long-range atomic order of crystals and therefore it play a major role in determining physical and chemical properties of bone mineral, such as solubility and crystal size (Wopenka and Pasteris, 2005; LeGeros, 1981). Carbonate ion presence in bioapatite lead to the $\nu_2(CO_3)$ and $\nu_3(CO_3)$ vibrational modes, detected in the IR spectrum in the range from 890 to 840 cm^{-1} and from 1600 to 1300 cm^{-1}, respectively (Fig. 1). A further distinction can be made between vibrational bands due to carbonate ions occupying the A or B crystallographic site: it is almost accepted the attribution of the $\nu_3(CO_3)$ vibrational modes at ~1465 and ~1542 $cm^{-1}$for A-type carbonate and at ~1462 and ~1415 cm^{-1} for B-type carbonate, as well as the $\nu_2(CO_3)$ at ~880 cm^{-1} for A-type carbonate and at ~872 cm^{-1} for B-type carbonate (Rey et al., 2011). The possible presence of secondary calcite, frequently detected in archaeological bones as the result of secondary mineral phases precipitation in bone micro-porosity during diagenesis, can be monitored. In fact, while $\nu_2(CO_3)$ and $\nu_3(CO_3)$ vibrational modes overlap with those of carbonate ions in the bioapatite crystal structure, $\nu_4(CO_3)$ at 712 $cm^{-1}$is characteristic for calcite. As for phosphates functional group, the strongest absorption bands corresponds to $\nu_3(PO_4)$ and $\nu_4(PO_4)$ vibrational modes and range from 1200 to 900 cm^{-1} and from 700 to 500 cm^{-1}, respectively; weaker bands, corresponding to $\nu_1(PO_4)$ and $\nu_2(PO_4)$ are at 962 cm^{-1} and 472 cm^{-1}, respectively (Rey et al, 2011) (Fig. 1). The $\nu_4(PO_4)$ vibrational mode shows two bands at ~604 and ~565 cm^{-1} (and a shoulder at ~575 cm^{-1}), whose separation is correlated to atomic disorder and/or crystal size of bioapatite. Weiner and Bar-Yosef (1990) defined a crystallinity parameter, named infrared splitting factor (IRSF), calculated as the sum of peak intensities at 604 and 565 cm^{-1} divided by the intensity of the valley between them, thus quantifying the splitting extent of the two peaks. Therefore, FTIR spectroscopy can provide simultaneous information on collagen preservation, carbonate content, and crystallinity of the bone mineral fraction. So, this method will enable us to monitor these parameters thought the multiple burial phases at Al Khiday along the almost entire Holocene.

3. Materials and Methods

3.1 Archaeological samples

The archaeological site 16D4 (or Al Khiday 2) is located in central Sudan near Khartoum, on the western bank of the White Nile, at 3.5 Km from the river course and 22 Km south from the confluence with the Blue Nile. Extensive archaeological excavation (Usai and Salvatori, 2005; Usai and Salvatori, 2007; Salvatori and Usai, 2009; Salvatori et al 2011; Zerboni, 2011) , carried out within the "El Salha archaeological project" since 2005, brought to light 190 graves belonging to at least three different burial phases: pre-Mesolithic, Neolithic and Meroitic (Usai et al., 2010; Dal Sasso et al., 2014-a). From the early Holocene onwards the same area have been used as a burial ground several times. The pre-Mesolithic phase (90 graves excavated so far) is chronologically constrained by the Mesolithic use of the site, whose features, cutting in some cases the older burials, dates to 6700-6300 cal. years BC, providing a terminus ante quem for this burial phase (Salvatori et al., 2011; Salvatori, 2012; Usai et al., 2010). The site was subsequently used as a cemetery during the Neolithic period (38 graves; 4550-4250 cal years BC) and later on during the Meroitic period (43 graves, between the 1st century BC and the 2nd century AD) (Usai et al., 2010). The Chronology of the burial phases was assessed on the basis of radiocarbon ages obtained on archaeological materials and soils sediments stratigraphically related to the graves (Usai et al., 2010; Salvatori et al., 2011). A possible fourth burial phase (19 graves) was identified on the basis of both archaeological evidences and the macroscopic bone preservation state (Usai et al., 2010), coupled with histological analysis (Dal Sasso et al., 2014-a). However, the lack of grave goods and uncertainties on the relationship between graves and the archaeological stratigraphy make this burial phase of uncertain chronological attribution and was tentatively labelled as Mesolithic. 12 pre-Mesolithic, 5 Mesolithic, 5 Neolithic and 6 Meroitic graves were selected as representative of the four burial phases. From each grave a femur (F) and a humerus (H) were sampled, hence a total number of 56 bone samples were here analysed by ATR-FTIR spectroscopy (Tab. 1).

3.2 Standard samples for calibration curves

Significant variations among the burial phases, in terms of diagenetic alteration, were observed at the micro-scale level and secondary calcite was detected in pre-Mesolithic, Mesolithic and Neolithic bone samples (Dal Sasso et al., 2014-a). The $\nu_2(CO_3)$ and $\nu_3(CO_3)$ vibrational bands of calcite overlap to those of structural carbonate of bioapatite, thus affecting the assessment of the preservation state of bioapatite by monitoring its carbonate content. Therefore, in order to remove the contribution of calcite to the $\nu_2(CO_3)$ and $\nu_3(CO_3)$ vibrational bands of spectra and retrieve that of structural carbonate of bioapatite, the following method has been developed. A set of 8 standard

samples were prepared by adding 1, 1.5, 2, 2.5, 5, 10, 15 and 20 wt.% of calcium carbonate (Merck) to a deproteinated modern ox bone. In this case, as archaeological bones are totally deprived of collagen (Usai et al., 2010), deproteinated bone was used as reference material. On the basis of results obtained by FTIR measurements, calibration curves were established in order to quantify secondary calcite in archaeological bones and decouple the overlapped contribution to the $\nu_2(CO_3)$ and $\nu_3(CO_3)$ vibrational modes, generated by carbonate groups contained in calcite and in bioapatite.

3.3 FTIR preparation and measurement

Sample preparation for ATR-FTIR measurement was minimal; the external surface of archaeological bone samples (which weight ranges from 100 to 200 mg each), encrusted by soil sediments, was mechanically removed by means of low-speed micro-drill equipped with an abrasive point. Attention was paid in order to avoid over-heating of samples during mechanical cleaning process. Then, samples were finely hand-ground in an agate mortar for about one minute in order to homogenize composition.

In order to reduce at minimum the variability on FTIR measurements using KBr pellet technique induced during sample preparation, the following protocol has been applied for all samples: 2.5 mg of bone powder were dispersed in acetone and further ground for 30 min with an agate ball micro-mill, then samples were homogenised with 300 mg of KBr in an agate mortar for 1 min. Transparent pellets (diameter of 12 mm) were created by means of a vacuum hydraulic press, under 11 tons/cm^2 pressure for 2.5 min. Pellets were then placed in oven at 110 °C overnight before measurement.

Spectra, both in ATR-FTIR and transmission modes, were collected with a Bruker Vector 22 spectrometer, equipped with a Specac Standard Golden Gate ATR accessory for ATR-FTIR measurements; 64 scans for each spectrum were acquired, in the range from 4000 to 400 cm^{-1}, with a spectral resolution of 2 cm^{-1}. Background was acquired subtracted from the spectra. Spectral analysis was performed using Omnic 9 software (Thermo Scientific). Measurements were performed at the Département de Préhistoire du Muséum national d'Histoire naturelle (Paris, France).

The following parameters were calculated for each spectrum:

- parameter correlated to the carbonate content of bioapatite (**CO_3/PO_4**): calculated dividing the intensity of the band at 1415 cm^{-1} ($\nu_3(CO_3)$ vibrational mode of B-type carbonate) by the peak

intensity at 1035 cm^{-1}assigned to the $\nu_3(PO_4)$ vibrational mode (Rink and Schwarcz, 1995 ; Grunenwald et al., 2014); since B-type carbonate is much more abundant than type-A, CO_3/PO_4 parameter calculated here is assumed to produce reliable results in monitoring the carbonate concentration in bioapatite (LeGeros, 1981; Sponheimer and Lee-Thorp, 1999; Wopenka and Pasteris, 2005);

- the amount of secondary calcite precipitated during diagenesis (**Cal/PO_4**): calculated dividing the peak intensity at 712 cm^{-1}($\nu_4(CO_3)$ vibrational mode characteristic for calcite) by the peak intensity at 1035 $cm^{-1}$of phosphate.;
- infrared splitting factor (**IRSF**): calculated summing the peak intensities of peak at 604 and 565 cm^{-1} and dividing by the intensity of the valley between them (Weiner and Bar-Yosef, 1990); it represents the crystallinity of bioapatite;
- collagen content parameter (**Amide I /PO_4**): calculated dividing the peak intensity of the Amide I band at 1660 cm^{-1} by the peak intensity of the phosphate band at 1035 cm^{-1}; this parameter was determined in order to check the actual collagen degradation.

The baseline used to calculate band intensities was defined by two points calculated as the local minimum in the region 2000-1800 and 1400-1200 cm^{-1} for the 1660 and 1415 cm^{-1} band, 1400-1200 and 900-750 cm^{-1} for the 1035cm^{-1} band, 660-620 and 510-470 cm^{-1} for the IRSF; the baseline used for the 712 cm^{-1} band is defined between 730 and 700 cm^{-1}. For clarity peak positions and baselines are reported in the following table.

Vibrational mode	Maximum peak position (cm^{-1})	Baseline (cm^{-1})
Amide I	1660	2000/1800 - 1400/1200
$\nu_3(CO_3)$	1415	2000/1800 - 1400/1201
$\nu_3(PO_4)$	1035	1400/1200 - 900-750
$\nu_4(CO_3)$	712	730-700
$\nu_4(PO_4)$	604	660/620 - 510/470
	565	660/620 - 510/471

4. Results

4.1 Calibration curves

Results obtained from ATR-FTIR on the 8 standard samples show that the detection limit for calcite in bone-calcite mixture is 2.5 wt.%: the 712 cm^{-1} band was not detected when analysing samples containing 1, 1.5 and 2 wt.% of calcite. Therefore, calibration curves were established considering just the results obtained from samples with 2.5, 5, 10, 15 and 20 wt.% of calcite. For each spectrum

CO_3/PO_4, Cal/PO_4 and IRSF was calculated. Fig. 2a displays an excellent relationship between Cal/PO_4 and calcite wt.% and, by linear regression, the following linear correlation function was determined:

$$[Cal/PO_4] = 0.0017[\text{calcite wt.\%}] - 0.0020 \quad (1)$$

This equation can be used to calculate the secondary calcite content in archaeological samples:

$$[\text{calcite wt.\%}] = ([Cal/PO_4] + 0.0020) / 0.0017 \quad (2)$$

As calcite $v_3(CO_3)$ vibration band is at almost the same position that $v_3(CO_3)$ of bone carbonate apatite, CO_3/PO_4 is affected by the presence of calcite in sample. A linear relationship can be observed between CO_3/PO_4 and Cal/PO_4 (Fig. 2b), and described by the function:

$$[CO_3/PO_4] = 3.5541[Cal/PO_4] + 0.2114 \quad (3)$$

This linear function shows that the slope is determined by the calcite content in the mixture and the intercept corresponds to the contribution of the sole carbonate contained in deproteinated bone sample. Therefore, this calibration curve can be used to obtain a correction (named CO_3/PO_4-corr) for the CO_3/PO_4 parameter, when secondary calcite is detected, using the function

$$[CO_3/PO_4\text{-corr}] = [CO_3/PO_4] - 3.5541[Cal/PO_4] \quad (4)$$

subtracting the contribution of calcite to the 1415 cm^{-1} band by calculating the intercept of this function, once measured CO_3/PO_4 and Cal/P. Equivalent calibration curves were obtained from measurement of the same samples by transmission FTIR (Fig. 2c and Fig. 2d, respectively) and linear functions were similarly obtained by linear regression:

$$[\text{calcite wt.\%}] = ([Cal/PO_4] + 0.0024) / 0.0016 \quad (5)$$

$$[CO_3/PO_4\text{-corr}] = [CO_3/PO_4] - 16.347[Cal/PO_4] \quad (6)$$

4.2 ATR-FTIR spectroscopy on archaeological samples

ATR-FTIR spectra do not show any appreciable band related to the organic fraction of bones, in particular band at ~1660 and ~1550 cm^{-1} assigned to Amide I and Amide II respectively (Fig. 1), proving an almost complete collagen loss for all the samples (or at least a collagen content under the detection limit of this technique). Therefore, Amide I /PO_4 values calculated for the four burial phases (Fig. 3a), ranging from 0.01578 to 0.03771 (Tab. 1), does not provide any measurement of the collagen content. This is furthermore proved by the absence of any significant trend among burial phases (Fig. 3a), neither any correlation with IRSF (Fig. 4a) nor CO_3/PO_4-corr (Fig. 4b), as documented also in other study cases, for which collagen was partially preserved (Lebon et al., 2010; Reiche et al., 2010, Lebon et al., 2014). Bioapatite crystallinity, expressed as IRSF, ranges from 4.04 to 5.22, from 4.64 to 5.81, from 4.16 to 5.79 and from 5.37 to 6.22 for pre-Mesolithic, Mesolithic, Neolithic and Meroitic samples, respectively (Fig. 3b) (Tab. 1), showing significant differences pre-Mesolithic samples, which have the lowest IRSF values, and the Meroitic samples, which register the highest values. Neolithic bones are those with a wider IRSF distribution, whereas, interestingly, Mesolithic ones have an average value higher than both the Neolithic and the pre-Mesolithic burials. In any case, the IRSF values of archaeological samples are always higher than those obtained from the modern standard samples, ranging from 3.76 and 4.09.

Calcite to phosphate ratios ranges from 0.00 to 0.04 for pre-Mesolithic, Mesolithic and Neolithic samples (with the exception of one Neolithic sample with Cal/PO_4 of 0.058, corresponding to the extraordinary high calcite content of 37%), while in Meroitic samples the 712 cm^{-1} band characteristic for calcite was not detected and therefore Cal/PO_4 values do not exceed 0.002 (Fig. 3c) (Tab. 1). Calcite content for pre-Mesolithic, Mesolithic and Neolithic samples (Fig. 3d), calculated by means of the calibration curve previously established, ranges from 2.5 to 20 wt.% (with the exception of the already mentioned Neolithic sample and one pre-Mesolithic sample containing 25% of calcite): no significant variations were observed among burial phases. Few samples (7) reported Cal/PO_4 values lower than 0.002, corresponding to a calcite content lower that the detection limit, established at 2.5 wt.% (Tab. 1).

Carbonate to phosphate ratio values ranges from 0.16 to 0.39, from 0.1 to 0.30, from 0.13 to 0.37 and from 0.09 to 0.15 for pre-Mesolithic, Mesolithic, Neolithic and Meroitic samples, respectively (Fig. 3e) (Tab. 1). However, it is worth to remember that this measure is affected by the presence of

secondary calcite in the bones, since the 1415 cm^{-1} band is given by the contribution of the $\nu_3(CO_3)$ vibrational modes of carbonate groups contained in calcite and bioapatite. This effect interests all the bones with the exception of Meroitic ones lacking in secondary calcite. The CO_3/PO_4-corr value was calculated for all those pre-Mesolithic, Mesolithic, Neolithic samples in which calcite was detected, using the function obtained from the formula (4). Conversely, this correction was not applied to the few (7) samples characterized by calcite content lower that 2.5 wt.%, thus not detected, and to Meroitic samples. Corrected carbonate to phosphate ratios (CO_3/PO_4-corr) range from 0.16 to 0.28, from 0.1 to 0.21 and from 0.11 to 0.24 for pre-Mesolithic, Mesolithic, Neolithic samples, respectively (Fig. 3f), being still higher than those obtained for Meroitic bones. Values ranging from 0.2 to 0.24 were obtained for modern standard samples used for the calibration curves.

Carbonate to Phosphate ratio values show a negative correlation with IRSF ($R^2 = 0.765$) (Fig. 5a), which is furthermore improved when CO_3/PO_4-corr is considered instead of CO_3/PO_4 ($R^2 = 0.921$) (Fig. 5b). This good correlation may also indicates that the contribution of calcite, present in few samples but under the detection limit (2.5 wt. %), to the $\nu_3(CO_3)$ can be assumed to be minimal.

Meroitic samples has higher IRSF and lower CO_3/PO_4-corr values with respect to pre-Mesolithic ones, while intermediated values were measured for Mesolithic and Neolithic samples. Modern standard samples show carbonate content comparable to some of the pre-Mesolithic samples, even if IRSF values are lower. A general accordance was observed for the same individual, since CO_3/PO_4-corr and IRSF values for humerus and femur sampled from each grave are very similar, within the accuracy of the measurement (Fig. 6). Only few cases show high intra-skeletal variability of both IRSF and CO_3/PO_4-corr values: the most evident ones are two Neolithic graves (grave 4 and grave 158, Fig. 6c), the variations of which are not systematic with respect of bone type, therefore higher or lower values were observed for femurs as well as for humeri. No correlation was observed between Cal/PO_4 and IRSF(Fig. 9b), nor between Cal/PO_4 and CO_3/PO_4-corr (Fig. 9a).

Standard deviation calculated on repeated measurements for IRSF, Cal/PO_4 and CO_3/PO_4 are 0.13, 0.002 (corresponding to 1 wt.% of calcite) and 0.02 respectively.

4.3 FTIR spectroscopy

All the FTIR spectra collected in transmission mode for the subset of samples do not show the occurrence of collagen related band at 1660 cm^{-1} (Fig. 1). IRSF values ranges between 3.16 and 4.19 for pre-Mesolithic samples, within this range are also Mesolithic and Neolithic IRSF values, while those measured for Meroitic samples ranges from 4.98 to 5.53.

Secondary calcite was detected in pre-Mesolithic, Mesolithic and Neolithic samples; Cal/PO_4 ranges from 0 to 0.033 corresponding to a calcite content ranging from 0 to 22 wt.% (calculated with calibration curve relative to FTIR spectra of the standard samples, function 4).

When considering the correlation of CO_3/PO_4 (ranging from 0.074 to 0.868) and IRSF (Fig. 8a) and the even better correlation between CO_3/PO_4-corr (ranging from 0.074 to 0.333) and IRSF (Fig. 8b), it is interesting to note that the Meroitic samples are characterised by higher IRSF and lower CO_3/PO_4-corr with respect to older burial phases. Modern standard samples show IRSF values ranging from 3.03 to 3.25 and CO_3/PO_4-corr values from 0.18 to 0.24.

5. Discussion

5.1 Comparison between FTIR analytical techniques

Collagen vibrational bands were not detected by any of the two analytical techniques, thus proving the loss of the organic matrix in archaeological samples during burial.

IRSF values calculated from FTIR spectra are always lower than those calculated from ATR-FTIR spectra, and the values obtained from the two method are well linearly correlated ; (R^2 = 0.9) (Fig. 7a). A good accordance between IRSF values can be described, once taking into account a mean overestimation of about 0.9 (ranging in this case from 0.63 to 1.31) for IRSF values calculated from ATR-FTIR spectra. Lower IRSF values measured by FTIR in transmission mode may be due to a minimal peak broadening effect to the addition of KBr to the sample (Hollund et al., 2012).

Also calcite content show a good linear correlation (R^2 = 0.91) when the results of the two methods are compared (Fig. 7b), and a mean overestimation of 1.6 wt.% of calcite for ATR-FTIR measurements is observed with respect to the FTIR ones (differences range from 0 to 5 wt.%).

When considering the correlation between CO_3/PO_4-corr and IRSF obtained from the FTIR spectra (Fig. 8b), despite the lower number of samples, results are comparable with those obtained from ATR-FTIR spectra (Fig. 5b), especially in terms of trend among samples of different burial phases .

As for the calibration curves, Fig. 2a and Fig. 2c, in which the linear correlation between Cal/PO_4 and calcite wt.% is described, can be considered equivalent, since the variation in the calcite wt.% calculated with the two functions, obtained from the linear regression, is lower than the standard deviation of Cal/PO_4 calculated on repeated measurements. Different is the situation for calibration curves referring to the linear correlation between CO_3/PO_4 and Cal/PO_4 (Fig. 2b and 2d): CO_3/PO_4 ranges from 0.25 to 0.74 and from 0.21 to 0.32 for FTIR and ATR-FTIR measurements, respectively, implying a steeper slope for the FTIR calibration curve. This evidence suggests a

higher sensitivity of FTIR analytical techniques to the $\nu_3(CO_3)$ vibrational modes. Nevertheless, since a good accordance of the correlation trends between CO_3/PO_4-corr and IRSF obtained from the two analytical techniques was observed (Fig. 8b), despite systematic variations of single diagenetic parameters, this should not be considered as a discriminating criteria for choosing one analytical technique than another, at least for this type of study. Therefore, these results indicates that ATR-FTIR spectroscopy, applied to bone diagenesis study, provides equivalent information than FTIR spectroscopy, but with the advantages of sample preparation method, as previously noted (see introduction of this study).

5.2 Diagenetic trajectory

The histological and micro-morphological study on these bones, previously carried out by Dal Sasso et al. (2014) with the purpose of investigating the bone diagenesis at the micro-scale level, pointed out the occurrence of alteration patterns due to microbial activity, secondary mineral phases precipitation and dissolution. All these features resulted to be related to local burial and environmental conditions, compatibly with data obtained from archaeological and geomorphological investigations at Al Khiday (Salvatori et al., 2011; Zerboni et al., 2011; Cremaschi et al., 2007) and with the palaeoenvironmental reconstruction at regional level (Gasse, 2000; Nicoll, 2004; Williams, 2009; Williams and Jacobsen, 2011; Zerboni, 2013). Pre-Mesolithic and Mesolithic bones experienced a more humid burial environment with respect to the subsequent burial phases, in accordance with palaeoenvironmental records which indicates higher water availability, due to stronger monsoonal activity, leading to higher flooding level of the White Nile and formation of seasonal swamps in the area. Neolithic graves likely encountered drier environmental conditions with respect to the more ancient burials, as by middle Holocene gradual climatic changes towards drier conditions, characterised by weaker monsoonal activity, and progressive decrease in rainfall and water availability. By the Meroitic period, and later on, more arid climate conditions were established, and consequently bones underwent diagenetic processes typical of arid or semi-arid environment.

Collagen, the preservation of which strictly depends on climatic and burial conditions, particularly temperature and pH of soil solution (Hedges et al. 1995; Collins et al. 2002; Smith et al., 2007), can be lost for chemical hydrolysis, alteration of the mineral fraction of bone and/or microbial degradation (Collins et al., 2002). Chemical hydrolysis is particularly effective when high temperature and extremes pH values occur in the burial environment, alkaline in particular. Microbial activity, detected by characteristic alteration patterns described as non-Wedl microscopic

focal destruction (non-Wedl MFD) by Hackett (1981), determines dissolution and reprecipitation of bioapatite. This process leads to the exposure of collagen to the pore solution and to microbial enzymes with consequent collagen degradation. Collagen exposure to pore fluids can also be accounted when bioapatite recrystallization occurs. In this case study collagen loss was observed for all burial phases. Microbial attack, with the typical non-Wedl MFD, was detected in pre-Mesolithic, Mesolithic and Neolithic bones, while it completely lack in Meroitic ones. Therefore, a combined contribution of both chemical hydrolysis and microbial attack may have been responsible for collagen loss in the bones from Al Khyday. In turn, collagen loss may play a significant role in bioapatite recrystallization, as nanocrystals are in this case exposed to the burial environment, thus more susceptible to alteration (Collins et al., 2002).

Higher IRSF values for archaeological bones with respect to modern ones are usually observed when studying altered bones. Bioapatite nanocrystals tend to recrystallize (presumably with Ostwald ripening process –Ostwald, 1897) into a more thermodynamically stable structure, implying more ordered crystal structure, increased crystal dimensions and therefore a significant reduction of the specific surface area (Nielsen Marsh and Hedges, 2000; Hedges et al., 1995). This diagenetic process can be proved by a good correlation between crystallinity parameter (IRSF) and carbonate content (CO_3/PO_4-corr), as observed in the bones from Al Khiday (Fig. 5b). The higher are IRSF values, the lower carbonate content is. Interesting to note is that, with respect to modern samples, Meroitic bones are the most altered, while the pre-Mesolithic ones show an IRSF - CO_3/PO_4-corr ratio closer to that of unaltered samples. Obviously, we cannot exclude that ionic exchange between bioapatite and the environment occurred during burial, so that IRSF and CO_3/PO_4-corr values similar to the modern ones do not necessarily imply a good preservation of the in vivo composition of bioapatite. These observations suggest that recrystallization process is more affected by burial and environmental conditions rather than the age of the burial. In this case, expecting a degree of recrystallization to be proportional with time, without considering changes in the burial conditions, can be lead to misleading conclusions. Moreover, these results show that the same burial conditions experienced by Meroitic bones differently affected the more ancient burial phases, already altered by several diagenetic processes occurred in the previous millennia. Different local pH conditions in the burial environment may also be responsible of these differences observed among burial phases. As for this case study, Dal Sasso et al. (2014-a) established on the basis of textural relationships between different types of diagenetic alterations, a diachronic sequence of diagenetic events: pre-Mesolithic, Mesolithic and Neolithic burials suffered first of microbial attack, presumably shortly after burial; then secondary calcite precipitation was related to changes of evapotranspiration conditions during the alternation of wet and dry periods, which punctuated the

early and middle Holocene. Therefore, precipitation of secondary calcite, meaning an alkaline burial environment, at a certain point of the diagenetic history of these bones may be responsible for a low recrystallization rate for bioapatite, as proved by Berna et al. (2004). Despite the occurrence of pedologic calcium carbonate rich horizons at Al Khiday site(Zerboni, 2011), the complete absence of secondary calcite in Meroitic bones suggests a limited circulation of water within the sediments after the Neolithic period, in accordance with the drier climate conditions in which bones were buried, and possibly a less alkaline burial environment with respect to that of the previous burial phases, thus determining an increase in the recrystallization rate (Berna et al., 2004) in the Meroitic bones. However, despite these considerations, no correlation is observed between the actual content of secondary calcite determined by Cal/PO_4 and CO_3/PO_4-corr (Fig. 9a) and IRSF (Fig. 9b). Moreover, no appreciable differences in secondary calcite content was observed among pre-Mesolithic, Mesolithic and Neolithic burial phases (Fig. 3d). Therefore, recrystallization process seems to be more influenced by the presence or absence of secondary calcite rather than its amount (Fig. 9b).

On the basis of the distribution of IRSF and CO_3/PO_4-corr values (Fig. 5b), despite being highly variable, pre-Mesolithic and Meroitic samples are well distinguishable in two groups, while Mesolithic and Neolithic samples are spread within intermediate values. When the distribution of these values are considered within each burial phase (Fig. 6), a good accordance of IRSF and CO_3/PO_4-corr values obtained on humerus and femur of the same individual can be observed (with few exceptions, such as Neolithic graves 4 and 158). High variability within a single burial phase may be due to changes in local burial conditions; this may also explain those few cases of high intra-skeletal variability, as particularly localised changes in burial conditions might have occurred.

6. Conclusions

This case study illustrates the effects of diagenetic processes along a wide chronological period covering the almost entire Holocene, and in particular describes the variability of diagenetic alteration of bones due to climate changes. These results obtained from an extensive FTIR spectroscopy investigation suggest that differences in diagenetic alteration observed among burial phases are directly influenced by palaeoenvironmental conditions and by climate changes occurring at regional level. However, variations of local burial conditions may play a significant role in determining the alteration state of bones, thus increasing the alteration variability, in terms of values provided by diagenetic parameters as defined from FTIR spectroscopy, within a single burial phase.

A comparison between results obtained from two different analytical techniques indicates that ATR-FTIR, even if occasionally used for bone diagenetic studies, can be applied in order to produce reliable results, with the advantages of a minimal sample preparation and fast analytical procedure. Moreover, the number of diagenetic parameters that can be obtained from FTIR spectra provides valuable information on chemical and structural alteration of bone material. We therefore encourage the application of ATR-FTIR spectroscopy as a screening method, that can be applied to investigate the variability of diagenetic alteration on a large set of samples, enabling the selection of the better preserved samples potentially suited for subsequent analyses, such as radiocarbon dating.

Table 1. Diagenetic parameters calculated from spectra acquired in ART and transmission modes

ATR-FTIR								
Burial phase	**Grave number**	**Sample**	**IRSF**	**Cal/PO_4**	**CO_3/PO_4**	**Amide I/PO_4**	**calcite%**	**CO_3/PO_4-corr**
pre-Mesolithic	Grave 24	24F	4.284	0.01168	0.25830	0.01918	8.0	0.21679
		24H	4.149	0.01145	0.26856	0.02552	7.9	0.22787
	Grave 55	55F	4.492	0.00581	0.25210	0.02609	4.6	0.23145
		55H	4.161	0.01754	0.30015	0.02140	11.5	0.23781
	Grave 69	69F	4.793	0.02839	0.26194	0.01652	17.9	0.16104
		69H	4.510	0.02709	0.32696	0.01854	17.1	0.23068
	Grave 88	88F	4.063	0.03255	0.39222	0.01615	20.3	0.27653
		88H	4.037	0.02117	0.33864	0.02350	13.6	0.26340
	Grave 132	132F	4.674	0.00297	0.23057	0.02884	2.9	0.22001
		132R	4.247	0.00409	0.24679	0.02362	3.6	0.23225
	Grave 156	156F	4.302	0.00511	0.24712	0.02322	4.2	0.22896
		156H	4.304	0.00476	0.26987	0.02428	4.0	0.25295
	Grave 157	157F	4.273	0.00594	0.28404	0.02570	4.7	0.26293
		157H	4.112	0.01750	0.34382	0.02278	11.5	0.28162
	Grave 160	160F	4.690	0.03825	0.35831	0.01785	23.7	0.22237
		160H	4.735	0.02412	0.27471	0.01759	15.4	0.18899
	Grave 170	170F	5.218	0.00117	0.15836	0.02711		
		170H	5.113	0.00000	0.17849	0.03034		
	Grave 172	172F	4.949	0.01238	0.23936	0.02134	8.5	0.19536
		172H	4.716	0.00367	0.21641	0.02812	3.3	0.20337
	Grave 174	174F	4.742	0.00185	0.20516	0.02694		
		174H	4.859	0.00180	0.18677	0.02698		
	Grave 177	177F	4.625	0.00053	0.21392	0.02699		
		177H	4.413	0.00266	0.22350	0.02578	2.7	0.21405
Mesolithic	Grave 31	31F	5.160	0.02424	0.23286	0.01578	15.4	0.14671
		31H	5.016	0.01418	0.23597	0.02184	9.5	0.18557
	Grave 120	120F	4.898	0.01196	0.21215	0.02147	8.2	0.16964
		120H	5.202	0.00918	0.17903	0.01937	6.6	0.14640
	Grave 128	128F	4.804	0.00817	0.23788	0.02742	6.0	0.20884
		128H	4.914	0.02322	0.29698	0.02280	14.8	0.21445
	Grave 163	163F	5.499	0.00269	0.14203	0.02284	2.8	0.13247
		163H	5.805	0.00262	0.11171	0.01691	2.7	0.10240
	Grave 164	164F	5.673	0.00193	0.11782	0.01865		
		164H	5.554	0.00410	0.12337	0.01646	3.6	0.10880
Neolithic	Grave 3	3F	4.838	0.05784	0.36600	0.02162	35.2	0.16043
		3H	5.133	0.00160	0.15527	0.02233		
	Grave 4	4F	4.367	0.00499	0.26234	0.03369	4.1	0.24461
		4H	5.789	0.00377	0.12529	0.01958	3.4	0.11189
	Grave 103	103F	4.614	0.00633	0.23322	0.03014	4.9	0.21072
		103H	4.508	0.01108	0.25332	0.02675	7.7	0.21394
	Grave 107	107F	5.473	0.00691	0.16830	0.02293	5.2	0.14374
		107H	5.070	0.01973	0.20754	0.01970	12.8	0.13742
	Grave 158	158F	4.160	0.00449	0.24902	0.02737	3.8	0.23306
		158H	5.628	0.00612	0.13639	0.01747	4.8	0.11464
Meroitic	Grave 50	50F	5.639	0.00132	0.12350	0.03404		
		50H	6.134	0.00070	0.09334	0.02535		
	Grave 115	115F	5.711	0.00081	0.10416	0.02673		
		115H	5.562	0.00000	0.11916	0.02819		
	Grave 136	136F	6.220	0.00068	0.08514	0.01850		
		136H	5.632	0.00090	0.11707	0.02247		
	Grave 137	137F	6.125	0.00019	0.09944	0.02262		
		137H	5.368	0.00006	0.15149	0.02966		
	Grave 159	159F	5.667	0.00162	0.14164	0.03771		
		159H	5.592	0.00042	0.13489	0.02917		
	Grave 166	166F	5.759	0.00098	0.09966	0.02456		
		166H	5.671	0.00000	0.12200	0.02583		

FTIR							
Burial phase	**Grave number**	**Sample**	**IRSF**	**Cal/PO_4**	**CO_3/PO_4**	**calcite%**	**CO_3/PO_4-corr**
pre-Mesolithic	Grave 88	88F	3.436	0.03273	0.86814	22.0	0.33310
		88H	3.302	0.01544	0.51612	11.2	0.26372
	Grave 156	156F	3.470	0.00503	0.32354	4.6	0.24131
		156H	3.161	0.00212	0.28791	2.8	0.25325
	Grave 170	170F	3.908	0.00020	0.14066		
		170H	4.186	0.00023	0.14243		
Mesolithic	Grave 128	128F	4.031	0.00472	0.23863	4.5	0.16147
		128H	3.881	0.01400	0.43026	10.3	0.20140
Neolithic	Grave 103	103F	3.482	0.00422	0.29884	4.1	0.22986
		103H	3.505	0.00816	0.35280	6.6	0.21941
Meroitic	Grave 136	136F	5.534	0.00022	0.07440		
		136H	4.979	0.00025	0.09486		

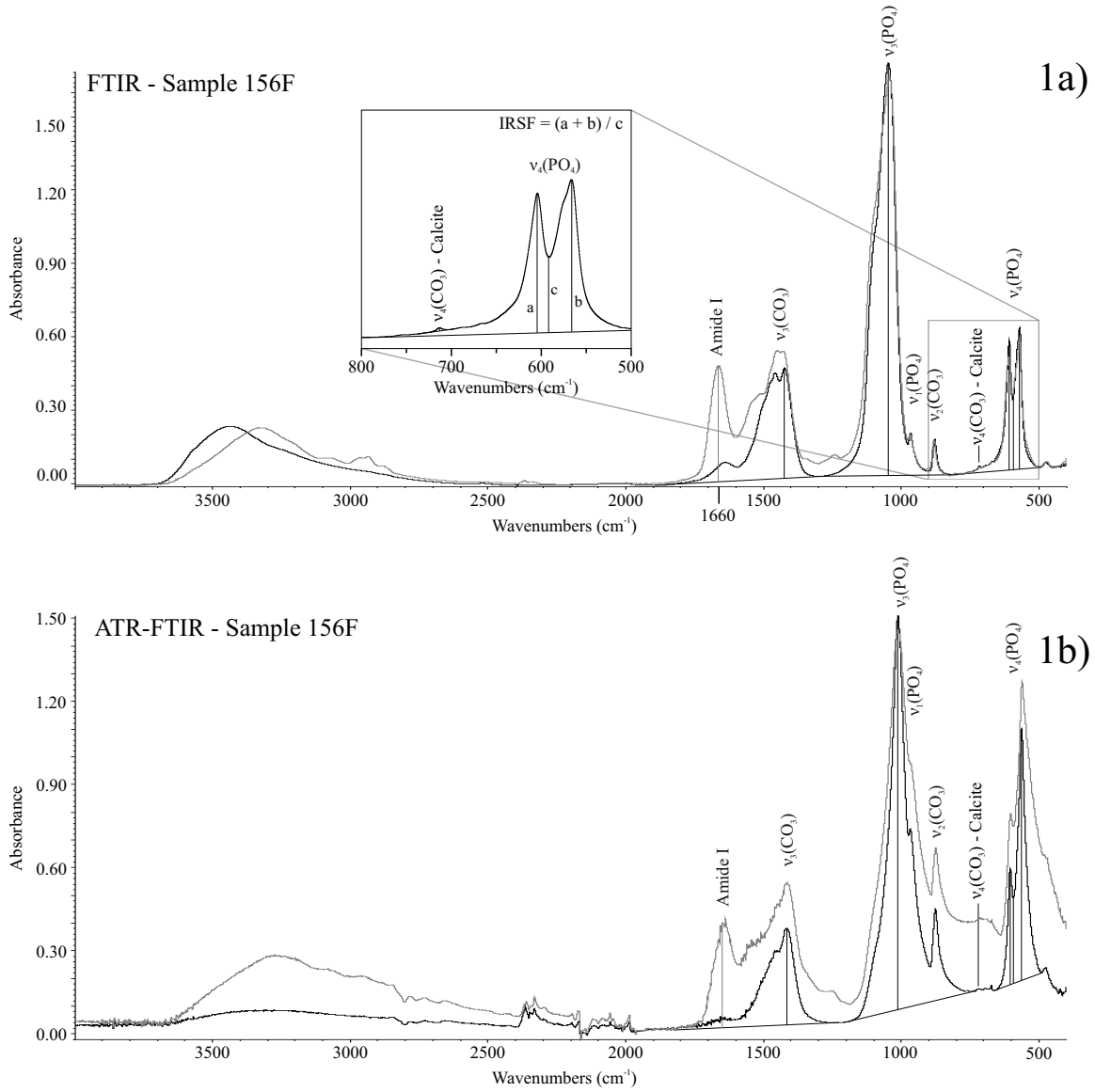

Fig. 1. Examples of FTIR spectra of bone acquired in transmission (a) and ATR (b) modes. Attribution of bands to vibrational modes of phosphate and carbonate groups and amide I is reported. Peak intensities and baseline used to calculate Amide I/PO_4 CO_3/PO_4 Cal/PO_4 and IRSF diagenetic parameters are shown. The spectra of an archaeological (black) bone sample (156F) and a modern (light grey) standard sample (2.5 wt.% of calcite), used for calibration curves, are reported.

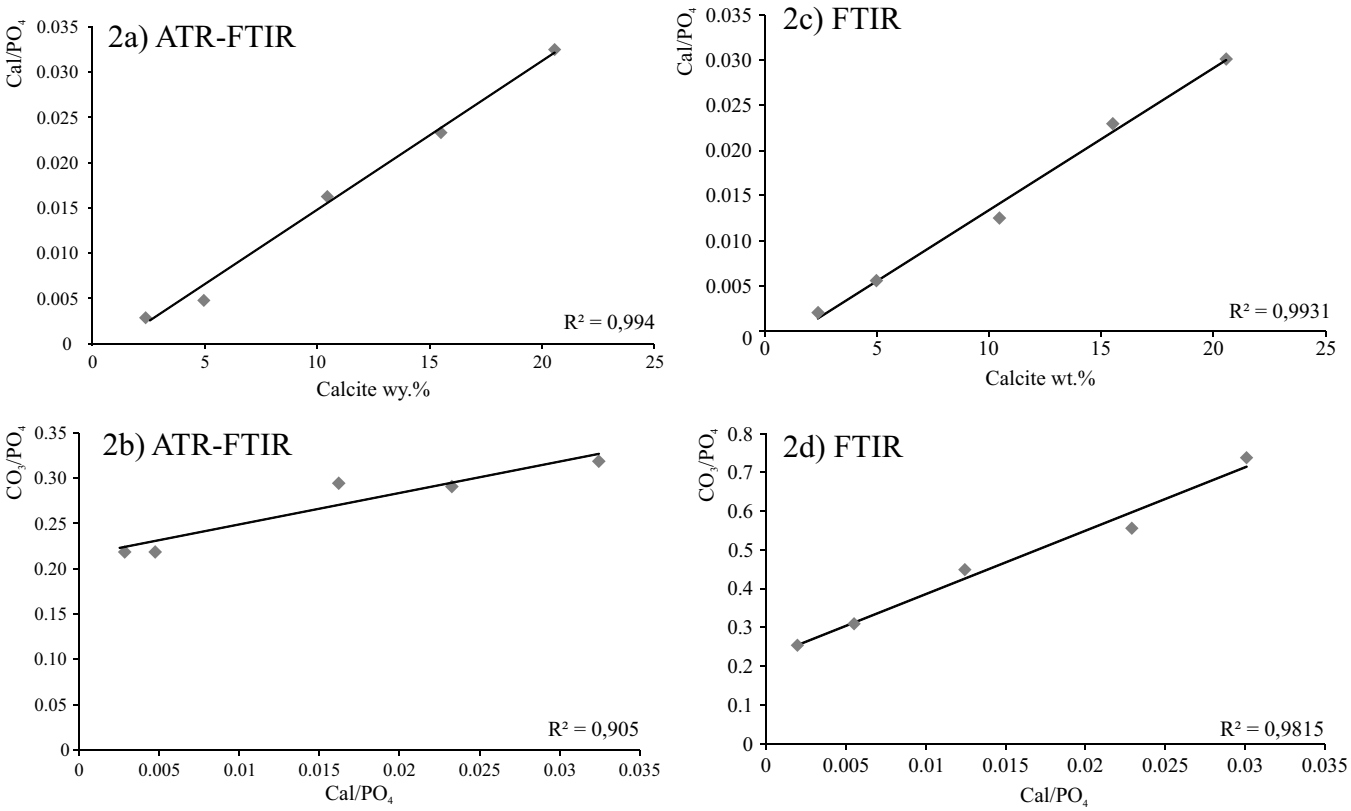

Fig. 2. Calibration curves used to quantify secondary calcite and to correct the CO_3/PO_4 ratio for bone samples containing secondary calcite. 2a. Cal/PO_4 ratio plotted against Calcite wt.% of modern standard samples (ATR-FTIR). 2b. CO_3/PO_4 ratio plotted against Cal/PO_4 of modern standard samples (ATR-FTIR). 2c. Cal/PO_4 ratio plotted against Calcite wt.% of modern standard samples (FTIR). 2b. CO_3/PO_4 ratio plotted against Cal/PO_4 of modern standard samples (FTIR)

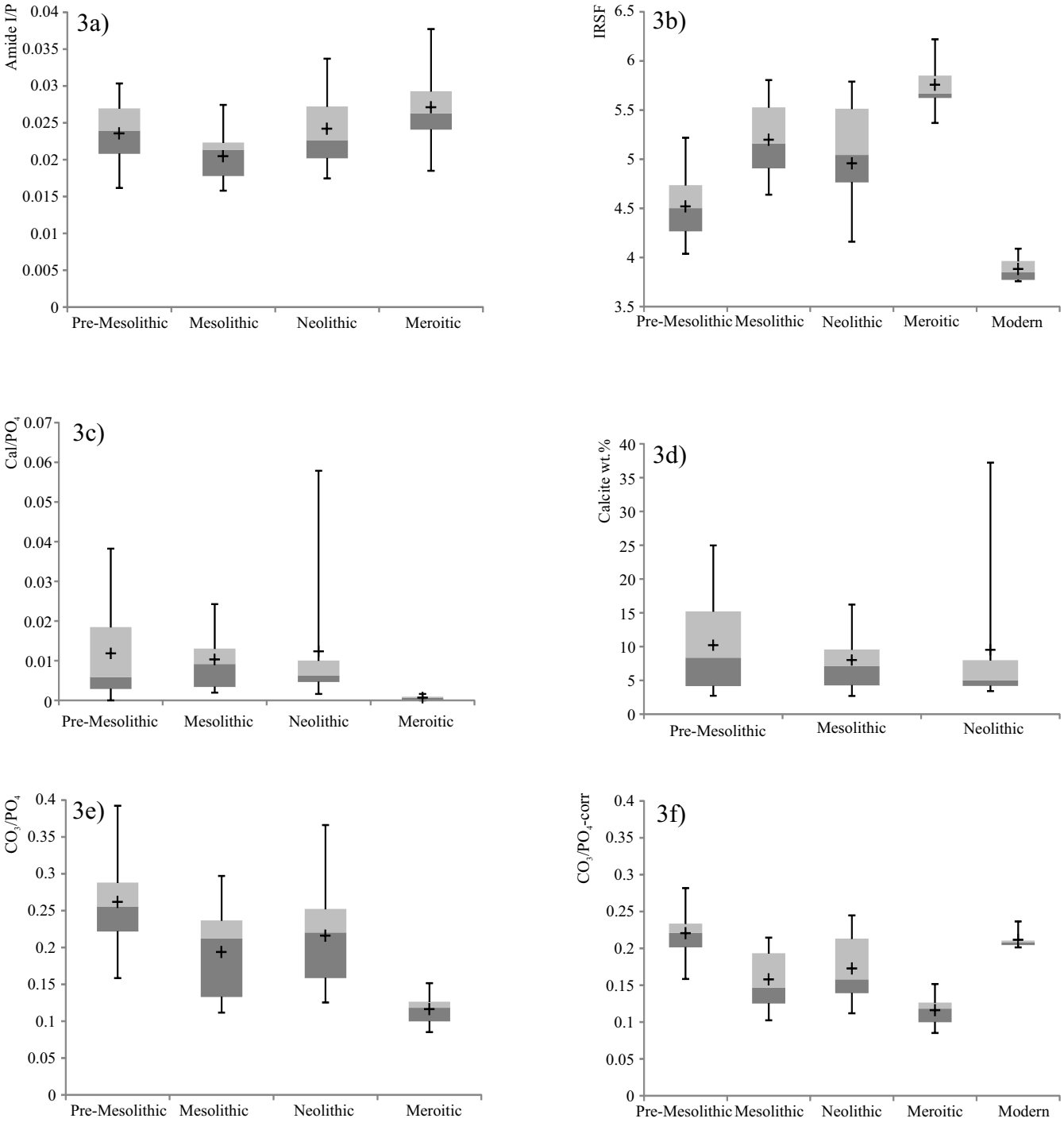

Fig. 3. Box plot of the frequency distribution of diagenetic parameters calculated from ATR-FTIR spectra of pre-Mesolithic, Mesolithic, Neolithic and Meroitic burial phases: 3a. Collagen content index: Amide I/PO_4 ratio; 3b. Infrared splitting facto: IRSF; 3c. Parameter related to the secondary calcite content: Cal/PO_4; 3d. Calcite percentage, not calculated for Meroitic samples: Calcite wt.%; 3e. Parameter related to the carbonate content of bioapatite CO_3/PO_4; 3f. Correction of CO_3/PO_4 taking into account the contribution of calcite to the $\nu_3(CO_3)$ vibrational bands: CO_3/PO_4-corr.

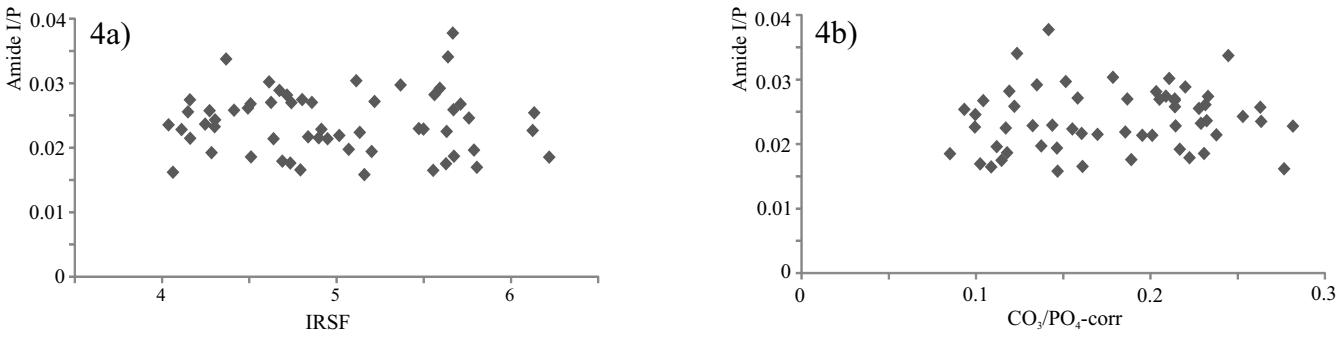

Fig. 4. 4a. Amide I/PO_4 ratio plotted against IRSF and 4b. Amide I/PO_4 ratio plotted against CO_3/PO_4-corr of archaeological bone samples (ATR-FTIR).

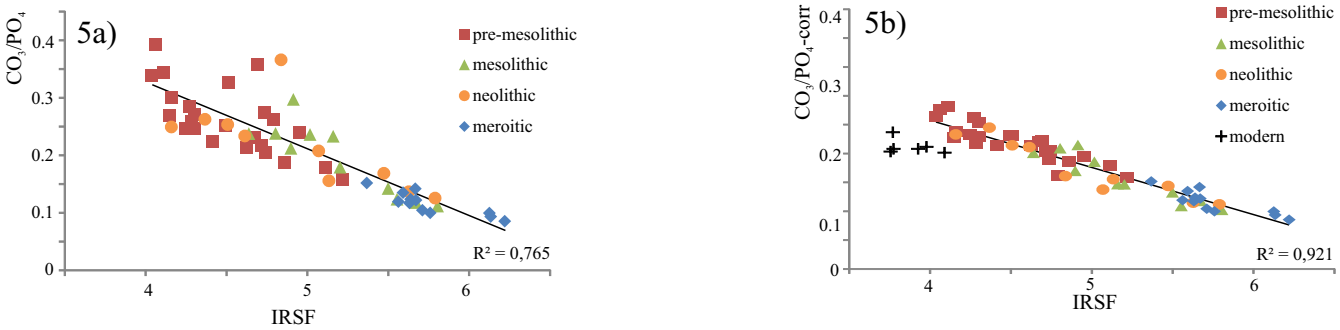

Fig. 5. 5a. CO_3/PO_4 ratio plotted against IRSF of archaeological bone samples, taking into account the burial phase (ATR-FTIR); 5b. CO_3/PO_4-corr ratio plotted against IRSF of archaeological bone samples, taking into account the burial phase (ATR-FTIR), modern samples are shown as reference .

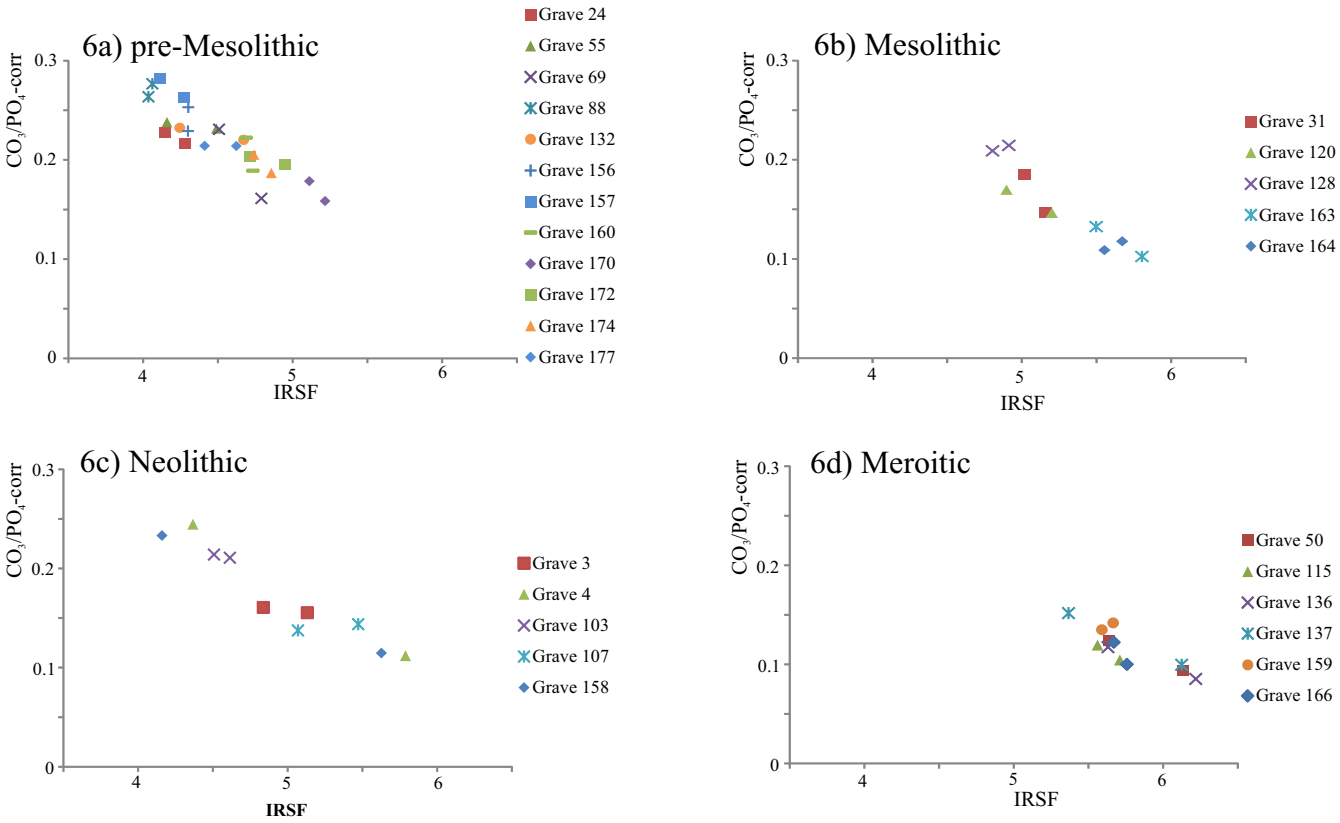

Fig. 6. 6a. CO_3/PO_4-corr ratio plotted against IRSF pre-Mesolithic bone samples (ATR-FTIR); 6b. CO_3/PO_4-corr ratio plotted against IRSF Mesolithic bone samples (ATR-FTIR); 6c. CO_3/PO_4-corr ratio plotted against IRSF Neolithic bone samples (ATR-FTIR); 6d. CO_3/PO_4-corr ratio plotted against IRSF Meroitic bone samples (ATR-FTIR).

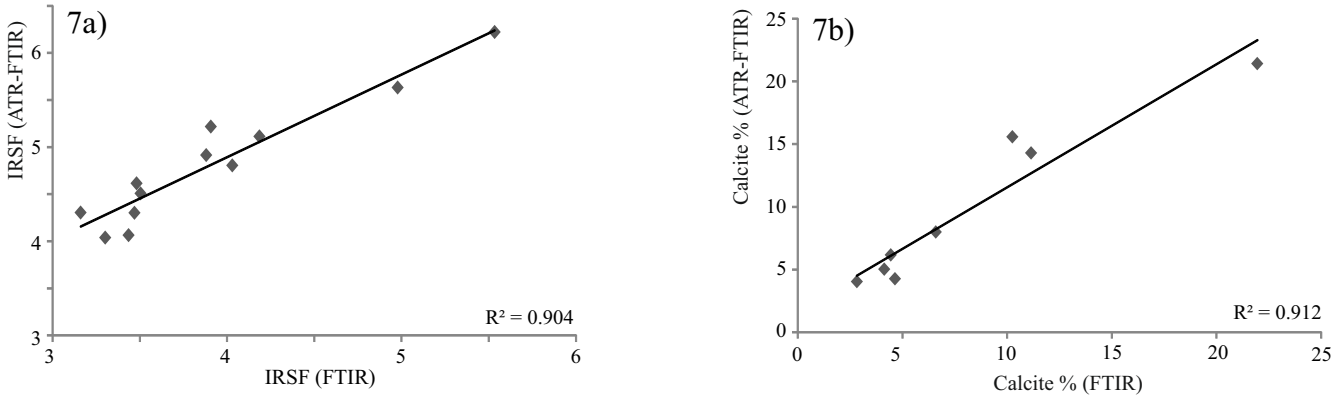

Fig. 7. Comparison between 7a. IRSF values; and 7b. Calcite wt. % content; of archaeological samples calculated from ATR-FTIR and FTIR spectra.

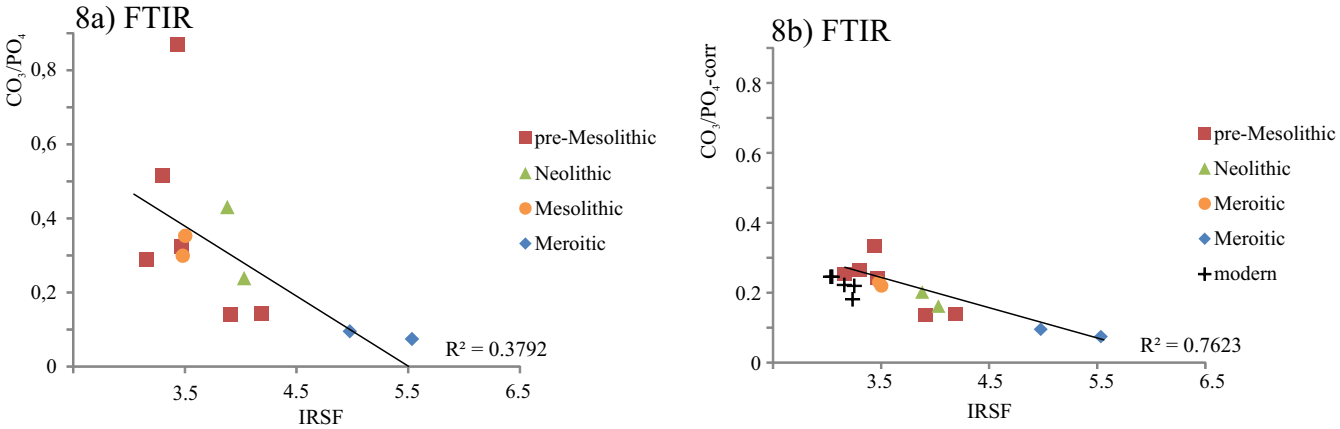

Fig. 8. 8a. CO_3/PO_4 ratio plotted against IRSF of archaeological bone samples, taking into account the burial phase (FTIR); 8b. CO_3/PO_4-corr ratio plotted against IRSF of archaeological bone samples, taking into account the burial phase (FTIR), modern samples are shown as reference .

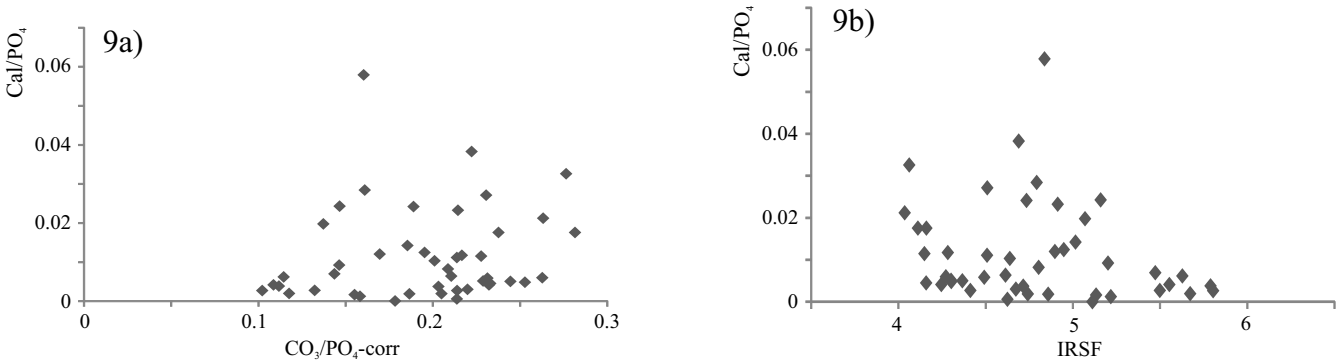

Fig. 9. 9a. Cal/PO_4 ratio plotted against CO_3/PO_4-corr and 9b. Cal/PO_4 ratio plotted against IRSF of archaeological bone samples (ATR-FTIR).

CHAPTER 3

Measurement of bioapatite crystallinity: influence of sample preparation

1. Introduction

Bone diagenesis is a complex phenomenon involving different processes that alter the in vivo composition and properties of bone material during burial. Physical and biochemical alteration of bones, recovered during archaeological excavations, occurs at different scale levels and with different extent, mainly depending on the variability of pre-burial and burial environmental conditions. Numerous studies have been carried out in order to reconstruct the diagenetic and taphonomic history of archaeological bones, to define alteration types and extent, to understand how and by which way diagenetic processes may affect bone preservation and assess reliability of retrieved information on the in vivo bone composition (Hedges, 2002; Nielsen-Marsh and Hedges, 2000; Smith et al., 2007; Lee-Thorp, 2008; Sponheimer and Lee-Thorp, 1999; Weiner, 2010). From these, several diagenetic parameters have been proposed in order to quantitatively or semi-quantitatively describe bone diagenesis, and therefore the preservation state of bone, from the macro- to the nano-scale (Hedges et al., 1995). Among these, the *crystallinity*, provides information on the preservation state of bioapatite, the mineral fraction constituting bone material. As a matter of fact, bones undergo a certain degree of recrystallization during diagenesis (Berna et al., 2004; Weiner 2010). Bioapatite is a nano-crystalline phase, which composition resembles that of hydroxyapatite ($Ca_{10}(PO_4)_6(OH)_2$) but considerably depart from stoichiometry, as a number of elements enter the structure in minor and trace quantity and ionic substitutions and vacancies occur (LeGeros, 1981; Elliot, 2002, Gómez-Morales, 2013). Ionic substitutions in the bioapatite structure influence the long-range atomic order of crystals and therefore they play a major role in determining the physical and chemical properties of mineral bone, such as solubility and crystal size (Wopenka and Pasteris, 2005; LeGeros, 1981). In particular, carbonate ions substitution, which is the most significant among ionic substitutions (4-7 wt.% of bioapatite), is known to be a crystal growth inhibitor and responsible for solubility increase. After the death of the individual, bioapatite nanocrystals tend to recrystallize (presumably by Ostwald ripening process – Ostwald, 1897) into a more thermodynamically stable and more ordered crystal structure, in which crystal dimensions increase, with a subsequent reduction of the specific surface area (Berna, 2004; Nielsen Marsh and Hedges, 2000; Hedges, 2002). Variability in the recrystallization degree is determined by the combined effect of several factors, mainly related to environmental and local burial conditions, such as soil composition, pore water chemical composition, temperature and moisture, as well as by possible pre-burial activities such as defleshing, boiling or burning.

In order to monitor and quantitatively describe changes in bone crystallinity, several crystallinity indexes have been proposed, calculated from results obtained by different analytical techniques. The most extensively used among these indexes is the infrared splitting factor (IRSF), as defined by Weiner and Bar-Yosef (1990) (Fig. 1), and calculated from infrared spectra of bioapatite samples. IRSF is defined within the $\nu_4(PO_4)$ vibrational mode of phosphate, which shows two bands at ~604 and ~565 cm^{-1} (and a shoulder at ~575 cm^{-1}); it is calculated as the sum of peak intensities at 604 and 565 cm^{-1} divided by the intensity of the valley between them, thus quantifying the splitting extent of the two peaks. Termine and Posner (1966) showed a linear correlation between the extent of the splitting of the $\nu_4(PO_4)$ vibrational bands and the crystallinity percentage of mixtures of crystalline and amorphous calcium phosphates: the broader are the peaks, the lower is crystallinity (and IRSF value). Fourier transform infrared (FTIR) spectroscopy is sensitive to functional groups and their chemical environment but it cannot differentiate between actual crystal size and atomic order/disorder, despite a correlation between atomic disorder and crystal size was proved by Wopenka and Pasteris (2005). Both these two factors are thought to contribute to crystallinity as assessed by IRSF index (Hedges, 2002; Weiner, 2010). IRSF values are reported to range from 2.5 to 2.9 for fresh bones whereas they can reach values of 7 for calcined or fossil bones (Weiner, 2010). Transmission FTIR spectroscopy, involving KBr pelleting method for sample preparation, is the most extensively used analytical technique in bone diagenesis studies, despite sample preparation can heavily affect IRSF measurements (Thompson et al., 2011), especially in relation to the grinding extent (Surovell and Stiner, 2001). When performing transmission FTIR spectroscopy, peak broadening is also influenced by scattering effects due to particle size (Duyckaerts, 1959) of the analysed sample dispersed in the KBr pellet: the larger is the particle size, the broader is the peak. Therefore, peak broadening is due to a combined effect of atomic disorder and particle size. Recent FTIR studies on calcite (Poduska et al., 2011; Regev et al., 2010) and on biogenic apatite (Asscher et al., 2011a) show that these two effects can be decoupled through the grinding curve method. Measurements carried out after repeated grinding of the same sample show sharper and more intense peaks, and indexes calculated on infrared spectra versus grinding intensity (cycles), describe a trend lines, the offset of which can differentiate the extent of atomic disorder among samples. Moreover, this method should overcome the problem of sample preparation influence on IRSF determination. This approach has been applied to modern and fossil bone, dentine and enamel (Asscher et al., 2011a; 2011b) showing that grinding curves, obtained by plotting IRSF versus the full with at half maximum (FWHM) of the 1035 cm^{-1} peak ($\nu_3(PO_4)$ vibrational mode), can distinguish between enamel of different taxa, between bone and enamel, and can be used to monitor diagenetic changes of bioapatite in fossil samples.

In the present research the grinding curve method is applied to the study of archaeological human bones with the main aim to establish a reliable comparative method between IRSF values measured on a set of samples, in order to monitor diagenetic changes in bioapatite.

In addition, since bone crystallinity can be determined also by X-ray powder diffraction (XRPD), as bioapatite nanocrystals act as coherently scattering domains producing a diffraction pattern, a subset of bone samples was also analysed by XRPD. Small-sized crystallites lead to broadening of line profiles (Sherrer, 1918), and for nano-materials this is particularly evident; therefore line-broadening analysis was carried out in order to obtain information on crystallite size of bioapatite (which, however, can differ from the crystal size measured on bone samples by electron microscopy (Weiner, 2010; Ungár et al., 2005), being often underestimated. Results were then compared with IRSF values in order to explore a possible correlation.

2. Materials and methods

2.1 Archaeological samples

Bone samples analysed in this study come from the archaeological site 16D4 (or Al Khiday 2), located in central Sudan near the Al Khiday village, 20 km south of Khartoum, on the western bank of the White Nile. Archaeological excavation, carried out within "El Salha archaeological project" since 2005 (Salvatori et al., 2011), brought to light 190 graves belonging to four different burial phases. The same area has been used as a burial ground at least for four times during almost the entire Holocene. A terminus ante quem for the most ancient burial phase (named pre-Mesolithic) have been established to the 6700-6300 cal. years BC; then the area was used as a cemetery during the Neolithic period (4550-4250 cal. years BC) and later on during the Meroitic period (1st century BC and the 2nd century AD). A fourth burial phase was identified, but given the lack of grave goods and uncertainties on the relationship between graves and the archaeological stratigraphy, it was tentatively labelled "Mesolithic", despite the uncertain chronological attribution (Usai et al., 2010; Dal Sasso et al., 2014-a). A set of bone samples representative for each burial phase was selected. Histological and micro-morphological study (Dal Sasso et al., 2014-a) and FTIR spectroscopic study in attenuated total reflection (ATR-FTIR) mode (Dal Sasso et al., in prep – Chapter 2), revealed a great variability in types and extent of diagenetic alteration among burial phases, which were related to changes in palaeoenvironmental and local burial conditions occurred during the Holocene. In fact, on the basis of archaeological and geomorphological investigations at Al Khiday (Salvatori et al., 2011; Zerboni et al., 2011; Cremaschi et al., 2007) and palaeoenvironmental reconstruction at regional level (Gasse, 2000; Nicoll, 2004; Williams, 2009; Williams and Jacobsen,

2011; Zerboni, 2013), during the wide span of time covered by these burial phases profound climatic changes occurred in the region. Pre-Mesolithic and Mesolithic bones encountered a more humid burial environment, due to higher monsoonal activity, with respect to the subsequent burial phases; by middle Holocene, when during the Neolithic use of the site, gradual climatic changes led to drier conditions with a progressive decrease in rainfall and water availability, and by the Meroitic period more arid climate conditions occurred. Therefore, considering the variability of diagenetic alteration observed, this set of samples well suites the purposes of this research. Bone samples here analysed are femur fragments belonging to 12 pre-Mesolithic, 5 Mesolithic, 5 Neolithic and 6 Meroitic graves.

2.2 FTIR spectroscopy

2.2.1 Experiment 1

The external bone surface, encrusted by soil sediments, was mechanically removed by means of low-speed micro-drill equipped with an abrasive point. Attention was paid in order to avoid over-heating of samples during mechanical cleaning process. Then, ~1 mg of sample was lightly hand-ground in an agate mortar for few seconds and KBr was added and homogenised. Powder was then pressed, using a hydraulic press, under 2 tons/cm^2 pressure, and a 7 mm in diameter transparent pellet was obtained. After the first measurement, half of the pellet was reground with other KBr and a new pellet was created and probed. This procedure was repeated other two times, so four spectra at different grinding steps (and with different sample: KBr ratio) were acquired for each sample.

Spectra were collected with a Nicolet 380 FTIR spectrometer equipped with a DTGS detector; 32 scans for each spectrum were acquired, in the range from 4000 to 400 cm^{-1}, with a spectral resolution of 4 cm^{-1}. Spectral analysis was performed using Omnic 9 software (Thermo Scientific). Measurements were performed at the Kimmel Center for Archaeological Science – Weizmann Institute of Science (Rehovot, Istrael). IRSF, as defined by Weiner and Bar-Yosef (1990), and FWHM of the 1035 cm^{-1} peak were calculated for each spectrum. The baseline was defined by two points calculated as the local minimum in the region 660-620 and 510-470 cm^{-1} for the IRSF, 1400-1200 and 900-750 cm^{-1} for the 1035 cm^{-1} peak.

2.2.2 Experiment 2

A femur fragment from one Meroitic grave (grave 50) was selected and two sample preparation protocols (hereafter Experiment 2A and Experiment 2B) were applied. Experiment 2A resembles

the protocol applied in Experiment 1: after external surface removal, bone sample was lightly hand-ground in an agate mortar; 1mg of bone powder was ground with 100 mg of KBr for 30 seconds, then a 12 mm in diameter transparent pellet was obtained with a hydraulic press under 8 tons/cm^2 pressure. After each measurement half of the pellet was reground with ~50 mg of KBr; powder was then pressed again and another spectrum acquired, for a total of 6 spectra.

In Experiment 2B, 2 mg of bone sample were hand-ground in an agate mortar with 500 mg of KBr; after 30 seconds 100 mg of the powder was pressed into a pellet, with the same conditions applied in Experiment 2A, and a spectrum was acquired. The remaining powder was ground for further 30 seconds, then other 100 mg were pressed into a new pellet. Other 3 pellets were then created with a grinding-time step of 1 minute. This protocol is basically similar to that applied in the previous experiments, with the difference that the sample: KBr ratio is constant from the first to the last grinding step, without any dilution of the sample, as happens in Experiment 1 and Experiment 2A. Spectra were collected with a Nicolet Nexus 870 FTIR spectrometer equipped with a DTGS detector; 64 scans for each spectrum were acquired, in the range from 4000 to 400 cm^{-1}, with a spectral resolution of 2 cm^{-1}. Spectral analysis was performed using Omnic 9 software (Thermo Scientific).Measurements were performed at the Dipartimento di Scienze Chimiche, University of Padova (Padova, Italy).

2.3 X-ray powder diffraction

A subset of bone samples (4 pre-Mesolithic, 3 Mesolithic, 3 Neolithic and 4 Meroitic) were finely ground with an agate mortar and analysed by XRPD. Analysis was performed with a PANalytical X'Pert PRO diffractometer in Bragg-Brentano geometry, equipped with a Cu X-ray tube, operating at 40 kV and 40 mA, and a X'Celerator detector. Diffractogram were acquired in the range from 3° to 80° 2θ, with a step size of 0.02° 2θ and counting time of 1 s per step. Rietveld refinement (Young, 1993) analysis was performed on diffractograms using the MAUD program (Lutterotti, 2010). Instrumental contribution to line broadening was determined by measuring the NIST Si 640c standard sample, with the same experimental conditions. The crystal structure of Holly Springs hydroxyapatite reported by Sudarsanan and Young (1969) was adopted as structural model for bioapatite of bone samples. A polynomial function with 6 parameters was used to describe the background, while a pseudo-Voigt function was adopted to model the diffraction profile and residual was minimized by least square method. Scale factor, background parameters, isotropic atomic displacement parameter (maintained equal for all atoms) and unit cell parameters were refined. Other atomic thermal parameters, site occupancy and atomic position remained fixed

during refinement. The crystallite-size contribution to line broadening, taking into account its anisotropy, was determined by the spherical harmonics model proposed by Popa (1998), implemented in MAUD, by refining the spherical harmonics coefficients. The March-Dollase model for preferred orientation was tentatively applied to (002) reflection, even though refined parameters indicated a weak contribution for preferred orientation.

3. Results and discussion

Grinding curves for all archaeological bone samples (Experiment 1) were obtained by plotting IRSF values versus the FWHM of the 1035 cm^{-1} peak (Fig. 2). For clarity reason experimental points (+) belonging to the same sample were linked with a straight line and samples were grouped by colours, according to the burial phase attribution. As proven by Asscher et al. (2011a; 2011b), curves offset to higher IRSF values indicates higher atomic order in bioapatite, thus enabling one to monitor the extent of diagenetic alteration of bioapatite, as higher atomic order implies a higher recrystallization degree. In this case the grinding curve approach can actually differentiate archaeological bones belonging to different burial phases. In particular, Meroitic and pre-Mesolithic samples are quite well differentiated while Mesolithic and Neolithic samples range between them and are partially overlapped. Pre-Mesolithic samples are characterised, in addition to the overall lower IRSF values, by a lower variability of FWHM values, the minimum values of which (at the last grinding step) are always lower than the other burial phases. Higher FWHM values were observed by Asscher et al. (2011b) for modern bones with respect to fossil ones and related to a lower atomic order in modern bioapatite. In this case, higher FWHM values observed for pre-Mesolithic samples may be indicative of a lower recrystallization extent of bioapatite if compared to Mesolithic, Neolithic and Meroitic samples. Among the four burial phases, Meroitic bones show the highest recrystallization degree. This evidence is also supported by the results obtained on the same set of samples by ATR-FTIR (Dal Sasso et al., in prep – Chapter 2), where IRSF and relative carbonate content, among other diagenetic parameters, were investigated. However, despite the good accordance between these results, the trend line for grinding curves in this case study differs substantially from what observed by Asscher et al. (2011a; 2011b). After repeated grindings, FWHM should decrease and IRSF should increase until no significant value changes are noted. In this case we observed a steady decrease of FWHM values, but also IRSF decreases, with rare exceptions, after the second or the third grinding step. Moreover, once fitted the experimental data with a linear regression model, the linear correlation between IRSF and FWHM with increasing grinding, proved by Asscher et al. (2011a; 2011b), here is not observed. Only 6 out of 28 samples show a correlation coefficient (R^2)

higher than 0.95, while several samples do not show any correlation (Tab. 1). In order to investigate the reason of this discrepancies, a sample (50F, the Meroitic femur sampled from grave 50) for which no linear correlation was observed between experimental points obtained after subsequent grinding steps (R^2 = 0.01), was prepared according to the method of Experiment 2 and measured. More in detail, Experiment 2A reproduced a sample preparation analogous to that adopted during Experiment 1, but in which with grinding time and sample dilution were more accurately monitored. FTIR spectra acquired for Experiment 2A (Fig. 3) show that, at each grinding step, peak intensities decrease. This evidence indicates that, despite the intensities should have increased for effect of the particle size reduction (Poduska et al. 2011), the contrasting effect of sample dilution in KBr heavily affects the measurement. In fact, spectra obtained from the same sample prepared with the protocol described in Experiment 2B (Fig. 4), without any dilution along subsequent grinding step, show the expected intensity increase and peak sharpening, as observed in previous researches both on bones and on other materials (Asscher et al., 2011a; Poduska et al., 2011; Regev et al., 2010). Moreover, grinding curve obtained from Experiment 2A shows a completely different trend than that of Experiment 2B (Fig. 5). The first, resembling the trend already observed in Experiment 1 (Fig. 2), shows a decrease in IRSF values after few grinding steps, and a very poor linear correlation (obtained by linear regression of experimental points) between FWHM and IRSF (R^2 = 0.19). On contrary, the grinding curve obtained from Experiment 2B shows an excellent linear correlation between FWHM and IRSF values (R^2 = 0.99), higher IRSF and lower FWHM values with respect to that obtained for Experiment 2A. This evidence proves that dilution heavily affect parameters measurement from FTIR spectra, both in terms of absolute values and trends. Moreover, even if a parameter is normalised within the spectrum, such as IRSF (that results from a peak ratio), dilution seems to considerably affect its determination: this may be caused by the increase of signal-to-noise ratio (especially for very diluted samples, as in grinding 6) and probably by the instrument sensitivity decrease due to dilution effect, even if peak sharpening with increasing grinding is in any case recorded in the spectrum. At this point further measurements of the same sample, prepared with the protocol adopted for Experiment 2B, at different dilutions would clarify if and at which extent dilution can affect the determination of FTIR diagenetic parameters.

Since measures of experiment 1 and 2 were carried out using different apparatuses, another important issue that has to be taken into account is the possibility of comparing results acquired with different instruments, as well as from different laboratories or research groups. In this case study Experiment 1a and Experiment 2 were conducted with a Nicolet 380 and a Nicolet Nexus 870 FTIR spectrometer, respectively, both equipped with a DTGS detector. When plotting grinding curves obtained from Experiment 1 and 2 in the same graph, differences in absolute values, not

negligible, are evidenced (Fig. 6). Further analyses are required in order to understand the reasons of this variability, more specifically to both define which are the experimental parameters that mainly influence results and verify if any correlation between results obtained with different experimental setups may be established.

In light of these results, it can be not so easy to compare crystallinity, expressed as IRSF, among a set of samples in order to retrieve information on the diagenetic history and preservation state of bones, even considering the same experimental conditions. As suggested by Asscher et al. (2011a; 2011b), given the equation of a grinding curve obtained by linear regression of experimental data points, IRSF values can be calculated for arbitrary FWHM values. Therefore, reliable comparison between IRSF values of different samples can be achieved when IRSF values are calculating for a chosen FWHM value. With this approach the contribution to peak broadening due to particles scattering effects should be considered systematic for all samples, thus negligible when comparing IRSF values within a set of samples, the spectra of which were acquired with the same experimental conditions. However, in our case, the poor correlation between IRSF and FWHM, obtained from grinding curves in Experiment 1, do not enable us to calculate reliable IRSF values for an arbitrary FWHM value. Longer grinding times according to the protocol of Experiment 2B can be experimented to explore if good correlation between values can be observed in grinding curves: in such a case, calculated IRSF values will be confidently assumed to be less affected by sample preparation, therefore enabling us to compare values between different samples as well as with other crystallinity indexes obtained from other analytical techniques.

Bioapatite crystallinity, and in particular the apparent crystallite size, was here also measured by XRPD on a subset of the samples analysed by FTIR. The quality of Rietveld refinement was monitored by the agreement factor (Rwp), lower than 5% for every sample (Tab. 1), and residuals (Fig. 7).

The results of the model fit show a clear anisotropic contribution to the line broadening due to crystallite size, and in particular to the elongation along the c-axis of crystallites (Fig. 7). Moreover, the model provided the (average) apparent crystallite size along crystallographic directions. In Tab.1 are reported crystallite size (expressed in nanometres) obtained for the analysed samples along (002) and (300) crystallographic directions, corresponding to the c-axis and the a-axis, respectively. In order to explore the crystallinity variations among samples, the c-axis crystallite size was here selected as term for comparison, since crystallites are elongated along this crystallographic direction and the (00l) reflections of biogenic apatite in the diffractograms are less affected by peak overlapping (Fig. 7), thus providing more reliable results. Crystallite-size values

along the c-axis ranges from 44 to 82 nm (Table 1), and although the number of analysed samples is low within each burial phase, Meroitic bones have highest crystal size (Fig. 8). Despite the fact that IRSF values from Experiment 1 are heavily affected by sample preparation, a comparison with crystallite size obtained from XRPD was tentatively established. For each sample, crystallite size was plot against the minimum and the maximum IRSF registered in the grinding curve (Fig. 9), expecting the minimum and the maximum value to be the most and the less influenced by scattering effects, respectively. Crystallite size and minimum IRSF values are linearly correlated ($R^2 = 0.55$) and the correlation significantly improves when considering the maximum IRSF values ($R^2 = 0.79$). This indicates that results obtained from two different analytical techniques are consistent and the crystallinity variation observed among samples is confirmed.

4. Conclusions

On the basis of these preliminary results, a significant improvement of the correlation would be expected when IRSF values, calculated for a fixed FWHM value are compared to crystallite size. Despite the fact that further analyses are required in order to clarify some aspects of this research, these preliminary results are promising and the prosecution of this research may contribute towards the establishment of bioapatite preparation protocol for FTIR spectroscopy in transmission mode.

Table 1. Minimum (IRSF_min) and maximum (IRSF_max) values of IRSF calculated; R2 of linear regression calculated for the grinding curve of each sample (FTIR). Average crystallite size along the (002) and (300) crystallographic directions and Rwp (%) of the fit profile (XRPD).

Burial phase	Grave number	FTIR spectroscopy			XRPD		
		IRSF_min	IRSF_max	R^2	cryst.size (002) nm	cryst.size (300) nm	Rwp (%)
pre-Mesolithic	24	3.137	3.383	**0.97**			
	55	3.220	3.254	0.36	48	17	4.50
	69	2.820	3.334	0.38			
	88	2.855	3.112	0.18			
	132	3.253	3.288	0.88			
	156	2.931	3.126	0.59	47	17	4.80
	157	3.150	3.363	**0.94**			
	160	3.598	3.825	0.69			
	170	3.569	3.728	0.01	68	24	4.20
	172	3.493	3.583	0.34			
	174	3.325	3.693	0.69			
	177	3.020	3.101	0.07	52	19	4.60
Mesolithic	31	3.454	4.184	0.13	73	30	4.40
	120	3.393	3.936	0.26			
	128	2.985	3.329	0.16	67	24	4.00
	163	3.825	4.570	0.69	74	22	4.30
	164	3.644	4.259	**0.98**			
Neolithic	3	3.340	3.710	0.22	58	16	4.70
	4	2.973	3.185	0.06			
	103	3.433	3.944	0.89	66	21	4.40
	107	3.267	3.551	0.64			
	158	2.795	3.088	0.65	44	14	4.60
Meroitic	50	3.733	4.247	0.01	66	19	4.60
	115	4.150	5.164	**0.99**	81	23	4.6
	136	3.617	5.100	**0.94**	82	24	4.2
	137	3.197	4.554	**0.91**			
	159	3.834	4.045	0.74	60	17	4.40
	166	3.479	4.303	0.79			

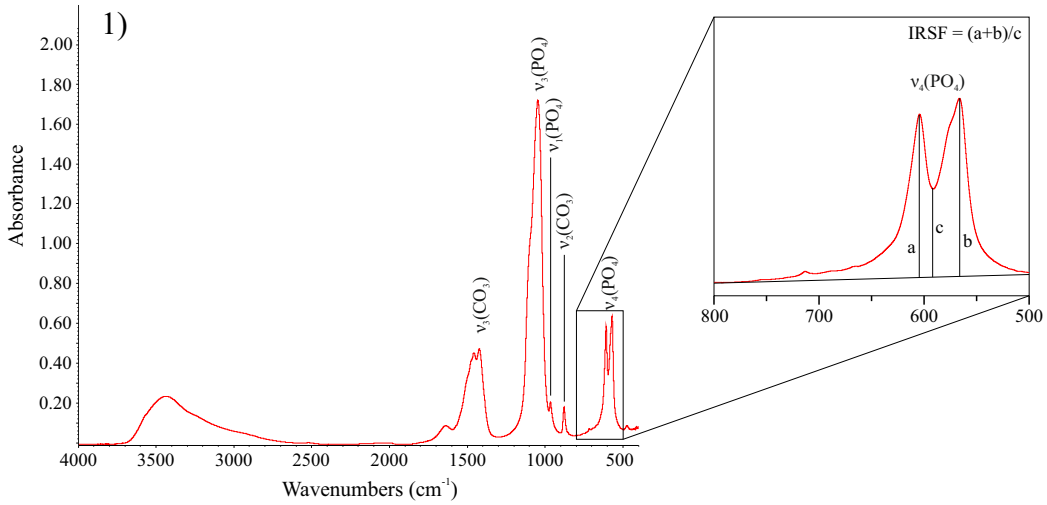

Fig. 1. Examples of FTIR spectra of bone (sample 156). Attribution of bands to vibrational modes of phosphate and carbonate groups is reported. The method adopted to calculate the IRSF (Weiner and Bar-Yosef, 1990) is also shown.

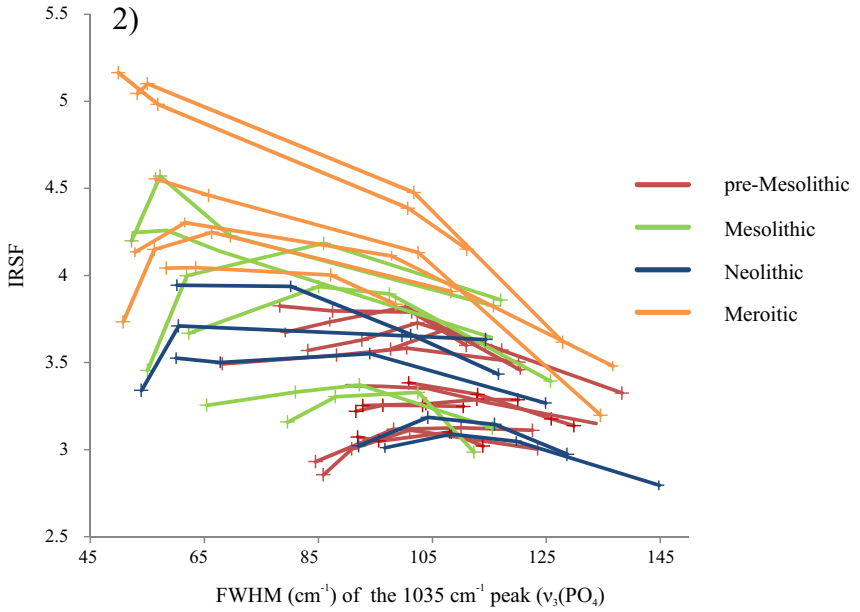

Fig. 2. Grinding curves of pre-Mesolithic, Mesolithic, Neolithic and Meroitic bones (Experiment 1)

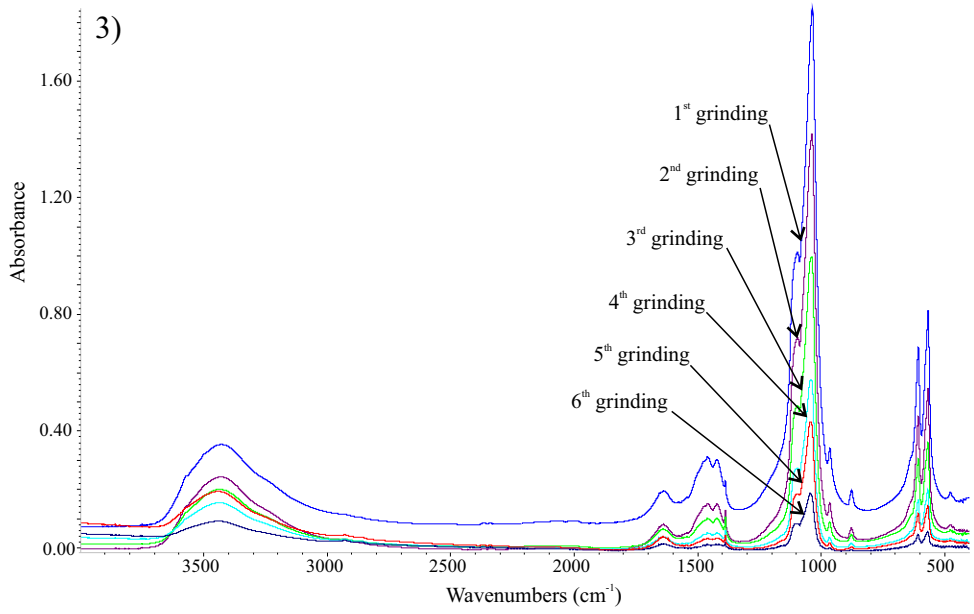

Fig. 3. FTIR spectra acquired for Experiment 2A

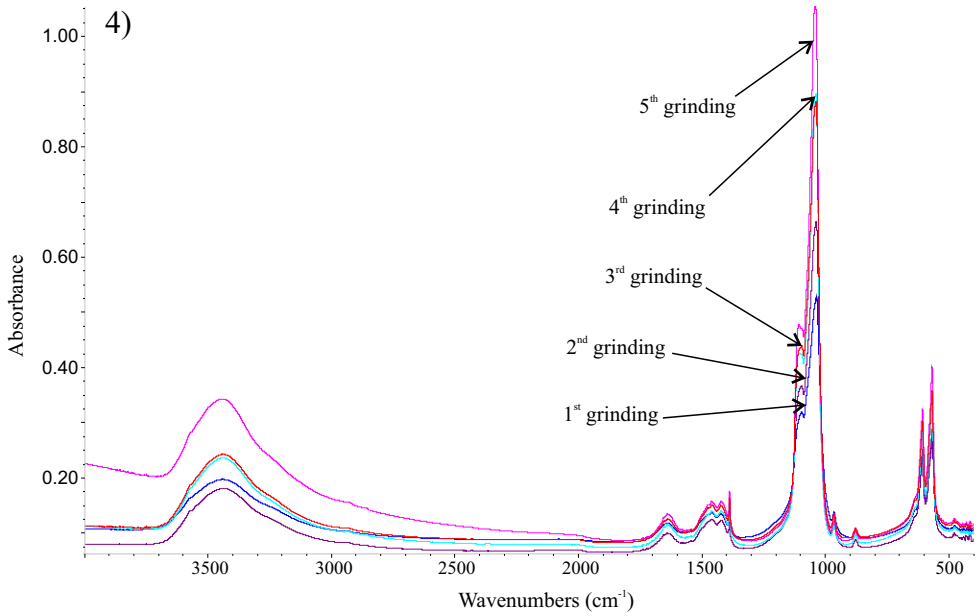

Fig. 4. FTIR spectra acquired for Experiment 2B

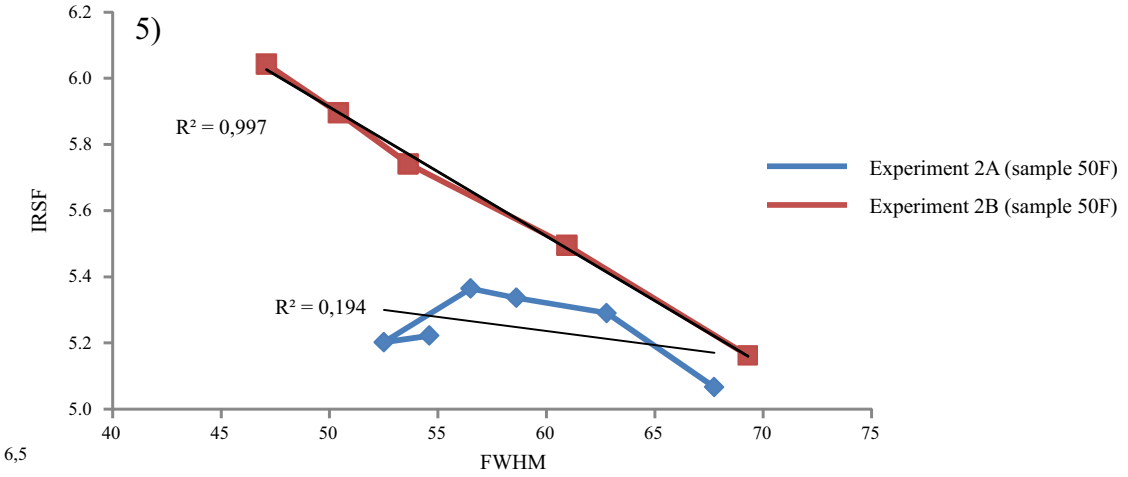

Fig. 5. Grinding curves of sample 50 (Experiment 2)

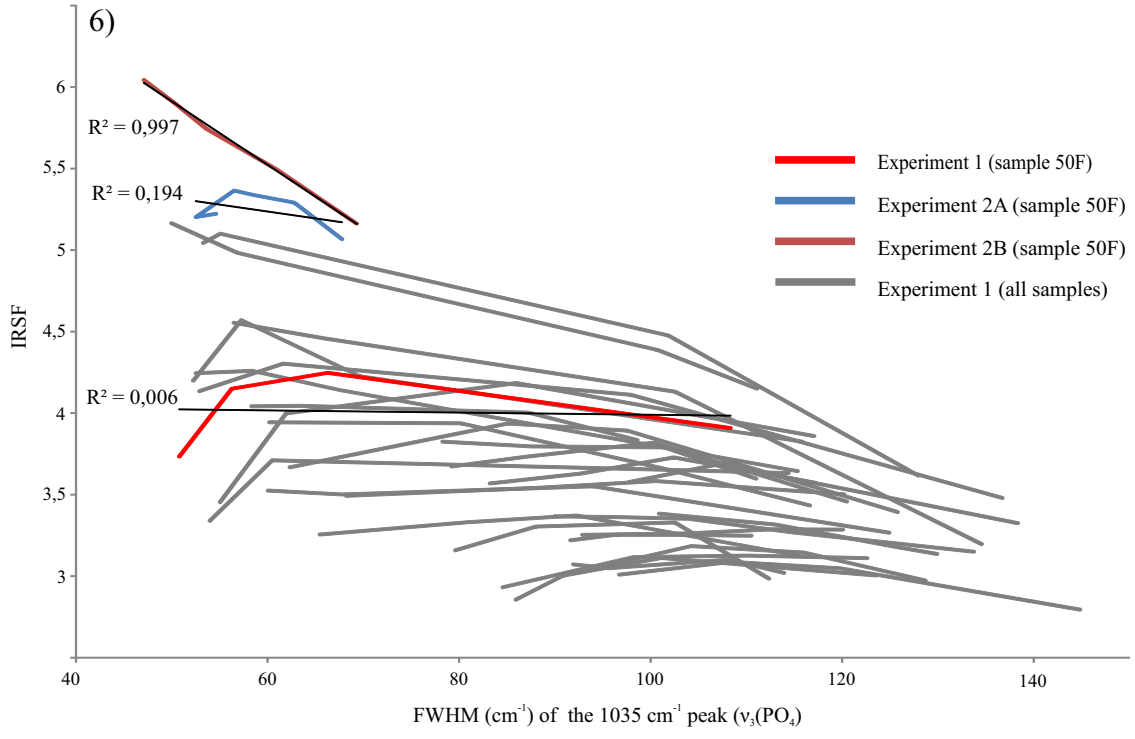

Fig. 6. Comparison of grinding curves produced by Experiment 1 and Experiment 2

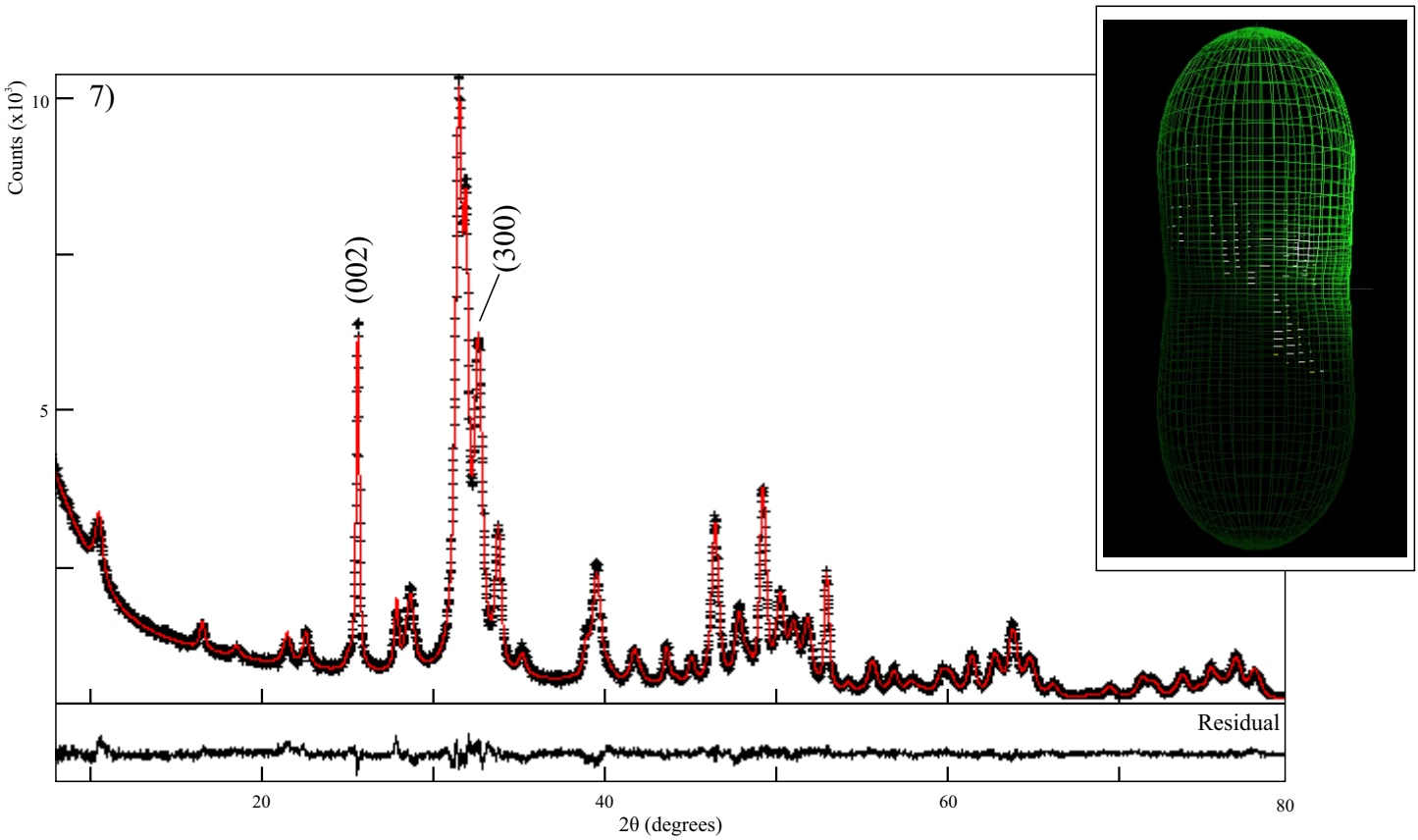

Fig. 7. Experimental diffractogram (points) and Rietveld fit profile (line) of sample 50F. A 3D model of the average shape of crystallites, elongated along the c-axis

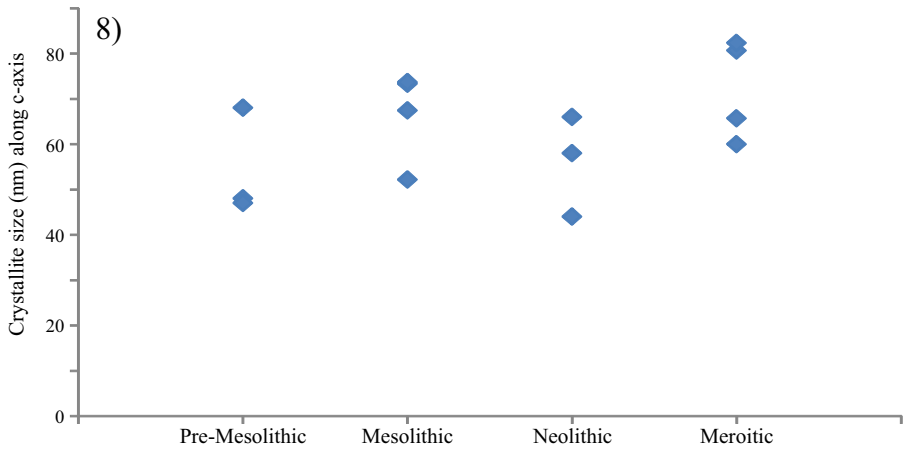

Fig. 8. Distribution of the average crystallite size alog the c-axis obtained from Rietveld refinement for pre-Mesolithic, Mesolithic, Neolithic and Meroitic bones

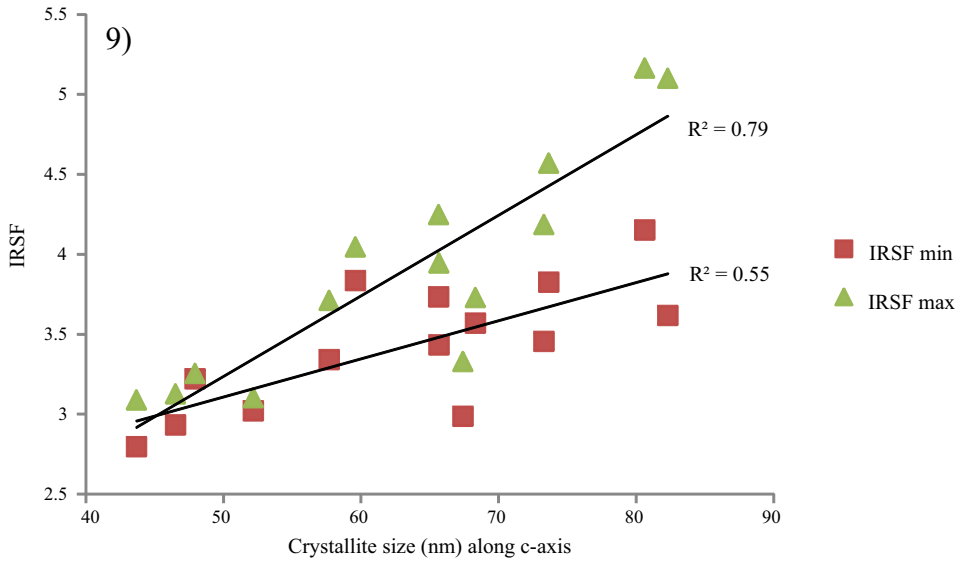

Fig. 9. Minimum and the maximum IRSF values registered in the grinding curves (FTIR - Experiment 1) plotted against the crystallite size (XRPD).

CHAPTER 4

Micro-Raman imaging of archaeological bone: a convenient screening method to investigate bone diagenesis

1. Introduction

Bone is a composite material, mainly constituted by mineral nanocrystals, an organic matrix and water, organised in a complex hierarchical structure described in terms organization levels, from the nano- to the macro-scale (Weiner and Traub, 1992; Weiner and Wagner, 1998). The organic fraction of bone is mainly constituted by type I collagen, while the mineral fraction is constituted by nanocrystals of biogenic apatite (bioapatite), whose structure and chemical composition resemble those of hydroxyapatite ($Ca_{10}(PO_4)_6(OH)_2$), even if several types of ionic substitutions (among them the most significant is the carbonate ion substitution) and vacancies occur (Wopenka and Pasteris, 2005; LeGeros, 1981; Elliot, 2002; Gómez-Morales, 2013). Pristine chemical and isotopic composition of bone retain valuable information on the living organism and its environment (Lee-Thorp, 2008). However, when retrieving this information from archaeological bones, diagenetic alteration has to be taken into account. In fact, from the death of the individual onwards, bone material undergoes several taphonomic and diagenetic processes leading to alteration of its constituents at different scale levels. The study of bone diagenesis has been carried out during the last decades with the main aims to model the diagenetic processes involved in bone alteration, to define and quantitatively describe the alteration types and extent and to contribute to assess the reliability of retrieved information with respect to the in vivo composition or isotopic signature of bone (Hedges, 2002; Nielsen-Marsh and Hedges, 2000; Smith et al., 2007; Lee-Thorp, 2008; Sponheimer and Lee-Thorp, 1999; Weiner, 2010). Several analytical techniques have been applied to study archaeological and fossil bones (and teeth) in order to assess their preservation state and understand mechanisms of diagenetic alteration; among them, extensively applied are optical microscopy (OM), scanning and transmission electron microscopy (SEM and TEM), X-ray powder diffraction (XRPD), Fourier transform infrared spectroscopy (FTIR), Raman spectroscopy, X-ray fluorescence (XRF) and mass spectrometry (Hackett, 1981; Bell, 1990; Weiner and Price, 1986; Roche et al., 2010; Person et al., 1995; Thomas et al., 2007, Lee-Thorp, 2008, Reiche et al., 2003; Lebon et al., 2010; Dal Sasso et al., 2014-a). Depending on the analytical techniques applied, valuable information on bone preservation state can be obtained, from the nano- to the macro-scale level. The choice of the most suitable analytical technique is based on the type of information that needs to be achieved, the aims of the study, as well as the sample preparation protocol required for the selected technique. As for sample preparation, two aspects have to be considered: first, when

dealing with archaeological and cultural materials, since destructive and semi-destructive analyses may represent a non-negligible issue, the amount of sample required is an important factor to be taken into account; second, anyhow, sample preparation (i.e. samples can be powdered or embedded in epoxy resin or thin sectioned, etc) influences the type of retrieved information. Widely used analytical techniques (i.e. XRPD and IRSF), applied to powdered samples, provide valuable information, but sample heterogeneity cannot in these cases be described, being bulk techniques. Besides the complex structure of bone tissue itself, heterogeneity of diagenetic alteration types and extent at the micro- (and macro-) scale level were proved by histological and microstructural analyses (Hedges et al., 1995; Jans et a., 2004; Fernández-Jalvo et al., 2010; Dal Sasso et al., 2014-a). For these reasons, spatially resolved analyses provide additional information with respect to bulk analysis on bone preservation state, investigating intra-sample variability of isotopic and chemical composition as well as structural properties of bone material (Vašinová Galiová, 2013; Brady et. al., 2008, Reiche et al, 2010; Lebon et al., 2014).

On these bases, micro-Raman (μ-Raman) spectroscopy was applied in this research in order to investigate diagenetic alteration of an early-Holocene archaeological human bone. Raman spectroscopy is an analytical technique, which probes molecular vibrations; it is, therefore, sensitive to molecular bonds and their chemical environments as well as chemical composition and structure of the analysed material (Smith and Clark, 2004). This technique allows samples to be qualitatively and semi-quantitatively investigated in any physical state, as gas, liquid, crystalline or amorphous solid. When coupled with a microscope, selective analyses on the different constituents of heterogeneous materials can be performed at the micro-scale. Moreover, if provided with a software-controlled motorized stage, a point-analysis grid on a selected area of the sample allows to acquire multispectral maps, thus providing a highly informative method to monitor the sample spatial heterogeneity, as well as supplying numerous measurements for one sample, producing a statistically significant amount of data to be analysed. When applied to bone material, μ-Raman spectroscopy is a valuable analytical method, as organic and mineral fractions can be simultaneously investigated, at the same time considering the intrinsic spatial heterogeneity of bone tissue itself, and, if analysing archaeological bones, distribution of diagenetic alteration can be monitored.

Besides Raman spectroscopy, also infrared (IR) spectroscopy produces a vibrational spectrum, supplying similar information. IR spectroscopy has been extensively applied in material characterization field as well as in bone diagenesis studies. Over the last decades, the development of system configuration and instrumental components of Raman spectrometers overcame many limitations (i.e. lower sensibility and higher instrumental cost) that disfavoured its application in the

past, in favour of IR spectroscopy. Now, comparing the two techniques, several advantages can be acknowledged by applying Raman spectroscopy: i) it is a non-destructive analysis and no sample preparation is needed; ii) sharper peaks limits peak overlapping, thus facilitating qualitative analysis; iii) it is not sensitive to water eventually present in the sample, nor to atmospheric gases (as CO_2); iv) improvement of spatial resolution (Smith and Clark, 2004). As for IR mapping, acquisitions in transmission mode require the sample embedded in epoxy resin and cut in thin (2-5 μm) sections by ultra-microtomy (Reiche et al., 2010). This complex, and not always feasible, sample preparation method can be avoided when IR mapping is performed in attenuated total reflection (ATR) mode, where minimal sample preparation is required. Nevertheless, good contact between the ATR crystal and the sample is necessary in order to perform the measurement and a polished section of the sample is recommended (Lebon et al., 2014). In both cases, spatial resolution is at least one order of magnitude lower than that achieved by μ-Raman mapping (1 μm). If on one hand these represent the main restrictions for IR mapping, on the other hand Raman spectroscopy has also some limitations when applied to material characterization, the most significant of which is the fluorescence effect induced by organic material, atomic fluorescence or fluorophores (Smith and Clark, 2004) that can partially or completely overwhelm characteristic peaks of the analysed sample.

Despite the fact that μ-Raman spectroscopy analysis (Morris and Mandair. 2010; Awonusi et al., 2007; Penel et al. 1998) as well as μ-Raman mapping (Timlin et al., 1999; Otto et al., 1997; Kazanci et al., 2006) are widely performed on bone material in biomedical and biomaterial characterization field, it is not so extensively applied to the diagenetic analysis of archaeological and fossil bones (Edwards et al., 2001; Thomas et al., 2007; Pucéat et al., 2004; King et al., 2011), even less μ-Raman mapping (Lebon et al., 2011).

The aim of this research is to investigate the effectiveness of μ-Raman mapping in studying the spatial heterogeneity of archaeological bones, and detecting types and distribution of diagenetic alteration within the sample.

2. Raman spectra of bones

Raman spectrum of bone shows molecular and structural information about collagen and bioapatite (Fig. 1a). Collagen bands are located in the region from 1720 to1600 cm^{-1}, from 1500 to1370 cm^{-1} and from 1200 to1350 cm^{-1} corresponding to the amide I, δCH_2 and amide III vibrational modes, respectively. Bioapatite shows several vibrational bands relative to phosphate and carbonate ions. Phosphate has a strong-intensity sharp peak at 961 cm^{-1} assigned to $\nu_1(PO_4)$ vibrational mode and

weak bands in the region from 1070 to 1032 cm^{-1}, from 650 to 550 cm^{-1} and from 480 to 400 cm^{-1} relative to $\nu_3(PO_4)$, $\nu_4(PO_4)$ and $\nu_2(PO_4)$ vibrational modes, respectively (Penel et al., 1998; Rey et al., 2011). Carbonate ions occur in bioapatite crystal structure (4-7 wt.%), mainly as substitution for phosphate ions (LeGeros, 1981; Sponheimer and Lee-Thorp, 1999; Wopenka and Pasteris, 2005), influencing the long-range atomic order of crystals and therefore playing a major role in determining physical and chemical properties of bone mineral, such as solubility and crystal size. Raman peak at 1070 cm^{-1} is assigned to $\nu_1(CO_3)$ vibrational mode.

3. Materials and Methods

In this research, a fragment of an archaeological human femur (sample 156F) was analysed; it belongs to a set of human bone samples collected during the excavation of 16D4 archaeological site, conducted within the "El Salha archaeological project" (Usai and Salvatori, 2005; Usai and Salvatori, 2007; Salvatori and Usai, 2009; Usai et al., 2010; Salvatori et al 2011). The site is located in central Sudan, on the western bank of the White Nile, about 20 Km south of Khartoum. Along almost the entire Holocene, the site was used several times as burial ground, thus multiple burial phases have been identified and a total number of 190 graves were brought to light. The bone fragment used in this study was sampled from grave 156, belonging to the oldest burial phase found in the site, the pre-Mesolithic, and dated to the early Holocene (Usai et al., 2010). Histological and micro-morphological (Dal Sasso et al., 2014-a) and FTIR study (Dal Sasso et al., in prep – Chapter 2) on pre-Mesolithic bones revealed a complex sequence of diagenetic events, related to palaeoenvironmental and burial conditions, that produced several alteration features: microscopic focal destruction due to bacterial and fungal activity, collagen loss, deposition of secondary mineral phases such as calcite and Mn and Fe oxides, mineral dissolution and bioapatite recrystallization have been detected. The sample analysed in this study was selected as representative of the pre-Mesolithic burial phase, in terms of types and extent of diagenetic alteration, as well as for the presence of apparently unaltered portions, the entirety of which can be tested by μ-Raman spectroscopy. The cortical part of a modern human rib was for comparison also analysed, under the same experimental conditions.

Even if no sample preparation is required for μ-Raman spectroscopy analysis, in order to compare results with other spatially resolved analysis and to easily identify features of the bone tissue microstructure and their relation with diagenetic alteration patterns distribution, minimal sample preparation was adopted. Bones where traversal sectioned using a low-speed micro-drill equipped with a diamond saw. While cutting, attention was paid in order to avoid over-heating of samples.

Sections were then polished using 1000, 2500 and 4000 grit sandpaper on a rotating stage with water as lubricant, and subsequently 1µm diamond suspension on a polishing cloth. Samples were finally cleaned in ultrasonic bath for few minutes and dried in oven at 40°C.

µ-Raman spectroscopy analysis was carried out with a DXR Thermo Scientific Raman microscope, equipped with a frequency-stabilized single mode diode 780 nm laser. This laser wavelength was chosen to reduce sample fluorescence effects, but still maintaining a high spatial resolution and Raman scattering efficiency (Smith and Clark, 2004). Acquisitions were carried out with a laser power of 20 mW, spectrograph aperture of 25 µm pinhole and using a 10x objective, thus providing a spectral resolution in the range 4-8 cm^{-1} and a spatial resolution of 3 µm. Rectangular areas of 110x75 µm (50x30 µm for the modern sample) were raster-scanned in a grid of points with a step size of 5 µm. For each spectrum 128 scans (4 sec of acquisition time each) were acquired in the range from 100 to 2200 cm^{-1}. Spectral analysis was performed using Omnic 9 software (Thermo Scientific); statistical treatment of data was then performed using Statgraphic Centurion XVI software package.

Several parameters can be calculated from Raman spectra in order to semi-quantitatively define chemical composition and structure of bone material as well as to monitor the effects of diagenetic alteration and the occurrence of secondary phases (Pucéat et al., 2004). In µ-Raman maps, each probed point correspond to a spectrum, from which, therefore, more parameters can be calculated, and a new map, representing the spatial distribution of parameter values can be created. In order to monitor the preservation state of bone, parameters related to the collagen content (Amide I/ PO_4), the carbonate content (CO_3/PO_4) and crystallinity of bioapatite, the amount of secondary calcite (Cal/PO_4) and Mn oxide (Mn/PO_4) precipitated during diagenesis were calculated. Amide I/ PO_4 was obtained dividing the peak intensity of the Amide I band at 1668 cm^{-1} by the peak intensity at 961 cm^{-1} assigned to the $\nu_1(PO_4)$ vibrational mode. CO_3/PO_4 was calculated dividing the intensity of the band at 1070 cm^{-1} ($\nu_1(CO_3)$ vibrational mode) by the peak intensity of phosphate at 961 cm^{-1}. In Raman spectroscopy, peak broadening is determined by the contribution of the actual crystallite size and atomic order/disorder of the analysed sample (small crystallite size and atomic disorder produce broader peaks; Pucéat et al., 2004); since this technique cannot differentiate between these two contributions, crystallinity can be indirectly monitored measuring the full width at half maximum (FWHM) of the phosphate 961 cm^{-1} peak. Since FWHM is inversely proportional to crystallinity, high FWHM values correspond to low crystallinity, thus indicating smaller crystallites and/or higher atomic disorder. The presence of secondary calcite can be easily detected by Raman spectroscopy (Fig. 1b), since calcite shows a strong intense peak at 1085 cm^{-1}, assigned to $\nu_1(CO_3)$ vibrational mode (Gunasekaran et al., 2006), that can be used to monitor its occurrence within the

sample: Cal/PO_4 parameter was here calculated by dividing the peak intensity at 1085 cm^{-1} by the peak intensity at 961 cm^{-1} of phosphate. Mn oxides show a very broad band from 800 to 400 cm^{-1}; since in this region also phosphate and carbonate bands are located, in order to avoid band overlapping, the Raman shift at 660 cm^{-1} was selected to calculate Mn/PO_4, which was obtained dividing its intensity by that of the phosphate peak at 961 cm^{-1}. All these parameters were established as intensity ratios in order to ensure a reliable comparability of results. Even if Raman peak intensity is proportional to the count of scattered photons, when analysing massive samples intensity variations may be caused by other uncontrolled variables (i.e. sample surface morphology), given the same experimental conditions. Despite this, the intensity of the 961 cm^{-1} peak was select as a parameter correlated to bioapatite density (BD), in order to monitor its distribution; its reliability will be discussed later on. The baseline used to calculate band intensities was defined by two points calculated as the local minimum in the region 1900-1700 and 1630-1500 cm^{-1} for the 1660 cm^{-1} band, 1200-1100 and 930-800 cm^{-1} for the 1085, 1070 and 961 cm^{-1} bands, 930-800 and 400-200 cm^{-1} for the 660 cm^{-1} band.

4. Results

4.1 The archaeological sample

The archaeological bone sample 156F was investigated in three different areas (Fig. 2, 3 and 4) along the transverse section (areas A, B and C). Areas A (Fig. 2a) and B (Fig. 3a) both cover a fraction between two osteons, from the Haversian canal to the outer margin, and part of interstitial lamellae: these two areas were selected among the best preserved areas of the section, as extensive bacterial attack caused a severe destruction of bone microstructure on large areas of the section. Haversian canals are completely filled in with secondary calcite. Area C covers a bone portion between three osteons, comprising the external part of osteons and interstitial lamellae; here Mn oxides were detected (dark brown spots in the microscope image of Fig. 4a). All the μ-Raman maps revealed a complete collagen loss, as bands associated to Amide I, CH_2 and Amide III were never detected in these area, instead observed in the modern bone sample (Fig. 1a, Fig. 5c). For this reason, Amide I/ PO_4 was not calculated for the archaeological sample.

The spatial distribution of bioapatite density (BD) (Fig. 2b, 3b and 4b) partially reflects bone microstructure, as slightly higher values are registered for the outermost part of osteon and interstitial bone tissue. BD lower values were observed in those portions in which microporosity, due to bacterial activity (Fig. 2b coordinates 70,70 and 30,100), or secondary mineral phases, such as calcite (Fig. 2b, right-top) and Mn oxides (Fig. 4b, left-bottom and right-top) occur. Crystallinity

and carbonate content of bioapatite were monitored with FWHM and CO_3/PO_4 parameters, respectively. Since each map is scaled on the basis of the range of values measured during the experiment, in order to facilitate the comparison between results acquired in the different areas, the frequency distribution of these values (FWHM, CO_3/PO_4) were plotted for each map (Fig. 6). Areas A (Fig. 2c) and B (Fig. 3c) show similar FWHM values, ranging from 13.8 to 14.7 (Fig. 6); quite homogeneous value distribution is observed, with slightly higher values (lower crystallinity) for interstitial bone tissue with respect to those for the osteon. More variability is detected for area C (Fig. 4c): overall higher values, ranging from 14.2 to 15.5, are observed for most of the investigated area, while two small portions are characterised by values ranging from 15.5 to 17.3 (Fig. 6). These latter portions are also characterized by lower BD values (Fig. 4b) and the occurrence of Mn oxides (for Mn/PO_4 values higher than 0.1 in Fig. 4e) and by the lowest CO_3/PO_4 values (Fig. 4d) registered among the three areas (Fig. 6). Beside these low values, in all the rest of this area (Fig. 4d), as well as in the other ones (Fig. 2d, 3d), CO_3/PO_4 values ranging between 0.16 and 0.20 (Fig. 6) are homogeneously distributed among the bone tissue section. Minimal variations towards higher values can be observed in areas A (Fig. 2d) and B (Fig. 3d) in those portions where higher FWHM values were registered. High values (greater than 0.2) observed in area A (Fig. 2d), on the right-top of the map, are due to occurrence of calcite, since the 1070 cm^{-1} peak is overwhelmed by the 1085 cm^{-1} peak of calcite. Secondary calcite was detected in areas A and B, while completely lack in area C. Besides occurring in the Haversian canal (Fig. 2e, right-top), calcite was also detected along the osteon microstructure, decreasing in concentration moving from the Haversian canal towards the osteon outermost part. This effect is more evident when considering spectra acquired along a profile (Fig. 3e and 3f), in which the 1085 cm^{-1} peak of calcite is detected up to 80 μm from the Haversian canal.

4.2 Modern sample

The area investigated on the modern bone section covers part of a Haversian canal and interstitial bone tissue (Fig. 5a). The organic fraction on bone material was easily detected and Amide I/ PO_4 was in this case calculated: slightly variations were observed (Fig. 5c) for his parameter, with higher values recorded in the outermost part of osteon. BD values are highly variable (Fig. 5b), ranging from 110 to 260, with higher values in the innermost part of osteon and interstitial bone tissue. FWHM values, always higher than in the archaeological bone, range from 16.7 to 17.5 (Fig. 6), showing slightly lower crystallinity in the proximity of the Haversian canal (Fig. 5d). CO_3/PO_4 values ranges from 0.20 to 0.24 (Fig. 6), with lower values in the innermost portion of the osteon.

Results obtained by µ-Raman maps for these parameters on the modern bone sample are in good accordance with literature data in biomedical field (Ascenzi et al., 1977; Paschalis et al., 1996). These authors proved that the parameters they calculated, and that can be considered equivalent to Amide I/ PO_4 and CO_3/PO_4 here considered, increase from the osteon edge to the Haversian canal, while crystallinity decreased.

5. Discussion

µ-Raman spectroscopy revealed several types of alteration on the analysed archaeological bone, due to diagenetic processes encountered during burial. The most evident alteration is the complete collagen loss, as none of the characteristic collagen Raman bands was detected among the analysed areas. Collagen loss is mainly due to chemical hydrolysis, alteration of the mineral fraction and microbial degradation of bone (Hedges, 2002; Collins et al., 2002): these processes are mainly driven by climatic and local burial conditions, in particular temperature and pH of soil solution. Chemical hydrolysis is particularly effective when occur high temperature and extremes pH values, alkaline in particular, in the burial environment. Moreover, the exposure of collagen to pore solution and to microbial enzymes, caused by bioapatite dissolution or recrystallization, favour collagen degradation. In turn, bioapatite recrystallization is favoured by collagen loss, as nanocrystals come into contact with the burial environment, becoming more susceptible to alteration. In this case, since microbial attack was extensively detected among bone section and an alkaline burial environment was hypothesized, due to the presence of secondary calcite precipitated in bone micro-pores (Dal Sasso et al., 2014-a), collagen loss is probably due to combined contribution of both chemical hydrolysis and microbial degradation of bone.

After the death of the individual, taphonomic and diagenetic processes promote bioapatite recrystallization: bioapatite nanocrystals tend to recrystallize (presumably with Ostwald ripening process – Ostwald, 1897) into a more thermodynamically stable crystal structure, characterised by a higher atomic order, increased crystal size and reduction of specific surface area (Berna, 2004; Nielsen Marsh and Hedges, 2000; Hedges, 2002). Recrystallization implies also the depletion of carbonate ions, as their occurrence in bioapatite crystal structure has been proven to increases the atomic disorder, inhibit crystal growth and increase solubility (Wopenka and Pasteris, 2005). The significant variability of recrystallization degree observed among archaeological and fossil bone samples coming from different sites is assumed to be caused by the contribution of several factors, mainly related to environmental and local burial conditions (i.e. soil composition, pore-water chemistry, temperature, moisture, etc.) as well as to pre-burial activities/treatments (i.e. defleshing, boiling or burning). In this case study, minimal variation in bioapatite crystallinity is observed:

areas A and B show slightly higher crystallinity within the osteon, with respect to interstitial bone tissue. At the same time, portions showing higher crystallinity register lover carbonate content, thus as expected when bioapatite recrystallize. Area C, covering the outermost portion of osteons and interstitial bone tissue, shows homogeneous crystallinity, in average slightly lower than that observed in areas A and B, as well as carbonate content (Fig. 6). No variations were detected in relation to bone microstructure, with the exception of the areas in C (Fig. 4c) where Mn oxides occur (Fig. 4e). Here, lower crystallinity and lower carbonate content are observed. On the basis of these data, interpretation may be ambiguous, however a conceivable explanation may be the weakness of the bioapatite signal (observed as lower intensity of Raman peaks) due to the simultaneously occurrence of secondary phases, such as Mn oxides. Despite these observations, when comparing crystallinity and carbonate content with the modern bone sample (Fig. 6), variation of FWHM and CO_3/PO_4 values from the modern to the archaeological samples is much higher than the minimal intra-sample variability observed in areas A, B and C. In particular, bioapatite of archaeological bone is definitely more crystalline and with a lower content of structural carbonate. This result highlights the fact that, at least in this case, despite the heterogeneity of bone tissue microstructure as well as of the in vivo composition and structure of bioapatite, major effect of recrystallization is observed at a higher scale level than the microscopic one as analysed by µ-Raman spectroscopy. As shown by these results, bioapatite recrystallization does not selectively occur for specific microstructural/histological features but extensively affect bone as a whole (or at least at the macro-scale level). Moreover, as crystallinity and carbonate content of bioapatite

Variability of the peak intensity of phosphate at 961 cm^{-1} (BD values) may be associated to variations in bioapatite density. Comparison of absolute values, also within the same analysed area, may be hazardous, since BD this is not a normalised parameter. Nevertheless, bone microstructure features are quite clearly identified also considering this parameter. BD can be a valuable tool for a preliminary screening of bone samples in order to detect and monitor the distribution of diagenetic micro-porosity and secondary phases.

Secondary calcite, precipitated within bone micro-porosity, was easily detected by the Raman peak at 1085 cm^{-1}, used to calculate Cal/PO_4 parameter. Calcite was observed not only within the Haversian canal, as also detected at the scanning electron microscopy (SEM) by Dal Sasso et al. (2014), but also within the bone tissue, as calcite permeates osteons up to 80 µm from the Haversian canal, presumably filling in the nano-porosity between bioapatite crystallites. Further investigation on this intimate association between calcite and bioapatite with other analytical technique may lead to a more complete understanding of bioapatite preservation in terms of chemical and isotopic

composition, in order to assess if ionic and/or isotopic exchange between the two mineral phases may have occurred.

Differences between the archaeological and the modern bones, in terms of variations in the above discussed parameters, can supply information on the preservation state of the archaeological bone. The complete loss of organic matter and the extent of bioapatite recrystallization indicate a poor preservation of bone tissue, even in portions less affected by microbial alteration, such as those on which the μ-Raman mapping was performed. Moreover, the quite homogeneous bioapatite recrystallization degree and the complete collagen loss observed in all the analysed areas suggests that these kinds of alteration are the results of processes that extensively affect bones at a larger scale level than the microscopic one investigated with this analytical technique. On the contrary, secondary mineral phases deposition is localised at the micro-scale level, with concentration gradients among bone microstructure. Deposition presumably occurs along microstructural trails within bone tissue such as the micro-porosity of the vascular system (as calcite in osteons) or micro-fractures, porosity and nano-porosity generated during diagenesis (Dal Sasso et al. 2014).

6. Conclusions

This research highlight the relevance of μ-Raman spectroscopy mapping on the study of bone diagenetic alteration, thus providing valuable spatially-resolved information on the preservation state of archaeological bone at the micro-scale. Reliable results have been obtained for qualitative analysis and phases identification. Moreover, the effectiveness of semi-quantitative analysis by the establishment of a set of parameters calculated on peak intensity ratio has been proved. The high spatial resolution of this technique enables one to precisely investigate the distribution of bone constituents and possible secondary phases, as well as bone material properties taking into account the heterogeneity of bone tissue itself. Moreover, when analysing diagenetic alteration at the micro-scale, the different effect of this process and its variability within the sample contribute towards the understanding the extent of diagenesis, which can be modelled in detail. Finally, the minimal (or none) sample preparation required and the easy and fast data acquisition process, make this technique extensively applicable as a screening method in the characterization of the preservation state of archaeological bones and in the identification of the better preserved (less altered) portions within a sample, on which performing possible further investigation, such as isotope analysis.

Fig.1

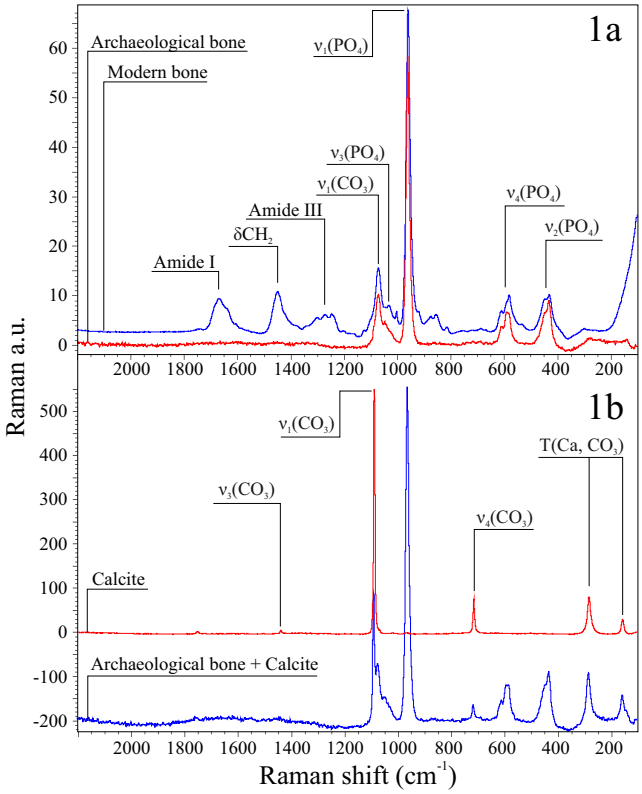

Fig.1. 1a. Representative Raman spectra of modern and archaeological (sample 156F) bone. Bands attribution is reported; 1b. Raman spectrum of pure calcite and calcite associated to the archaeological bone (156F).

Fig.2

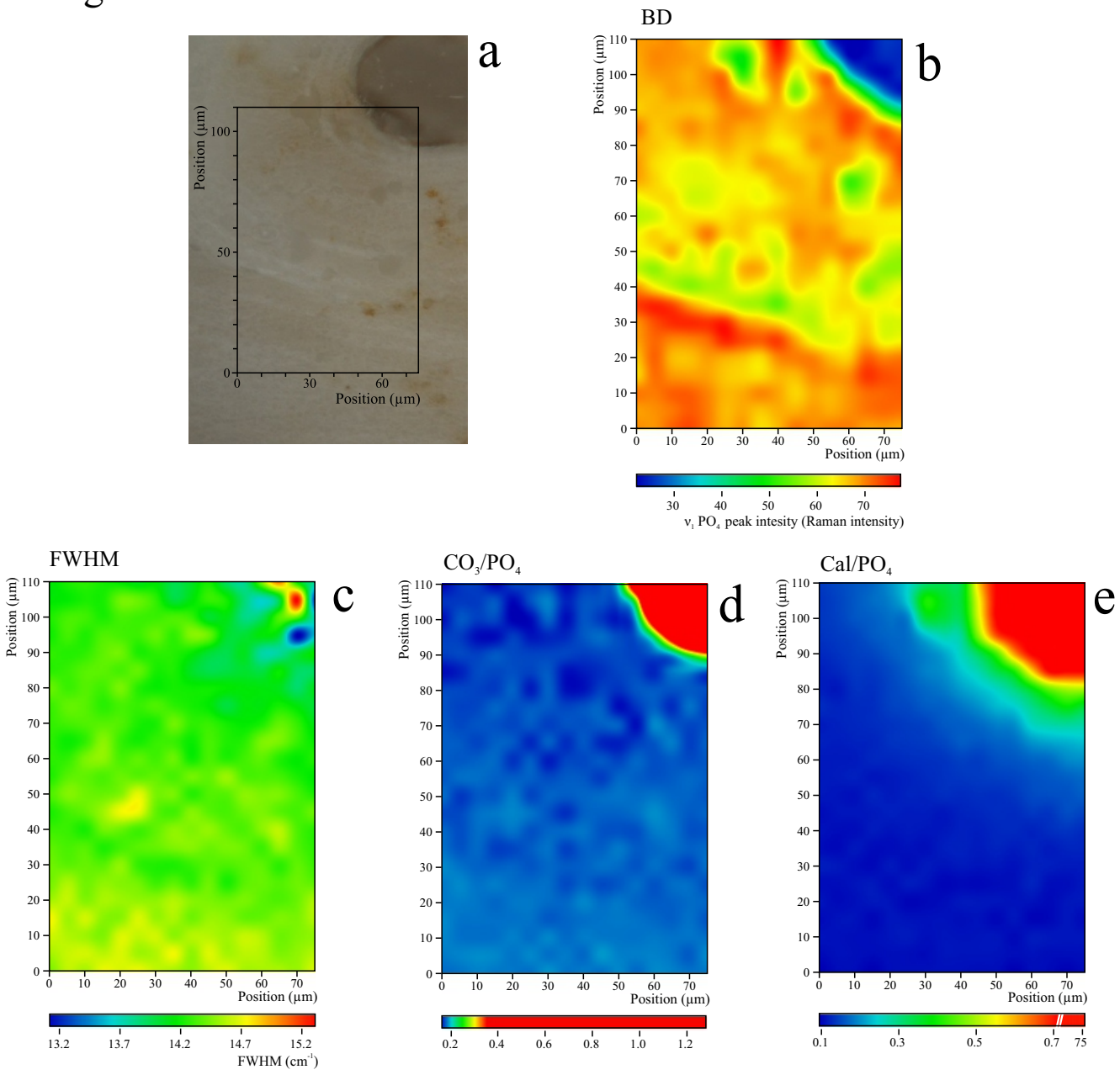

Fig.2. 2a. Sample 156F, area A (optical microscopy); µ-Raman map showing the spatial distribution of the 2b. Bioapatite density parameter BD; 2c. FWHM of the 961 cm^{-1} peak (which is inversely proportional to crystallinity); 2d. CO_3/PO_4. parameter, related to the structural carbonate of bioapatite; 2e. Cal/PO_4 parameter related to the content of secondary calcite.

Fig.3

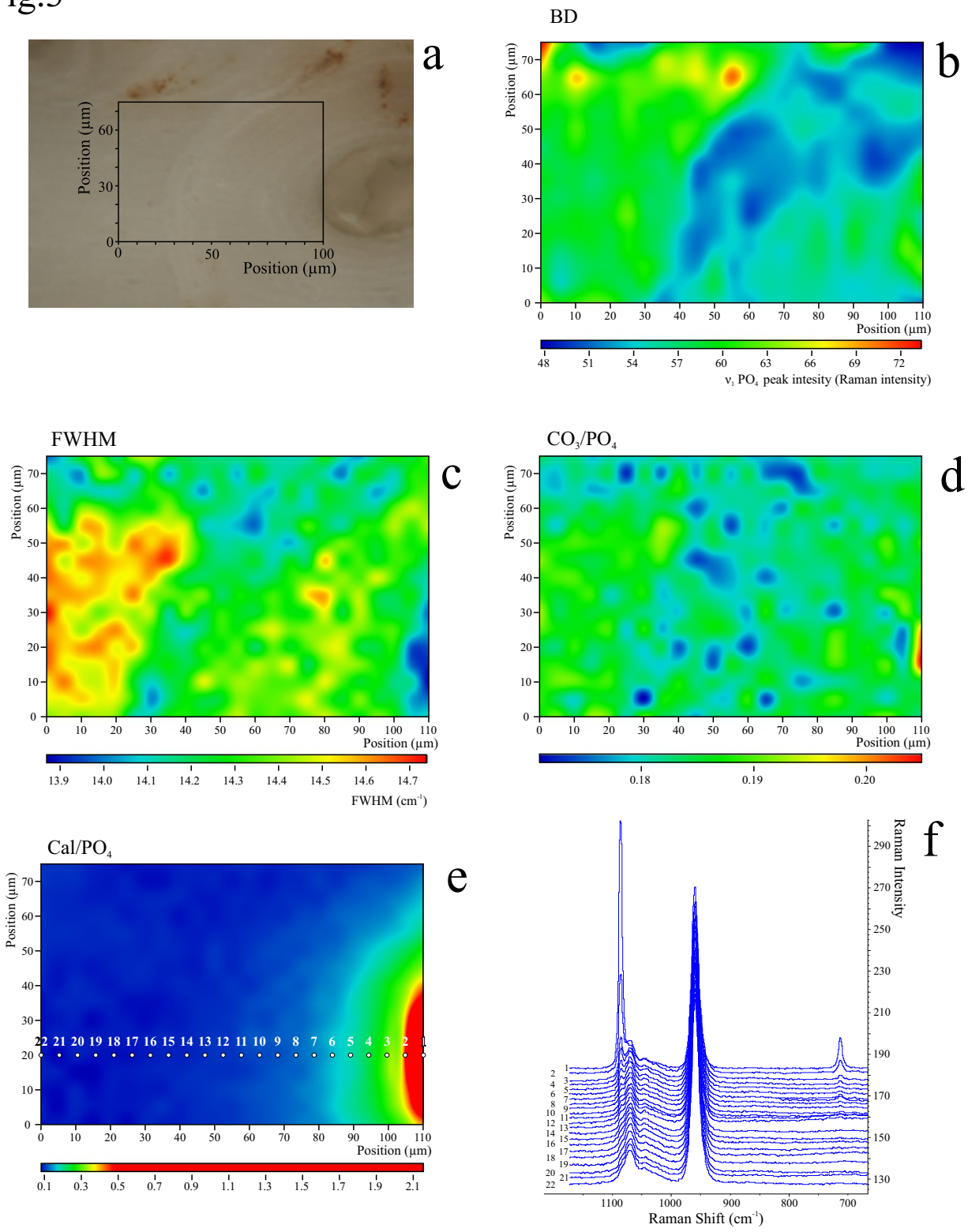

Fig.3. 3a. Sample 156F, area B (optical microscopy); µ-Raman map showing the spatial distribution of the 3b. Bioapatite density parameter BD; 3c. FWHM of the 961 cm^{-1} peak (which is inversely proportional to crystallinity); 3d. CO_3/PO_4. parameter, related to the structural carbonate of bioapatite; 3e. Cal/PO_4 parameter related to the content of secondary calcite. 3f. Raman spectra acquired along the profile shown in 3e from the Haversian canal towards the edge of the osteon.

Fig.4

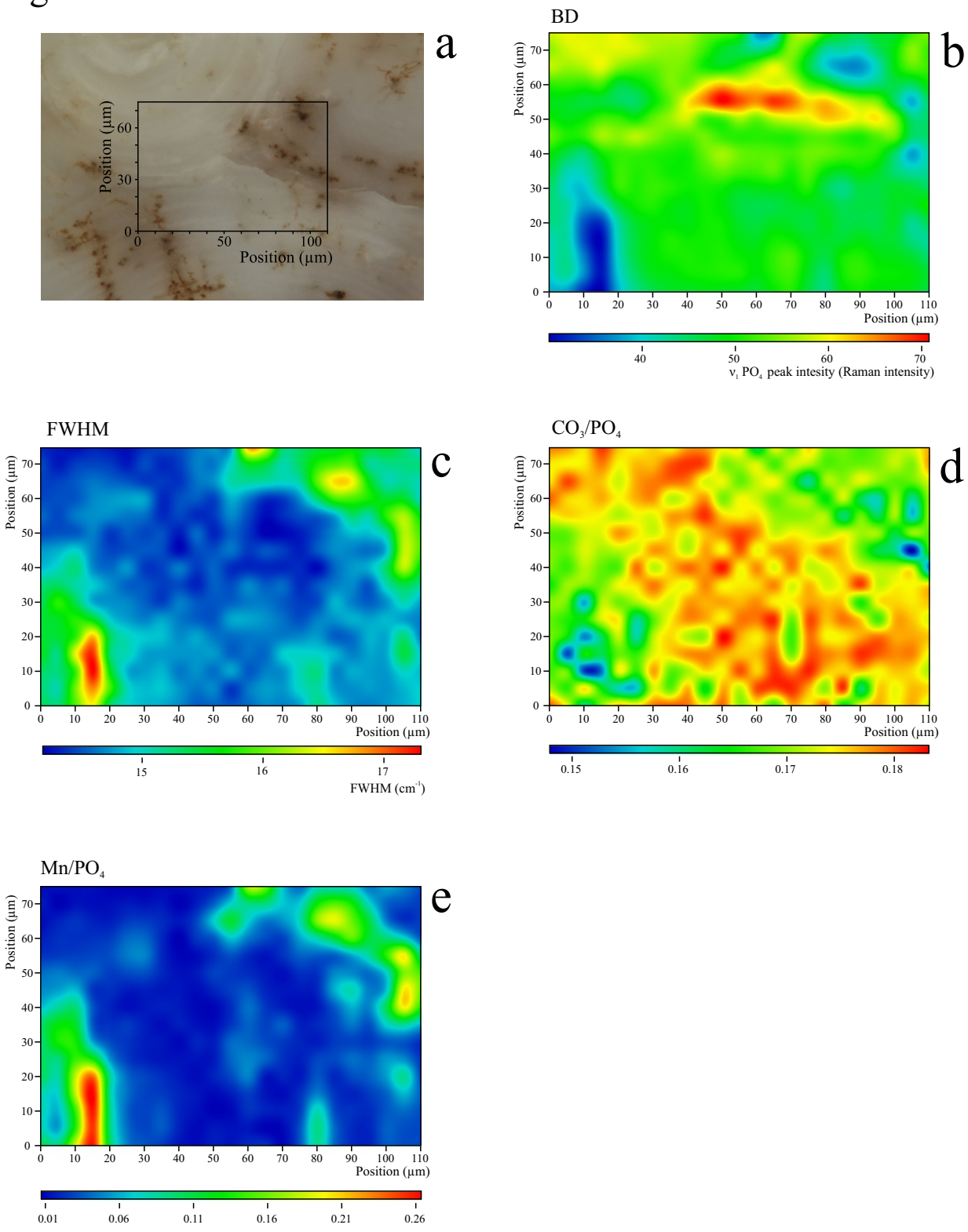

Fig.4. 4a. Sample 156F, area C (optical microscopy); µ-Raman map showing the spatial distribution of the 4b. Bioapatite density parameter BD; 4c. FWHM of the 961 cm^{-1} peak (which is inversely proportional to crystallinity); 4d. CO_3/PO_4. parameter, related to the structural carbonate of bioapatite; 4e. Mn/PO_4 parameter related to the content of secondary Mn oxides.

Fig.5

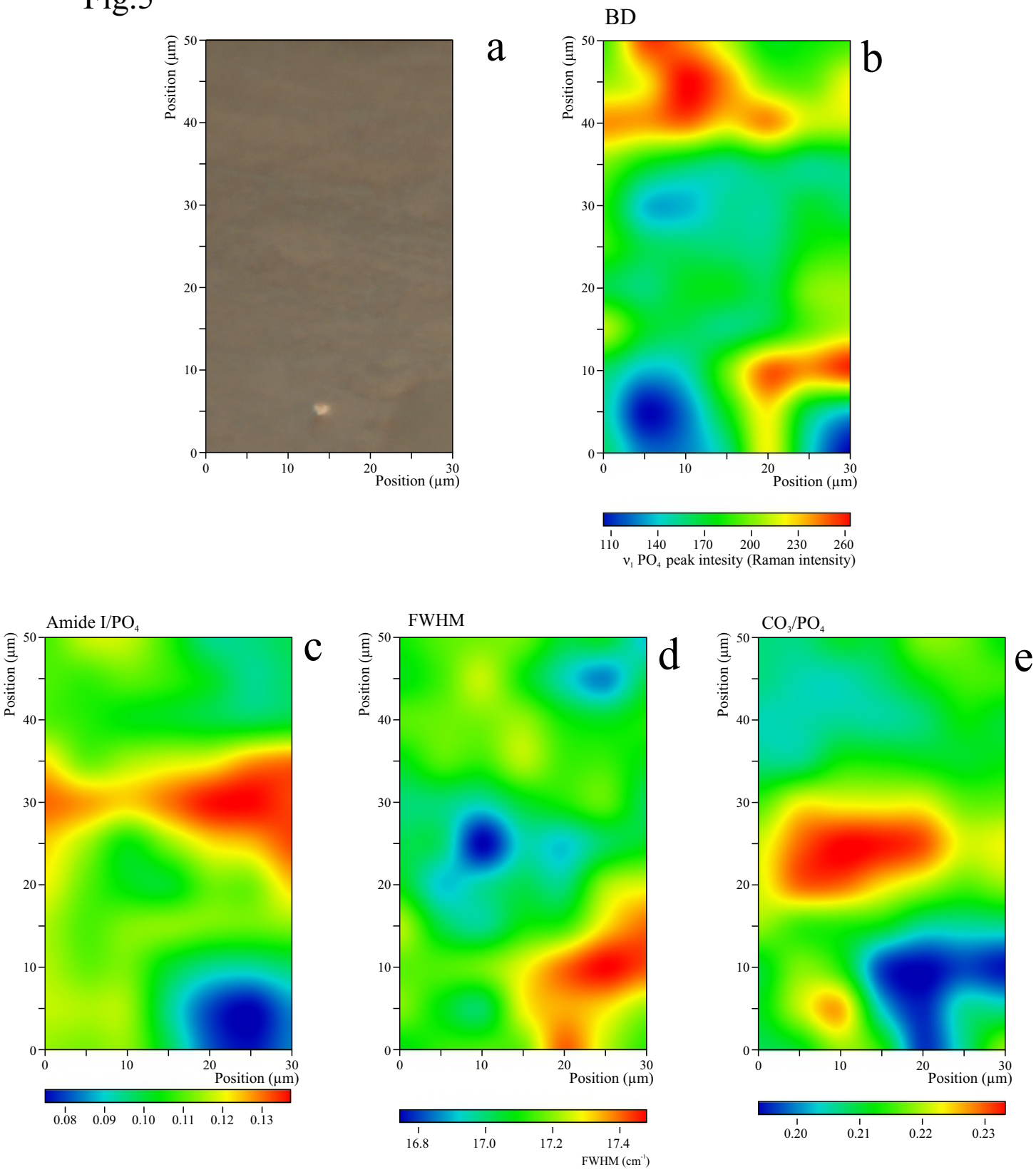

Fig.5. 5a. Modern bone sample (optical microscopy); µ-Raman map showing the spatial distribution of the 5b. Bioapatite density parameter BD; 5c. Amide I/PO_4 parameter related to the collagen content; 5d. FWHM of the 961 cm^{-1} peak (which is inversely proportional to crystallinity); 5e. CO_3/PO_4. parameter, related to the structural carbonate of bioapatite;

Fig.6

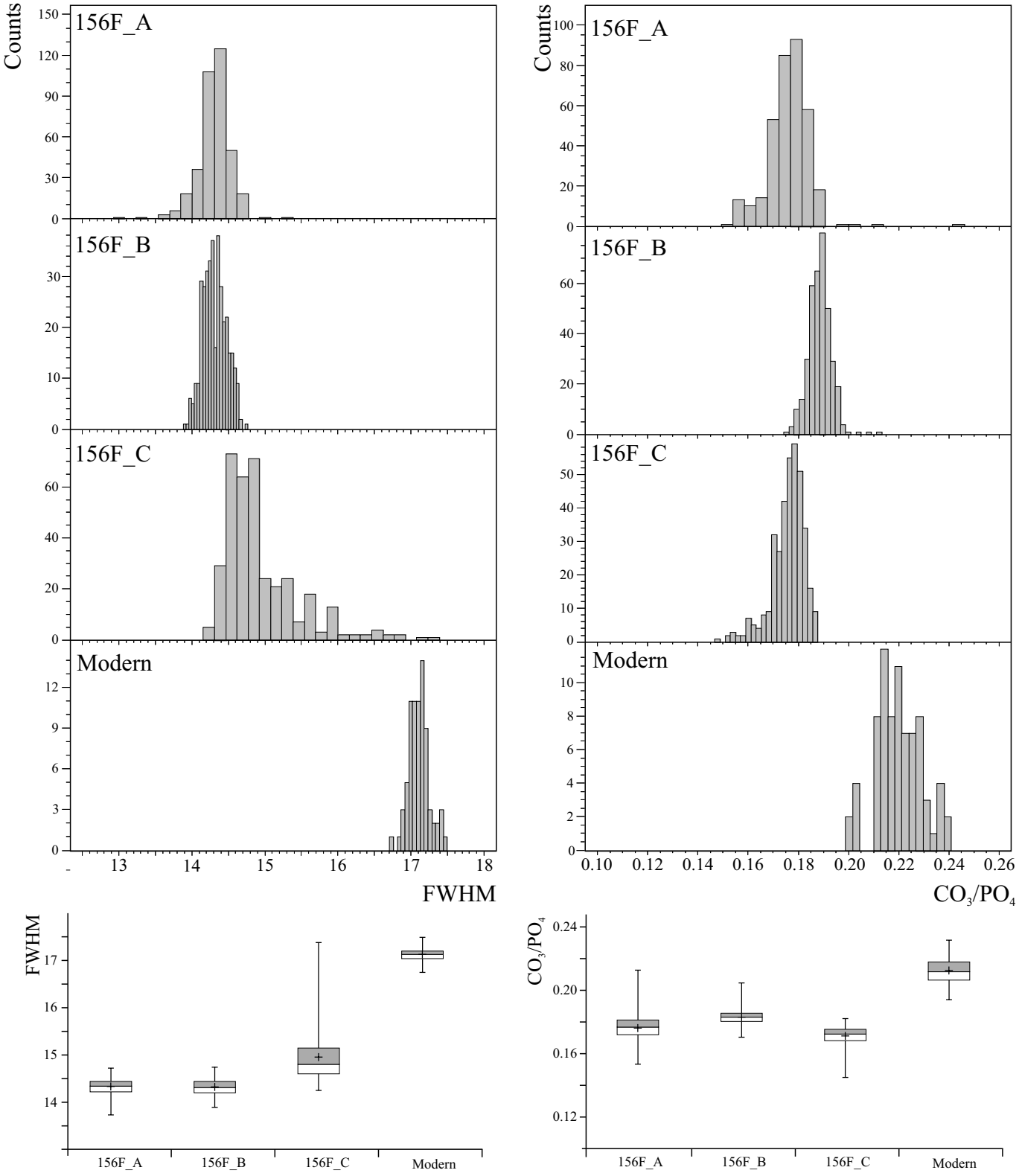

Fig.6. Frequency distribution of FWHM and CO_3/PO_4 values acquired for three areas of the archaeological sample 156F (156F_A, 156F_B, 156F_C) and for one area of the modern sample.

CHAPTER 5

Calcrete pedogenesis and interaction with anthropic activity at Al Khiday (Khartoum, Sudan): a multi-analytical approach to timing the calcrete development

1. Introduction

Pedogenic calcrete refers to a near-surface terrestrial accumulation of predominantly calcium carbonate, resulting from the introduction and cementation of calcium carbonate into a soil profile in different forms, i.e. powdery, nodular, laminar or massive (Wright, 2007). It often occurs in areas where vadose and shallow phreatic groundwater is saturated with respect of calcium carbonate. This general definition is applied to a large variety of calcitic horizons at different stages of development, abundantly occurring worldwide, at different latitudes and within different geological contexts. However, the majority of calcitic soil horizons are developed in arid and semi-arid regions. General assumption is that calcrete develops in soils, in which the circulating fluids (vadose and shallow phreatic groundwater) are saturated in calcium carbonate and, at the same time, are characterised by a net moisture deficit. Calcite accumulation is promoted by several physical-chemical processes as well as by biological-mediated processes (Cailleau, 2011), which, in turn, are influenced by climatic conditions.

In this research, a multi-analytical approach, consisting in the mineralogical, micromorphological, and geochronological analysis, was applied to the study of pedogenic calcrete from Central Sudan, in order to contribute towards the understanding dynamics and ages of its formation and development. Calcrete analysed in this study comes from a localised small area along the western bank of the White Nile, few km south of the Khartoum-Omdurman urban system (Fig. 1), selected within a large, multiphase archaeological site (currently under excavation), which is in tight relation with calcrete. Part of the vestiges of the site (pre-Mesolithic burials) is, in fact, englobed in the calcitic crust (Fig. 2a), whereas other features (Mesolithic pits, Meroitic graves) are clearly carved in the pre-existing carbonate horizon (Fig. 2b and 2c). This archaeological evidence, supported by detailed analytical studies both on the geomorphologic and palaeoenvironmental aspects (Zerboni, 2011; Williams et al., submitted), and on the anthropic activities during the wide span of time of occupation of the site, covering almost the entire Holocene (Usai and Salvatori, 2002; Usai, 2003; Usai and Salvatori, 2005; Salvatori and Usai, 2009; Usai et al., 2010; Salvatori et al., 2011; Salvatori, 2012; Dal Sasso et al., 2014a, 2014b) supply important information on the timing of calcrete formation. Therefore, results from calcrete samples analyses, coupled with this additional information, may contribute to a more complete understanding of processes involved in calcrete formation and development.

2. Study area and palaeoenvironmental setting

Calcrete horizon has been found during the archaeological excavation of site 16D4, carried out since 2006 within the "El Salha archaeological project" over an area of 1400 m^2 (Usai and Salvatori, 2002; Usai, 2003; Usai and Salvatori, 2005; Salvatori and Usai, 2009; Usai et al., 2010; Salvatori et al., 2011; Salvatori, 2012). The archaeological site is located on the western bank of the White Nile, near the Al Khiday village (Khartoum, Sudan), at 3.5 km from the present-day river course and about 22 Km south of its confluence with the Blue Nile (Fig. 1). It is set on a late Pleistocene sandy ridge, corresponding to the remnants of a longitudinal sandy river bar, at the limit of alluvial sediments deposited during the Holocene flooding of the White Nile (Zerboni, 2011). Archaeological excavation and geomorphological investigation (Usai et al., 2010; Salvatori et al., 2011; Zerboni, 2011) revealed a complex stratigraphy, resulting from anthropic activities, erosional and pedogenic processes for a wide span of time. The area had been used several times along almost the entire Holocene. A Mesolithic specialised use of the site was defined by the numerous pits (104) that have been excavated, characterised by different types of filling material and presumably with different functions (Zerboni, 2011), radiocarbon dated to 6700-6300 cal BC (Salvatori et al., 2011). In addition, the site was used several times as a burial ground; at least three different burial phases have been identified. The most ancient one, which chronology is still uncertain but surely pre-Mesolithic, is characterised by many individuals (at least 90) buried in a prone and elongated position. The chronology of this burial phase is constrained by the Mesolithic use of the area, as a number of skeletons (15) were found to be cut by radiocarbon- or archaeologically-dated Mesolithic pits (Salvatori et al., 2011), which indicate that the pre-Mesolithic burial phase is unambiguously older than 6700 cal BC. The site was subsequently used as a cemetery during the Neolithic period (38 graves; 4550-4250 cal years BC) and later on during the Meroitic period (43 graves, 50 cal years BC-250 cal years AD) (Salvatori et al., 2011; Usai et al., 2010).

Pre-Mesolithic burials, despite being the most ancient, are the most close to the present ground surface (10-20 cm deep), whereas the Meroitic graves are the ones excavated deeper from the current ground level. This is the result of intense erosional processes (mainly wind erosion) occurred between the first burial phase (pre-Mesolithic) and the subsequent use of the area. Evidence of wind deflation is still visible on the site surface, where the fine fraction of the archaeological deposit was removed and coarser fragments, such as stones, pottery, etc., are concentrated and accumulated.

Currently, the climate of the region is arid, with mean annual temperature ranging from 22 to 33 °C and average rainfall of ca. 130 mm (Elagib and Mansell, 2000). However, climate conditions were significantly different in the past and substantial climatic changes occurred at local and regional levels (Gasse, 2000; Nicoll, 2004; Williams, 2009; Williams and Jacobsen, 2011; Zerboni, 2013) during the wide span of time of use of the site (from the early Holocene to the beginning of the 1st millennium AD). In the early Holocene (9550-6050 cal years BC) the precipitation rate, and consequently also the environmental humidity, were higher, as well as the flooding level of the White Nile, due to a northward expansion of the Indian monsoon domain (Gasse, 2000; Williams, 2009). The formation of seasonal swamps in the surrounding area of the Al Khiday sites during the Mesolithic occupation of the area is attested by geoarchaeological and geomorphological evidence (Williams and Jacobsen, 2011; Zerboni, 2011). Since the middle Holocene (6050-1050 cal years BC), the progressive weakening of monsoon intensity led to rainfall decrease and overall reduction of water availability. In the late Holocene (since 1050 cal years BC), since the Meroitic period and later on, progressively drier environmental conditions occurred, up to the arid climate that now characterises central Sudan. In addition to this general trend, palaeoenvironmental records identified several periods of rapid climate changes during the early Holocene wet phase, when several short arid periods occurred (Williams, 2009).

The pedogenic processes responsible of calcrete formation and development are strongly dependent on water availability, which, in turn, depends on climate conditions; therefore the results obtained from the analysis of the studied samples will be discussed taking into account the variations of climate conditions along the Holocene, as attested by palaeoenvironmental studies.

3. Material and methods

The samples studied in this research come from a test trench, exposed in the sandy deposit and representing the local substrate, and brought to light during the excavation of a Mesolithic pit (pit number 151A). The section showed at least 70 cm of sand deeply cemented by calcium carbonate (calcrete). Six oriented and undisturbed calcrete blocks were collect, namely A1, A2, A3a, A3b, A3c and A3d, from the top to the bottom of the section (Fig. 3). A total of 9 samples (one for each block and an additional sample for A2, A3a and A3d blocks) covering the whole section were selected, englobed under vacuum in epoxy resin (Araldite 2020) and prepared in thin sections (3x5 cm). Micro-morphological analyses were carried out on thin sections by optical microscopy (OM), cathodoluminescence microscopy (CL) and scanning electron microscopy (SEM).

OM analysis was carried out with a petrographic microscope (Nikon Eclipse E660) under plane-polarized (PPL) and cross-polarized light (XPL). CL analysis was performed with a petrographic microscope (NIKON Labophot2-POL) equipped with a cold cathode stage (CL8200 MK3, Cambridge Image Technology Ltd) and operating at 15 kV and 200 mA. OM and CL images were acquired with a CANON Reflex EOS 600D. For SEM analysis, was used a CamScan MX 2500 coupled to a detector for Energy dispersive X-ray spectroscopy (EDS), equipped with a LaB6 cathode and operating at 20 kV and 160 nA. Thin-section description was done following the terminology proposed by Bullock et al. (1985) and Stoops (2003), and the interpretation mostly followed the concepts discussed in Stoops et al. (2010).

On the basis of micromorphological analysis of thin sections, samples were gently disaggregated in an agate mortar; distinctive calcitic pedofeatures along the calcrete section were mechanically and accurately separated by hand-picking under the stereoscopic microscope, and then radiocarbon dated by accelerated mass spectrometry (AMS) at the Center for Isotopic Research on the Cultural and Environmental heritage (CIRCE) laboratory (Terrasi et al., 2008). All AMS-^{14}C ages were calibrated according to the INTCAL13 dataset (Reimer et al., 2013) using the Calpal software (Weninger and Jöris, 2008). The method of multiple-group calibration was used to graphically represent and compare calibrated AMS-^{14}C ages (Weninger, 1986).

4. Results

4.1 Field description

The calcrete section, here studied, corresponds to the wall of the pit 151A, an archaeological feature radiocarbon dated to 6700-6300 cal years BC, during the Mesolithic use of the site. Calcrete horizon is established 30-50 cm under present soil level; the pedostratigraphic sequence includes a silty to sandy surface horizon, with very poor and initial evidence for pedogenesis, under which a thick sandy deposit occurs. The latter consists of medium to coarse sand, and sometimes including lenses of coarser grains (very coarse sand to small pebbles). It is interpreted as a fluvial deposits related to a Upper Pleistocene higher level of the White Nile (Zerboni, 2011). The calcitic horizon, up to 1 m thick, is nodular and can be interpreted as an early stage of calcrete development in soil profile (Machette, 1985; Wright, 2007), resulting from the illuvial concentration of calcium carbonate in a siliciclastic host material. Two main concentrations of calcium carbonate were identified. The upper part of the section, namely block A1, is constituted by quartz sand slightly cemented by calcium carbonate; calcite concentration within the sediments is detected as coalescent irregular calcitic nodules of few centimetres in diameter. A weakly cemented sandy lens,

corresponding to block A2, is interposed between the first and the second concentration of calcium carbonate; the latter corresponds to the lower part of the section, namely from A3a to A3d blocks. It is formed by cemented quartz sand and carbonate concretions, where calcitic nodules can be distinguished. Abundance of carbonate concretions as well as cementation increases with depth. From a pedological point of view, this evidence can be interpreted as a single calcrete, rather than a sequence of distinct calcitic horizons: in fact, calcrete developed on the same parent material, due to the same pedogenetic process.

The calcrete horizon, as observed in the whole archaeological excavation at 16D4, is at 30-50 cm depth from the current surface level, and it partially embeds the pre-Mesolithic graves (Fig.2a), whereas Mesolithic pits (Fig.2b), as well as graves belonging to successive burial phases (Fig.2c), are carved into it. Moreover, the lower part of most of the Mesolithic pits is characterized by filling material cemented by calcite, whereas some of them present a whitish and hard calcitic concretion englobing the archaeological materials. The origin of calcitic cement within archaeological feature, even if driven by similar environmental processes forming the calcrete, is thought to be due to the recrystallization of the abundant remains of Ca-rich ash originally constituting the infilling of pits (Zerboni, 2011). More recent archaeological materials, such as human bones of the Neolithic burials, were found to be permeated by secondary calcite, whereas Meroitic ones completely lack in this secondary phase (Dal Sasso et al. 2014).

4.2 Thin-section micromorphology

Thin sections of the blocks (A1 and A2) from the upper units show a groundmass with abundant sand- and silt-sized, sub-rounded to sub-angular in shape, quartz grains, with a bimodal grain-size distribution. The authigenic calcite is heterogeneously distributed among the sections giving to the slides a single- to double-spaced porphyric c/f (coarse/fine) related distribution, locally open porphyric or gefuric. Areas corresponding to the calcitic nodules, macroscopically identified, show a micromass mainly constituted by micrite and microsparite (Fig. 4a), much more abundant with respect to that observed for other portions of the poorly cemented samples (Fig. 4c). Allochthonous calcitic pedorelicts (Fig. 4b, 4k, 4l), well-rounded in shape and comparable in size with sandy quartz grains, are frequent. They are constituted by a micritic matrix stained by Mn and Fe oxides, and contain veins of sparitic to micro-sparitic calcite, generally occurring within this kind of nodules (Fig. 4k, 4l). Slides from the upper units also evidenced the occasional occurrence of wood ash (calcite pseudomorphs after calcium oxalate crystals; Canti, 2003), fish bone fragments and small charcoal. Anthropogenic features were observed in small localised areas of the thin section

(Fig. 4d), and possibly migrated from the infilling of the nearby Mesolithic pit, because of bioturbation. SEM analysis on calcitic nodules from these units revealed that the microsparitic groundmass is heterogeneous in terms of compositions an cementation degree: some areas are characterised by densely packed calcite crystals (Fig. 4e) with respect of other areas, where more sparce distribution of calcite crystals is observed (Fig. 4g). In other areas, calcite crystals occur within a clayey matrix (Fig. 4f). The great heterogeneity in the distribution of calcite crystals is detected also by CL, under which the microsparitic micromass appears with an orange luminescence, whose intensity is proportional to the density of calcite crystals (Fig. 4h). Poorly cemented areas are characterised by low luminescence due to scarcity or lack of calcite (Fig. 4i, 4j).

Thin sections from the lower unit (A3a, A3b, A3c, A3d) show areas characterized by slightly cemented quartz grains, sub-rounded to sub-angular in shape, and sand- and silt-sized, embedded into a micritic micromass (Fig. 5a). The distribution of mineral grains and calcite generally results in a single spaced to open porphyric, occasionally gefuric, c/f related distribution. Conversely highly carbonated areas (Fig. 5b, 5c), corresponding to older calcitic nodules englobed in the micritic micromass, are predominantly constituted by microsparitic calcite and quartz sand grains are extremely rare. Different textural pedofeatures were identified within calcitic nodules: some portions are characterized by well cemented calcite crystals forming clusters of sub-rounded to sub-angular shape, identifiable by OM (Fig 5b, 5c), CL (Fig 5d) and SEM (Fig 5e, 5f) analyses. These features are embedded in a matrix mainly constituted by calcite crystals similar in size, but less packed, sometimes associated to clay minerals. Moving to the bottom of the unit, the dimension of these calcitic clusters decrease and their margins, in contact with the surrounding matrix, are less defined (Fig. 5i). CL results show significant, but not systematic, luminescence variations of calcite crystals, both dispersed and well packed, along the section. In some cases homogeneously luminescent crystal were observed (Fig. 5g), in others the innermost part of crystals is less luminescent with respect to their margins and inter-grain cement (Fig. 5h). OM, CL and especially SEM images show an overall increase of calcite crystal size from the upper to the lower units. Allochthonous calcitic pedorelicts, sub-rounded in shape and impregnated by only Fe oxides (and not Mn and Fe-bearing oxides, as in the rounded ones identified in the upper unit) were observed in unit A3c and, less frequently, in unit A3d. Both the two types of pedorelicts show higher oxides concentration towards their margins and a thin layer of clay minerals coating the outer surface (Fig. 5j, 5k).

4.3 AMS-^{14}C dating

AMS radiocarbon dating was performed on different pedofeatures, identified by micro-morphologic analysis, and mechanically selected under the stereographic microscope. As for the upper units, allochthonous pedorelicts (A1-pedorelict) and calcitic nodules (A1-mt) from unit A1 were selected and dated. As for the lower unit, well cemented clusters identified in thin sections were found to be much more lithified than the surrounding powdery calcitic-rich matrix; therefore, three samples of cemented clusters (samples A3a-cl, A3c-cl and A3d-cl) and three samples of calcitic-rich matrix (samples A3a-mt, A3c-mt and A3d-mt) from blocks A3a, A3c and A3d were separated and dated. An old radiocarbon age, 27590 ± 440 cal years BC, was obtained for allochthonous pedorelicts (A1-pedorelict); well cemented clusters from blocks A3a, A3c and A3d show older ages (7670 ± 100, 7950 ± 580 and 9530 ± 240 cal years BC, respectively) with respect to the powdery calcitic-rich matrix from the same samples and from calcitic nodules of A1 block (4390 ± 80, 5970 ± 100, 5780 ± 80 and 4130 ± 240 cal years BC, respectively) (Tab. 1).

Table 1. ^{14}C ages, standard deviation (SD) and calibrated ages obtained on selected calcitic pedofeaures

Sample	^{14}C age	SD	2σ cal BC	2σ cal BP
A1-pedorelict	25439	153	28030-27150	29980-29100
A1-mt	5290	102	4370-3890	6320-5840
A3a-mt	5536	29	4470-4310	6420-6260
A3a-cl	8663	40	7770-7570	9720-9520
A3c-mt	7104	42	6070-5870	8020-7820
A3c-cl	8823	242	8530-7370	10480-9320
A3d-mt	6891	31	5860-5700	7810-7650
A3d-cl	10005	41	9770-9290	11720-11240

5. Discussion

5.1 Formation processes

The authigenic accumulation of calcium carbonate in siliciclastic host sediments suggests an external source for calcium carbonate. Conceivable sources may be identified in the geological bedrock of the area, as the limited quantity of calcite contained in the local sandstone and shales, is firstly dissoluted, then mobilized and finally re-precipitated thanks to circulating pore water. Further sources of carbonate may be represented by alkaline atmospheric dust, Nile overbank sediments, and, concerning the Holocene, anthropogenic calcitic ash, the latter being available only after the onset of pedogenetic processes related to the formation of calcrete. However, the most probable

source of calcium carbonate, forming calcrete horizon at 16D4 site, can be identified in Pleistocene sediments, highly cemented by calcium carbonate and heavily affected by pedogenesis. Evidence of this type of paleosols, occasionally outcropping in the region, can be found few hundreds of meters west from the 16D4 site. Here, dissolution and mobilization of calcium carbonate may have occurred during wet environmental phases by shallow groundwater. Moreover, these Pleistocene sediments are also the most probable source of allochthonous pedorelicts (those separated from block A1 dates to the 27590 ± 440 cal. BC) identified in the calcrete section. In fact, pedorelicts possibly derive from surface transportation, as suggested by their sub-rounded to rounded shape and the occurrence of clayey material adhering to their external surface, interpreted as a rolled pedofeature (Boschian, 1997; Zerboni, 2011).

Calcrete nodules are formed by accumulation of microcrystalline calcite; the small size of crystals suggests a relatively fast precipitation of calcite, associated with high evaporation rates. In this case, the contribution of microbially induced calcite precipitation is assumed to be minimal, as micromorphological features characteristic of biological activity (Newman et al., 1997; Richter et al., 2008) were not observed. The upper units are characterized by weak cementation and nodules are formed by microcrystalline calcite impregnating sand- and silt-size quartz grains. The lower unit shows a significant increase in accumulation of calcium carbonate and larger nodules. Occurrence of very few quartz grains within nodules, much more dispersed in the microsparitic groundmass with respect to those observed in less cemented portions of the sample, may indicates a displacive calcite crystal growth (Armenteros, 2009). Moreover, higher permeating cementation of sediments was observed in this unit. This may represent a subsequent development stage of calcrete horizon; however, features characteristic of subsequent stages observed in more developed calcrete profiles (Wright, 2007) here are lacking, thus suggesting an overall low development stage for this calcrete horizon.

Cathodoluminescence of carbonates, in terms of colours and intensities, is mainly induced by the occurrence, in trace quantity, of Mn^{2+} and Fe^{2+} in the calcite crystal structure, which, in turn, is related to geochemical conditions during crystallization. Therefore, even if only qualitatively, luminescence variations of calcite crystals observed in CL images indicates variations in chemical composition and/or redox conditions during precipitation and subsequent recrystallization (Hiatt and Pufahl, 2014). These data, coupled with information on the diachronic interaction between calcrete horizon and archaeological records, indicate that calcrete formation and subsequent development is a long-lasting process, acting at least in the Early and Middle Holocene.

5.2 Timing of calcrete

Radiocarbon dating of calcrete is not a routinely performed type of analysis, even if some studies are reported in literature (Achyuthan et al., 2010; Vogel and Geyh, 2008; Deutz et al., 2002; Geyh and Eitel, 1998; Wang et al., 1996). In fact, ^{14}C dating of calcite forming calcrete horizon might not lead to a straightforward interpretation of results. When calcite precipitates, its ^{14}C activity is in equilibrium to that of circulating pore water, which, in turn, may not be in equilibrium with atmospheric CO_2, due to the so defined "reservoir effect". This can cause an overestimation of the actual age of calcium carbonate. Moreover, when dissolution and recrystallization occurs, ^{14}C activity of former calcite is then superimposed to that of the new-generated calcite, in equilibrium with pore water circulating at that time (Geyh and Eitel, 1998).

Despite these difficulties, in this case study, the well-defined geomorphological, palaeoenvironmental, as well as the archaeological contexts provide valuable information in order to estimate the consistency of radiocarbon ages on calcrete samples. Moreover, some of these issues can be overcome by the very low amount (~ 10 mg) of sample required by AMS-^{14}C dating, enabling one to apply an accurate sampling strategy on small portions of the sample. In this case, we assume as minimal the reservoir effect, because circulating pore water is more conceivably provided by the White Nile flooding and, during early Holocene, rainwater rather than fossil groundwater. Moreover, the superficial location of the calcrete horizon may suggest equilibrium condition with atmospheric CO_2 due to interaction with vegetation and/or microbial activity during calcite precipitation (Cerling, 1984; Deutz et al., 2001). However, the main issue that have to be taken into account when dealing with radiocarbon determinations on pedogenic calcite is the overprinting effect, which is not negligible (Deutz et al., 2002). Calcrete forms over time as results of subsequent dissolution and reprecipitation processes, thus ^{14}C activity is time averaged and determination of the time of actual onset of calcite precipitation may be hazardous. In fact, calcrete can be reasonably considered an open system when environmental condition that promotes calcite dissolution and reprecipitation occurs. However, when changes in environmental conditions lead to the interruption of calcrete development, a closed system can be hypothesised. Therefore, radiocarbon ages of calcrete samples reasonably indicate the interruption of calcite recrystallization; this may provide valuable information on the timing of calcrete development. For these reasons, radiocarbon ages cannot be used to determine a stratigraphic sequence of calcrete formation, given the complexity of this process. However, micro-sampling should minimize the artificial homogenization of different generation of calcite, and radiocarbon ages may provide reliable information on the long-time scale calcrete evolution, even if single ages may be still partially affected by time-averaging effect.

The method of multiple-group calibration (Weninger, 1986; Weninger and Jöris, 2008) was here used to represent radiocarbon ages, in order to discern if close radiocarbon ages might refer to the same or different events as well as to ease the comparison with other radiocarbon age datasets. Results were compared with those obtained on fossil shells and calcitic deposits and indicating the late Quaternary high flown levels of the White Nile (Williams, 2009), radiocarbon dating defining the chronology of Holocene human occupation at the archaeological site of Al Khiday (Salvatori et al., 2011).

Allochthonous pedorelicts, radiocarbon dated to 27590 ± 440 cal. BC, can be interpreted as remnants of Pleistocene carbonates that were eroded and transported. As for authigenic calcite, in order to correlate radiocarbon ages of different calcrete pedofeatures and climate conditions occurred in this area, results were compared with radiocarbon ages obtained by Williams (2009) in a cumulative graph of calibrated radiocarbon ages (Fig. 6). Williams identified more humid climate conditions, characterized by higher flow of the White Nile, Blue Nile and main Nile river, during the periods 12750-11150, 7750-7050, 5950-5650, about 4350 and 1250-850 cal years BC. The phases were identified on the basis of radiocarbon determinations on freshwater fossil shells, indicating humid environments as well as palaeoenvironmental records (Williams, 2009).

Older radiocarbon ages were obtained for well-cemented clusters from blocks A3d, A3c and A3a (9530 ± 240, 7950 ± 580 and 7670 ± 100 cal year BC, respectively), corresponding to drier climate conditions (Fig.6), according to palaeoenvironmental evidence provided by Williams (2009). Younger radiocarbon ages, obtained from powdery calcitic-rich matrix from A3d and A3c blocks (dated to 5780 ± 80 and 5970 ± 100 cal year BC, respectively) as well as from calcitic-rich matrix from A3a block and from calcitic nodules from A1 block (dated to 4390 ± 80 and 4130 ± 240 cal year BC, respectively), show a good accordance with two periods characterized by more humid climate conditions, dated to 5950-5650 and about 4350 cal. years BC, respectively (Fig.6). Despite the low number of radiocarbon ages available up to now, consistency of results suggest a first onset of calcite precipitation during drier climate conditions. The occurrence of a net moisture deficit in the vadose zone as well as pore water saturated with respect to calcium carbonate, due to the reduction of the White Nile flow, promoted the calcite precipitation. Subsequently, more humid climate conditions led to partial dissolution of calcite, whereas climate changes towards drier conditions caused reprecipitation of calcite. Therefore, alternation of wet and dry periods caused the partial dissolution and reprecipitation of calcite, leading to a progressive calcite accumulation within sediments. Well-cemented clusters may be interpreted as remnants of previously precipitated calcium carbonate, which was partially dissolved during subsequent humid periods and then reprecipitated as less compact calcitic matrix.

These results suggest that calcrete pedogenesis occurred as a series of subsequent events of calcite dissolution and precipitation, discontinuously distributed along the late Pleistocene and Holocene, driven by environmental conditions. This interpretation is also supported by evidence offered by the archaeological records. Several burial phases were identified and attributed to different periods along the Holocene (Fig. 6), whereas pits, dated to the Mesolithic period, were established after the pre-Mesolithic burial phase (the oldest one). Mesolithic pits were cut into the calcrete horizon, whereas human bones, with the exception of those belonging to the most recent burial phase (Meroitic), are englobed by secondary calcite. Conversely, in Meroitic bones (dated to 50 cal years BC-250 cal years AD; Usai et al., 2010) calcite is absent, despite the fact that graves were cut within the calcrete horizon and placed deeper from the surface. On the basis of these evidence, mobilization of calcite in the last 2000 years, a period characterized by semi-arid to arid climate conditions (Gasse, 2000) and lower level of the White Nile flow (Williams, 2009), was absolutely negligible, indicating the occurrence of quiescent stages during calcrete development process under arid conditions, when the amount of circulating pore water is extremely limited.

6. Conclusions

The long-lasting process of calcrete formation and development at the site 16D4 (Khartoum, Sudan) was significantly influenced by changes from humid to dry environmental conditions. Calcrete was characterised by alternate periods of growth due to dissolution and precipitation and processes, and periods of quiescence or extremely slow growth rates. Despite the fact that radiocarbon dating of calcrete has severe limitations due to the uncertain determination of the contribution of ^{14}C by different sources, accurate sampling method coupled with additional information from a well-defined context may provide a reliable interpretation of results. A higher number of radiocarbon-dated samples could supply a more statistically significant dataset for radiocarbon ages as well as highlight the variability of ^{14}C determinations on this type of material. However, radiocarbon ages obtained in the present work confirm the general model for calcrete formation and development established in previous studies, suggesting a progressive accumulation of calcium carbonate within sediments.

Specifically for this context, the interest in deciphering the relationship between calcrete pedogenesis and archaeological records concerns the evaluation of the interaction between secondary calcite and archaeological materials. In fact, occurrence of secondary calcite in archaeological materials may represent a complex issue in all those cases in which calcite may alter archaeometric results. An example can be, in the specific case, represented by the radiocarbon

dating of archaeological bones performed on bioapatite (the mineral fraction of bone material) (Dal Sasso et al., in prep – Chapter 6). Calcite is a significant contaminant when measuring ^{14}C activity of bioapatite; despite chemical removal of secondary calcite, radiocarbon ages obtained are in good accordance with those obtained on calcrete and resulting much more younger than those hypothesized on the basis of archaeological and stratigraphic evidences (Fig.6). Since bioapatite is not a closed system with respect to the environment, carbonate exchange between calcite and bioapatite during burial may significantly affect the result when dating the archaeological bones. Therefore the study of soil sediments and burial environment is fundamental in order to assess the reliability of radiocarbon ages.

Moreover, a more complete comprehension of processes and timing of calcrete pedogenesis can supply valuable information in order to assess the preservation state of archaeological materials.

Figure 1: Location of archaeological sites 16D4, 16D4-b and 16D5 at Al Khiday, Khartoum, Sudan (from GOOGLE EARTH, version 7.1.2.2041; 15°25'27.80"N, 32°22'11.55"E, alt 106,82 Km, Image Landsat, [11/02/2014];

Figure 2a. Carbonate concretions partially embed pre-Mesolithic bones (grave 152).

Figure 2b. Mesolithic pit carved in the calcrete horizon

Figure 2c. Meroitic grave carved in the calcrete horizon

Figure 3. Exposed calcrete section sampled for this study (pit 151A). Location of calcrete blocks selected is marked.

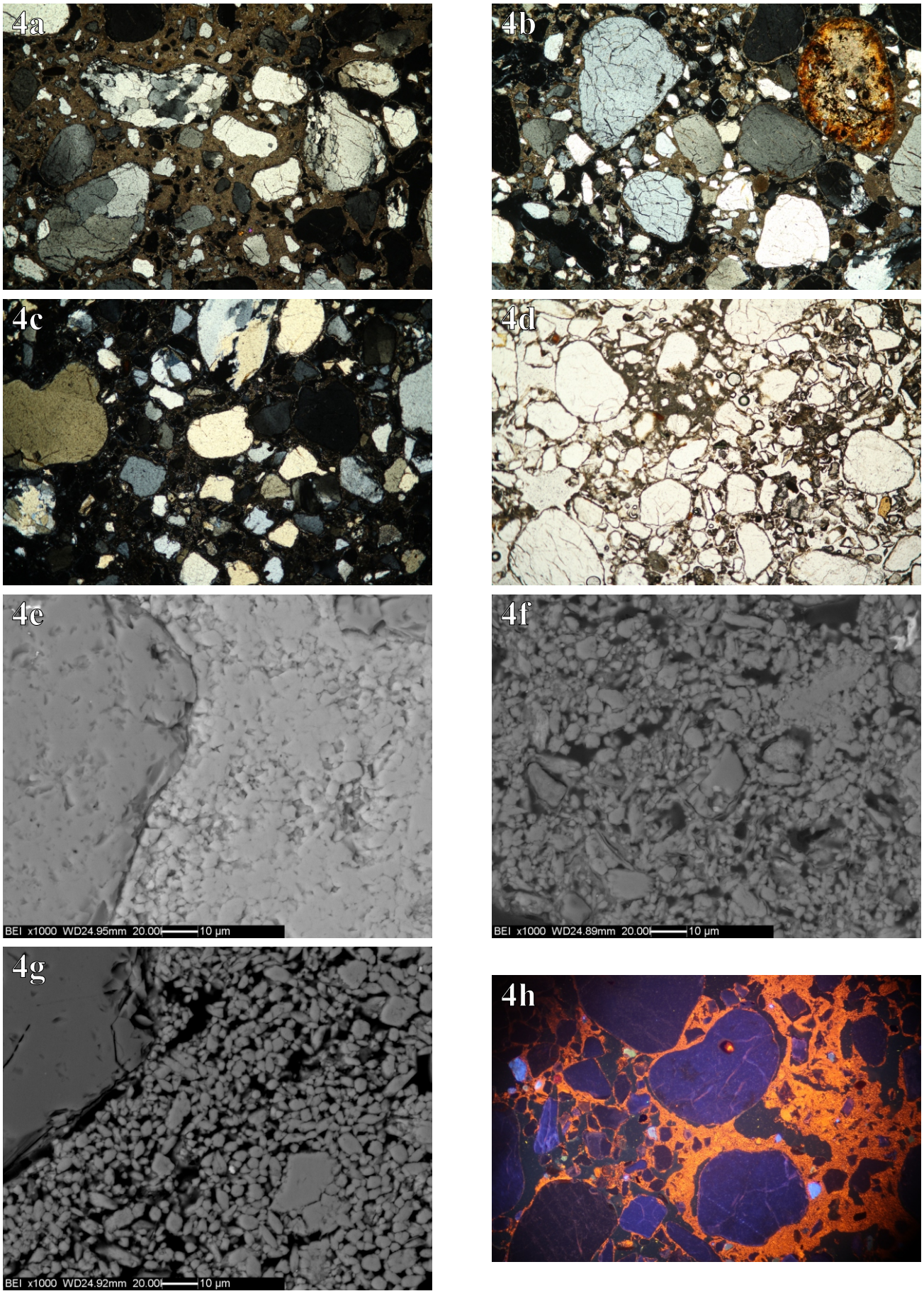

Figure 4. Microphotograph of: 4a. Micromass constituted by microsparite corresponding to a calcitic nodule in the upper unit (A1 - XPL, image width 4.4mm); 4b. Allochthonous calcitic pedorelict (A1 - XPL, i.w. 4.4mm); 4c. Quartz grains in a porphyric c/f related distribution, poorly cemented by authigenic calcite (A1 - XPL, i.w. 4.4mm); 4d. occurrence of wood ash and small charcoal deriving from the infilling material of the Mesolithic pit (A2 - PPL, i.w. 4.4mm). SEM-BSE image of different portions of calcitic nodule (A1) characterized by: 4e. Densely packed calcite crystals ; 4f. Calcite crystals associated to clayey matrix; 4f. Sparce distribution of calcite crystals. 4h. Microphotograph of microsparitic micromass cementing quartz sandy grains under CL microscopy (i.w. 2.8 mm)

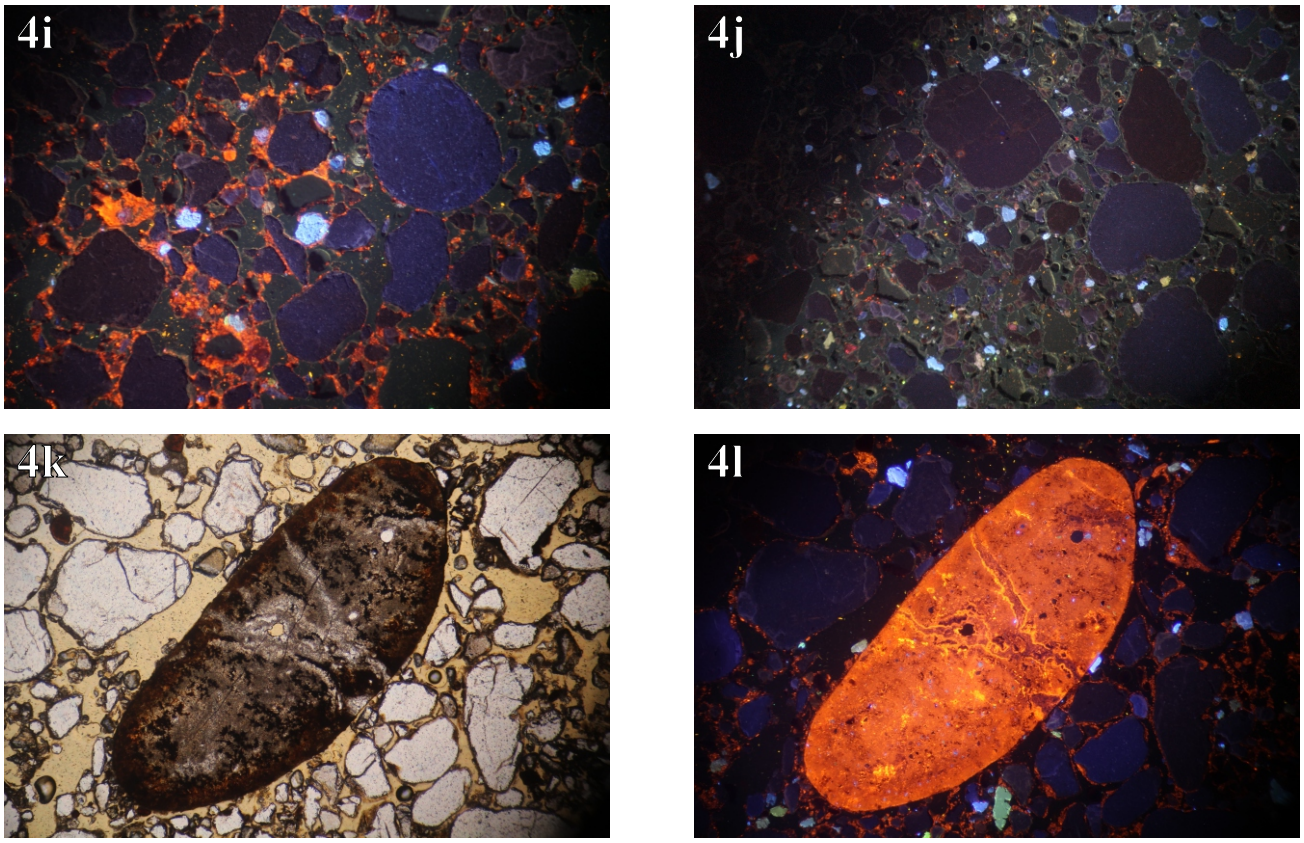

Figure 4. Microphotograph of: 4i, j. Poorly cemented areas are characterised by low luminescence due to scarcity or lack of calcite (A1 - CL, i.w. 2.8 mm); 4k, l. Allochthonous calcitic pedorelict, well-rounded in shape, constituted by a micritic matrix stained by Mn and Fe oxides, and contain veins of sparitic to micro-sparitic calcite (A1 - PPL (4k) and CL (4l) i.w. 2.8 mm)

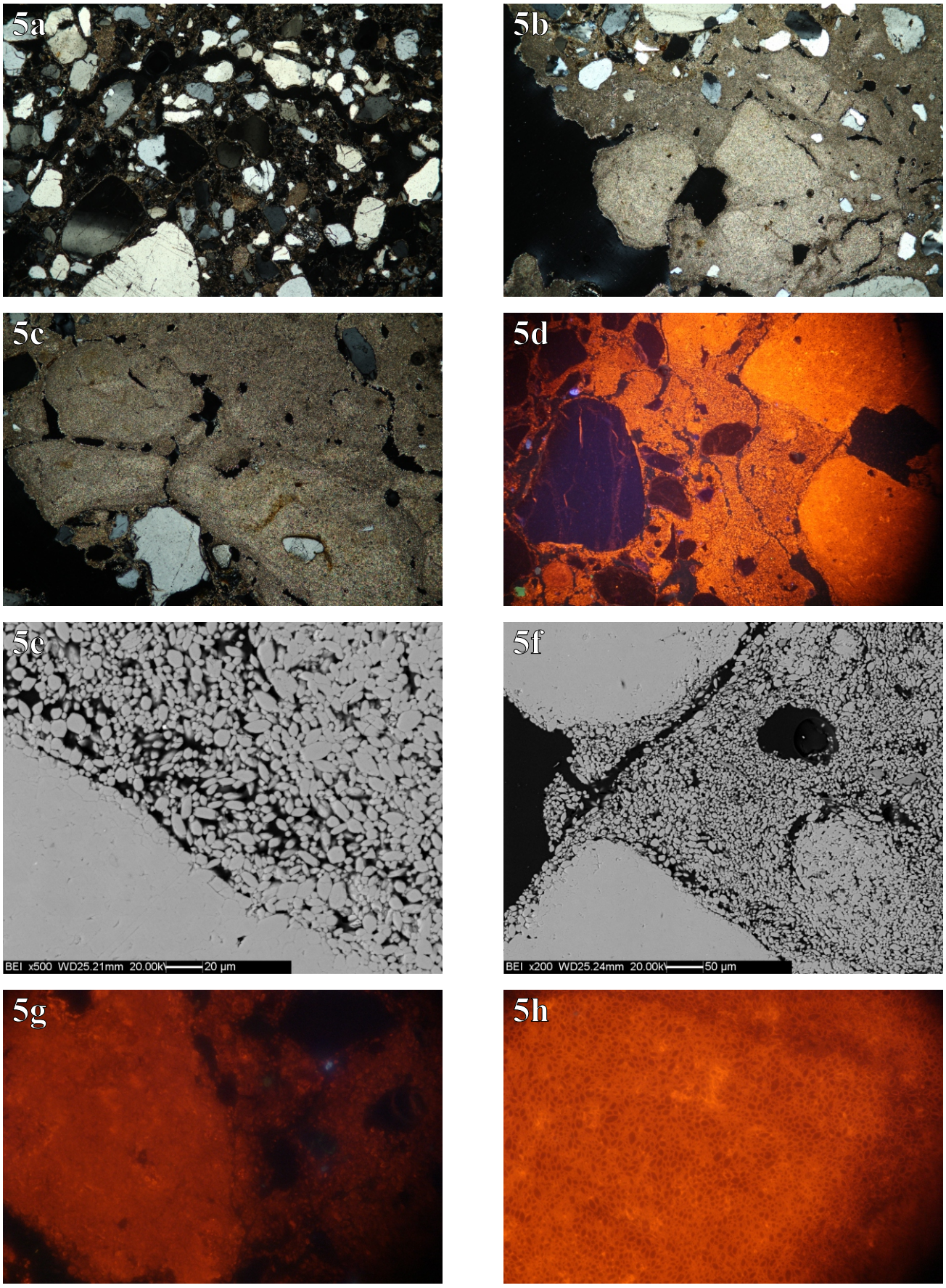

Figure 5. Microphotograph of: 5a. slightly cemented sand- and silt-sized quartz grainsembedded into a micritic micromass (A3a - XPL, i.w. 4.4mm). 5b, 5c, 5d. Highly carbonated areas corresponding to calcitic nodules predominantly constituted by microsparitic calcite. Clusters formed by well-cemented calcite crystals, sub-rounded to sub-angular shape, are shown (A3a - XPL (5b, 5c), i.w. 4.4 mm; CL (5d), i.w. 2.8 mm). 5e, 5f. SEM-BSE images of cluster portions embedded in a matrix characterized by less packed calcite crystals. 5g, 5h. well-cemented calcite crystal forming clusters, luminecence variations are shown (A3d (5g), A3A (5h), CL i.w. 0.7 mm)

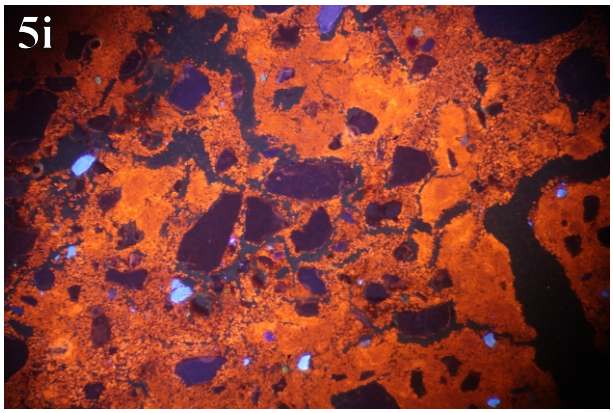

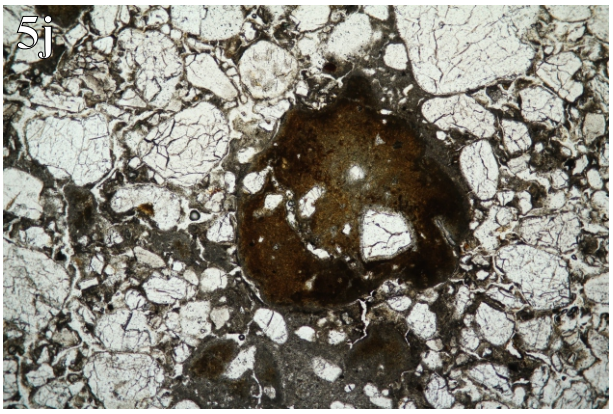

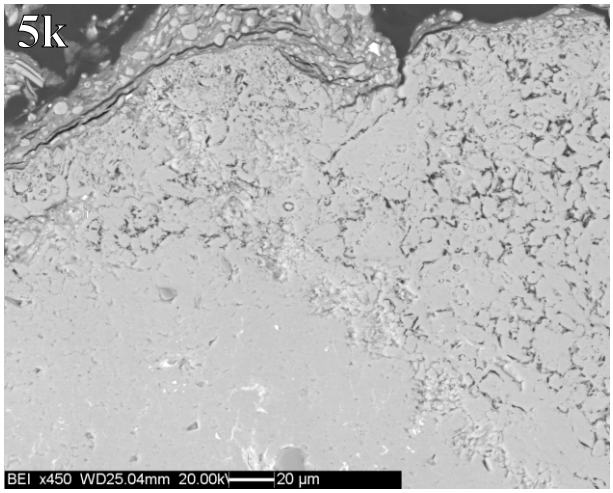

Figure 5. Microphotograph of: 5i. Portion of calcitic nodule with clusters characterized by less defined margins (A3d - CL, i.w. 2.8 mm); 5j. Allochthonous calcitic pedorelict sub-rounded in shape and impregnated by Fe oxides (A3c - PPL, i.w. 4.4 mm); 5k. SEM-BSE image of the outermost part of allochthonous calcitic pedorelict characterized by clay minerals coating its outer surface (A3c).

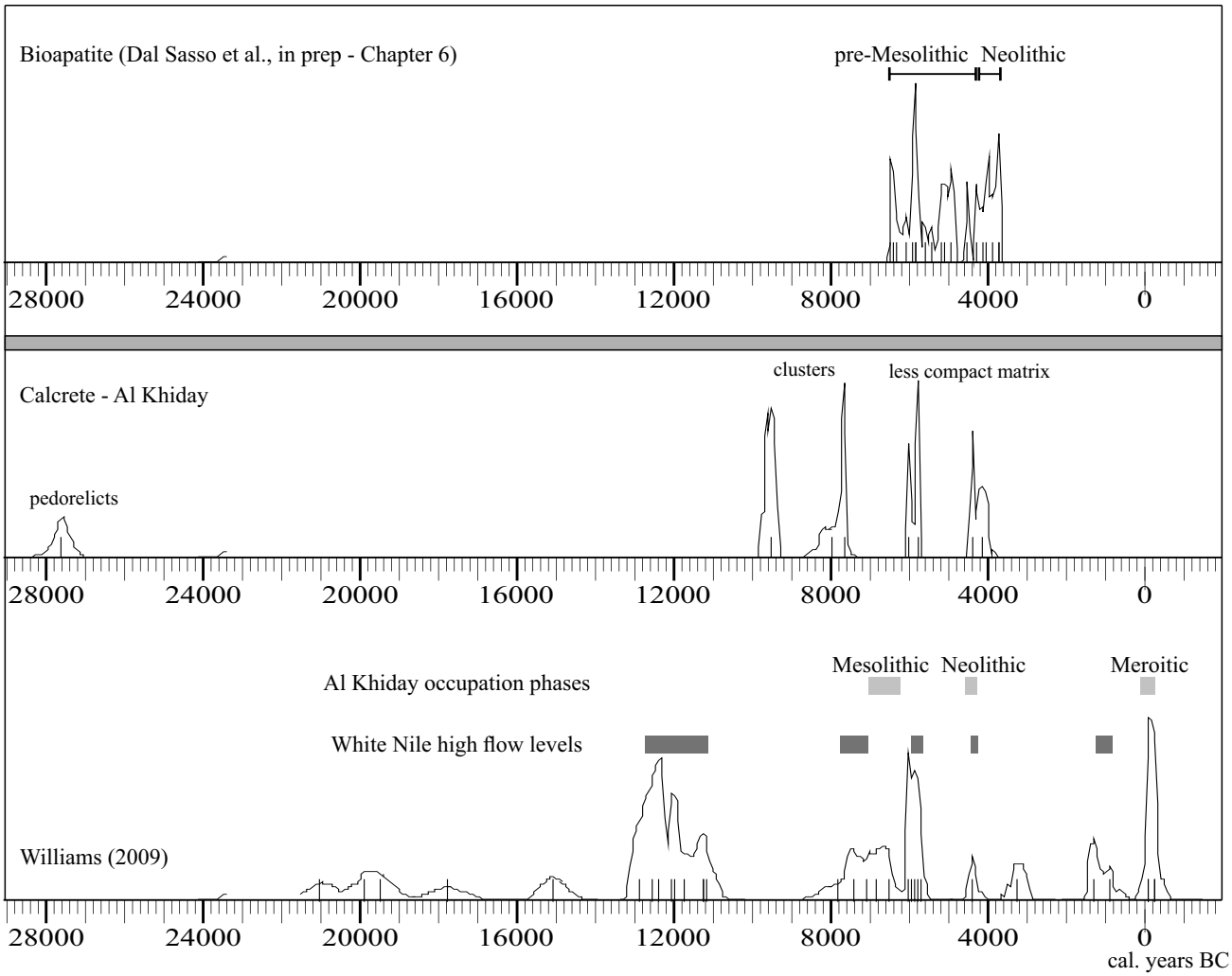

Figure 6. Cumulative calibrated dating probability of radiocarbon ages

CHAPTER 6

Radiocarbon dating of heavily altered bone apatite from the Al Khiday archaeological site (Khartoum, Sudan): is pristine apatite carbonate preserved?

1. Introduction

Human and animal bones are archaeological remains commonly found in prehistoric and historic burial areas and settlements. Under an archaeological viewpoint they are important records of the socio-cultural organization of ancient populations, since the typological, physical (anthropological and zooarchaeological on human and animal bones, respectively) and isotopic analysis of which can provide information on the social and economical activities, age, gender, individual mobility, health and diet. They can also record the post-depositional conditions and possible environmental and climate changes.

Under a compositional viewpoint, bones are composite materials, formed of an organic matrix (mainly type-I collagen) and a mineral phase, named bioapatite (Weiner and Wagner, 1998). Bioapatite is constituted by nanocrystals of highly non-stoichiometric hydroxyapatite ($Ca_{10}(PO_4)_6(OH)_2$), as several types of ionic substitutions in the crystal structure occur (LeGeros, 1981; Elliot, 2002). Among them, the most significant is the substitution of phosphate ions, and to a lesser extent of hydroxyl ions, by carbonates, which enter the crystal structure of bioapatite as result of metabolic processes (Elliot, 2002). Carbonate ions are thought also to stabilize the surface of apatite nanocrystals. The presence of ionic substitutions in the bioapatite structure influences the long-range atomic order of crystals, introducing crystal lattice defects. This, in turn, makes crystallites to be more soluble, smaller in size, with higher specific surface area, and more prone to ion exchange (Wopenka and Pasteris, 2005).

After the death of an organism and during burial, bones undergo several taphonomic and diagenetic processes, causing the alteration of organic and mineral constituents. Collagen deterioration, ions depletion or uptake, bioapatite recrystallization, microbially mediated alteration and secondary mineral phases precipitation are common processes during bone diagenesis (Hedges et al., 1995; Hedges, 2002; Nielsen-Marsh and Hedges, 2000; Smith et al., 2007; Lee-Thorp, 2008; Sponheimer and Lee-Thorp, 1999; Weiner, 2010; Dal Sasso et al., 2014).

Radiocarbon dating of archaeological bones is routinely performed, however it may represent a challenging task when bone is poorly preserved. When collagen completely lacks, structural carbonate incorporated in the bioapatite crystal lattice represents a valuable source of ^{14}C for bone dating (Haynes, 1968; Hassan et al., 1977; Saliège et al., 1995;Cherkisky, 2009; Zazzo and Saliège, 2011; Zazzo, 2014). However, diagenetic alteration of bioapatite can significantly affect the

radiocarbon determination on bones, as secondary carbonates as well as carbon isotope exchange between bioapatite and the surrounding environment occur. Secondary carbonates can be easily removed by chemical treatments, consisting mainly in weak acid attacks, which selectively dissolve secondary carbonates. A more problematic issue is represented by carbon isotope exchange, the extent of which for diagenetically altered bioapatite is not clear and presumably depends mainly on the diagenetic history of bone. Therefore, in order to assess the reliability of radiocarbon ages on bioapatite, reference ages for comparison are needed.

In this research, archaeological human bones from the Al Khiday cemetery (Khartoum, Sudan) were radiocarbon dated. Here, archaeological excavations brought to light a multi-stratified cemetery characterized by several burial phases, spanning along almost the entire Holocene. Due to the poor preservation of bones and the complete loss of collagen in all the human remains at Al Khiday, radiocarbon dating on the bioapatite fraction was the chosen method. Reference ages, provided by the well-established chronology of the site and by the well-defined archaeological and palaeoenvironmental context (Usai and Salvatori, 2002; Usai, 2003; Usai and Salvatori, 2005; Salvatori and Usai, 2009; Usai et al., 2010; Salvatori et al., 2011; Zerboni, 2011; Salvatori, 2012; Williams et al., submitted), can be in this case used to chronologically define, or constrain, each burial phase. Therefore, this case study provide a suitable set of samples to test the reliability of radiocarbon dating of bioapatite for poorly preserved bone samples.

The aims of this research are: i) to explore the reliability of radiocarbon dating of bioapatite for heavily altered bone samples; ii) to provide a model for diagenetic alteration of bioapatite in terms of carbon isotope exchange; iii) to provide a more accurate chronology for the analysed burial phases, once the reliability of radiocarbon age on these samples is assessed.

2. Archaeological and palaeoenvironmental settings

Archaeological excavations at the 16D4 site (or Al Khiday 2) were conducted within the “El Salha archaeological project” over an area of 1400 m^2since 2005 (Usai and Salvatori, 2005; Usai and Salvatori, 2007; Salvatori and Usai, 2009; Usai et al., 2010; Salvatori et al 2011; Salvatori, 2012).

The archaeological site is located on the western bank of the White Nile, at 3.5 km from the present-day river course and 22 Km south of its confluence with the Blue Nile (Fig. 1). Since the early Holocene, the area had been used as a burial ground at different periods. A hundred and ninety graves have been excavated and attributed to at least three different burial phases (pre-Mesolithic, Neolithic and Meroitic). The oldest phase, the pre-Mesolithic (90 graves), is characterized by bodies buried in a prone and elongated position, a rarely documented burial ritual (Usai et al., 2010), and

without grave goods. The chronology of this burial phase is based on the archaeological stratigraphy. In fact, during the Mesolithic period, a specialised use of the area produced numerous pits (104 have been excavated, so far) characterised by different types of filling material and presumably with different functions (Salvatori, 2012; Zerboni, 2011). Since these features can be considered an archaeologically closed context, on the basis of radiocarbon dating of suitable material coupled with the study of pottery fragments found within the infilling material, pits were dated to 6700-6300 cal. years BC (Salvatori et al., 2011; Salvatori, 2012). Evidence of 16 of these pits cutting individuals buried in a prone position clearly indicates that this older burial phase precedes the Mesolithic use of the site. Thus, the Mesolithic pits provide a terminus ante quem for the pre-Mesolithic burial phase. The site was subsequently reused as a burial ground during the Neolithic period (38 graves; 4550-4250 cal years BC) and later on during the Meroitic period (43 graves, 50 cal years BC – 250 cal years AD). Radiocarbon dating of these burial phases were obtained on grave goods or associated material (shell, wood and charcoal) (Salvatori et al., 2011; Usai et al., 2010). A fourth burial phase (19 graves), presumably older than the Neolithic burials, was identified on the basis of archaeological evidences and the macroscopic bone preservation state, coupled with histological analysis (Dal Sasso et al., 2014-a). But the lack of grave goods and uncertainties on the relationship between graves and the archaeological stratigraphy make this burial phase of uncertain chronological attribution and was tentatively labelled as Mesolithic.

The archaeological record at the 16D4 site in Al Khiday covers a wide chronological period corresponding to almost the entire Holocene. The current climate condition of the region is arid, with mean annual temperature ranging from 22 to 33°C and average rainfall of ca. 130 mm (Elagib and Mansell, 2000). However, significantly different climate conditions occurred in the past as well as several short periods when rapid climate changes at local and regional levels occurred (Gasse, 2000; Nicoll, 2004; Williams, 2009; Williams and Jacobsen, 2011; Zerboni, 2013). The early Holocene (9550-6050 cal years BC) is characterized by higher precipitation rates and environmental humidity than currently observed, as well as higher flooding level of the White Nile, due to a northward expansion of the Indian monsoon domain (Gasse, 2000; Williams, 2009). Since the middle Holocene (6050-1050 cal years BC), the progressive weakening of monsoon intensity led to rainfall decrease and overall reduction of water availability. In the late Holocene (since 1050 cal years BC) progressively drier environmental conditions occurred, up to the arid climate that now characterise central Sudan. Moreover, during the early Holocene wet phase, several periods of rapid climate changes to short arid periods are attested (Williams, 2009).

Under a geoarchaeological viewpoint, 16D4 archaeological site is established on a late Pleistocene sandy ridge, corresponding to the remnants of a longitudinal sandy river bar, at the limit of alluvial

sediments deposited during the Holocene flooding of the White Nile (Zerboni, 2011). It rises few meters above the White Nile flooding plain. The surrounding of the site is marked out by dark sediments rich in organic matter, deposited by former seasonal swamps contemporary to the Mesolithic occupation of the area (Williams and Jacobsen, 2011; Zerboni, 2011; Williams et al., submitted). Progressive drier conditions characterized the Neolithic period, becoming more severe in the Meroitic.

The archaeological record is affected by the formation and development of a pedogenic calcrete horizon, occurring at 30-50 cm under the current surface level of 16D4 site (a representative sketch is in Fig. 4a). Some of the pre-Mesolithic graves are partially embedded in calcium carbonate concretions, whereas Mesolithic pits, as well as graves belonging to successive burial phases, are apparently carved into the calcrete horizon. Dal Sasso et al. (in prep – Chapter 5) proved, by micro-morphological study and radiocarbon dating of calcitic nodules sampled from calcrete horizon, that calcite was mobilized during humid periods. This dissolution and reprecipitation process caused also the precipitation of secondary calcite in more recent archaeological materials, such as in the Neolithic bones. Moreover, calcrete formation and development is a further evidence of climate condition changes. In fact, calcium carbonate accumulation in the sediments is caused by a long-lasting process characterized by subsequent events of calcite dissolution and precipitation, promoted by the progressive drying up of environmental conditions (Zerboni, 2011; Dal Sasso et al., in prep – Chapter 5).

The archaeological record underwent also erosional processes. The concentration of coarse fragments of archaeological material on the surface of the site, due to the removal of the finer fraction of the archaeological deposit, is the most evident effect of wind deflation. Moreover, pre-Mesolithic burials, despite being the most ancient, are the most superficial ones, being at a depth of about 10-20 cm from the present ground surface while the Meroitic graves are those excavated deeper. This clearly indicated that a significant amount of sediments was eroded after the onset of the first burial phase and before the more recent ones.

3. Materials and methods

Femur fragments from two pre-Mesolithic (156 and 170) and one Mesolithic (?) (163) graves were selected for radiocarbon dating of the bioapatite (hereafter named sample 156F, 170F, and 163F, respectively). Their preservation state was characterised by histological and micro-morphological analysis (Dal Sasso et al., 2014-a), by Fourier transform infrared spectroscopy (FTIR) (Dal Sasso et al., in prep-Chapter 2) and micro-Raman (Dal Sasso et al., in prep- Chapter 4) spectroscopy and by

X-ray powder diffraction (XRPD) (Dal Sasso et al., in prep- Chapter 3). Several diagenetic processes, related to specific palaeoenvironmental and burial conditions, caused significant alterations of bone material. Collagen was completely deteriorated and bioapatite underwent recrystallization. Moreover, a diachronic sequence of diagenetic events was identified on the basis of textural relationship between alteration features, identified in bone microstructure. Firstly, biological alteration occurred: areas of thin micro-tunnelling surrounded by hyper-mineralized rim, described as non-Wedl microscopic focal destruction (non-Wedl MFD) by Hackett (1981), were observed. Then Mn oxides precipitated within bone microstructure, and subsequently calcite. For the studied femur fragments, calcite content was estimated around 4 wt. %, less than 2 wt. %, and about 3 wt.% in 156F, 170F and 163F, respectively (Dal Sasso et al., Chapter 2). Discussion of results will take into account also radiocarbon ages of bioapatite samples from pre-Mesolithic, Mesolithic and Neolithic graves of Al Khiday cemetery published by Zazzo (2014) and Gaballo (2009) (Tab. 1).

3.2 Sample preparation and analysis

All the fragments were chemical attacked in order to remove all secondary carbonates. For this specific case study, a treatment method was designed, taking into account well established protocols already published (Nielsen-Marsh and Hedges, 2000; Balteret al., 2002; Lee-Thorp, 2008; Zazzo, 2014). Human bones scattered on the soil surface of Al Khiday site were used as test material. They presumably belong to the oldest burial phase (being stratigraphically the most superficial ones), which were eroded by atmospheric agents and exposed on the surface. These test materials were selected because completely comparable, in terms of composition and diagenetic history, to the archaeological samples selected for radiocarbon dating, thus representing a well-suitable material to test the effectiveness of chemical treatment in this case study. The aim of this test was to design a method that effectively removes secondary carbonates using a dilute acid solution and in a shorter time (1 h) than other protocols, in order to avoid possible recrystallization or ions exchange (Lee-Thorp and Van der Merwe, 1990; Koch et al., 1997; Garvie-lock et al., 2004). Weak and medium strength acids were tested, acetic acid and formic acid, respectively. Effectiveness of secondary calcite removal was checked by FTIR and XRPD analysis. The protocol implemented was the following. After the external surface of bone fragments was mechanically removed by means of low-speed micro-drill equipped with an abrasive point, samples were finely hand-ground in an agate mortar. About 2 g for each sample were pre-treated with 100 ml of H_2O_2 30% M for 1 h in order to oxidize eventual organic contaminants (Crowley and Wheatley, 2014). Samples where then rinsed

in ultrapure water and centrifuged for five times. Then, samples were treated with 100 ml of formic acid 0.2 M for 1 h with a magnetic stirrer and under a N_2 flux in order to avoid contamination with modern carbon from atmospheric CO_2. Samples were rinsed in ultrapure water and centrifuged for five times, then dried over a hot plate at 50°C under N_2 flux. Ultrapure water used during the entire treatment was previously boiled for 10 min in order to remove dissolved CO_2. The effectiveness of treatment was checked monitoring the calcite content/absence for each sample by XRPD. For samples 170F and 163F, treatment method was separately applied to two aliquots for each sample, in order to check the consistency of results. For clarity the treated samples will be named 156F*, 170F-a*, 170F-b*, 163F-a* and 163F-b* (* standing for treated, -a and -b indicating the two aliquots separately treated).

All the samples, before and after the treatment, were analysed by FTIR spectroscopy and X-ray powder diffraction . For the FTIR spectroscopy, 1 mg of powdered sample was mixed in an agate mortar with 100 mg of KBr for about 1 min. A 12 mm transparent pellet was obtained pressing the powder under 8 tons/cm^2 pressure for 3 minutes, using a hydraulic press. Spectra were collected with a Nicolet Nexus 870 FTIR spectrometer equipped with a DTGS detector: 64 scans for each spectrum were acquired, in the range from 4000 to 400 cm^{-1}, with a spectral resolution of 2 cm^{-1}. Spectral analysis was performed using Omnic 9 software (Thermo Scientific).

Bioapatite shows several bands in the IR region relative to carbonate and phosphate groups (Fig. 2a). Vibrational bands ranging from 890 to 840 cm^{-1} and from 1600 to 1300 cm^{-1} are assigned to the $\nu_2(CO_3)$ and $\nu_3(CO_3)$ vibrational modes, respectively. Calcite content was monitored by the occurrence of its characteristic peak at 712 cm^{-1}, attributed to the $\nu_4(CO_3)$ vibrational band, absent in pure bioapatite spectra. As for phosphates, bands corresponding to $\nu_3(PO_4)$ and $\nu_4(PO_4)$ vibrational modes range from 1200 to 900 cm^{-1} and from 700 to 500 cm^{-1}, respectively; weaker bands, corresponding to $\nu_1(PO_4)$ and $\nu_2(PO_4)$ are at 962 cm^{-1} and 472 cm^{-1}, respectively (Rey et al., 2011). Crystallinity of bioapatite was also monitored by the infrared splitting factor (IRSF). This index takes into account the combined effect of crystallite size and atomic order/disorder of bioapatite. It quantifies the splitting extent of the two peaks at 604 and 565 cm^{-1} ($\nu_4(PO_4)$ vibrational mode), dividing the sum of peak intensities by the intensity of the valley between them (Weiner and Bar-Yosef, 1990) (Fig.2a). Higher values of IRSF correspond to higher crystallinity degree.

The mineralogical analysis by XRPD was performed using a PANalytical X'Pert PRO diffractometer in Bragg-Brentano geometry, equipped with a Cu X-ray tube, operating at 40 kV and 40 mA, and a X'Celerator detector. The diffractograms were acquired in the range from 3° to 80° 2θ, with a step size of 0.02° 2θ and counting time of 1 s per step. The Diffractograms of samples

selected for radiocarbon dating, after chemical treatment, were acquired in the range from 28° to 32° 2θ, where the main peak (104) of calcite occur, with a step size of 0.02° 2θ and counting time of 5 s per step, thus reducing the signal : noise ratio and improving the detectability of phases, in order to verify if secondary calcite was completely dissolved by the chemical attack (Fig. 2b, Fig. 3).

Samples lacking in secondary calcite after the treatment were radiocarbon dated by accelerated mass spectrometry (AMS) at the Center for Isotopic Research on the Cultural and Environmental heritage (CIRCE) laboratory (Terrasi et al., 2008). All AMS-^{14}C ages were calibrated according to the INTCAL13 dataset (Reimer et al., 2013) using the Calpal software (Weninger and Jöris, 2008).

4. Results and discussion

4.1 Treatment method and preliminary analysis

Both acetic and formic acid resulted effective in the complete removal of secondary calcite for a treatment time of 1 h. Experiments were carried out with a ratio of 0.1 ml solution / 1 mg of sample. Different A preliminary tests with much more diluted solution were performed: since solutions 0.02 M acetic acid and 0.02 M formic acid didn't removed all the calcite, slightly more concentrated solutions 0.07 M acetic acid and 0.07 M formic acid were used, although they were not enough to completely remove the secondary calcite, despite the dissolution of 35% and 45% of the sample, respectively. A further experiment with solutions 0.2 M acetic acid and 0.2 M formic acid resulted in the complete removal of calcite.

Previous radiocarbon dating of bioapatite from teeth and long bones, performed on pre-Mesolithic, Mesolithic and Neolithic graves of Al Khiday cemetery by Zazzo (2014) and Gaballo (2009) (Tab. 1), but using a different and well-established dissolution protocol (acetic acid pre-treatment) to dissolve possible secondary carbonates. The alternative formic acid pre-treatment for radiocarbon dating was here tested, also using different concentrations, in order to evaluate if this preparation method would have been effective but at the same time less aggressive in terms of quantity also of apatite dissolved. Since the attack with a 0.2 M formic acid solution caused the loss of nearly 80% of the sample, experimental conditions were maintained but the ratio solution/sample was set to 0.05 ml solution / mg of sample: in such conditions of the loss of sample was reduced to 50-55%. FTIR and XRPD analysis proved the complete dissolution of secondary calcite in this test sample. These experimental conditions were then adopted to prepare the archaeological bones for

radiocarbon dating. As an example of the effectiveness of this treatment, FTIR spectra (Fig. 2a) and XRPD diffractograms (Fig. 2b) of sample 156F before and after treatment are reported.

FTIR spectra of all samples after treatment do not show the 712 cm^{-1} peak characteristic for calcite. Moreover, relative intensities of carbonate bands in the regions from 890 to 840 cm^{-1} and from 1600 to 1300 cm^{-1} decreased after treatment. IRSF values of 4.15, 3.91 and 5.25 were obtained from samples 156F, 170F, and 163F. After the treatment increased IRSF values were obtained for all samples: 4.29, 5.56, 5.64, 6.92 and 6.85 for samples 156F*, 170F-a*, 170F-b*, 163F-a* and 163F-b*, respectively.

XRPD diffractograms of samples after treatment show the effectiveness of calcite removal; no evidence of secondary phases crystallized during chemical treatment was observed. Results indicate a higher sensitivity of XRPD analysis in revealing the occurrence of calcite with respect to FTIR analysis (Fig. 2). No evidence of calcite was detected within analysed samples (Fig.3).

4.2 AMS-^{14}C dating

^{14}C ages of pre-Mesolithic samples 156F*, 170F-a* and 170F-b* are 5840 ± 120, 6450 ± 60 and 6440 ± 80 2σ cal BC, respectively; ^{14}C ages of Mesolithic (?) samples 163F-a* and 163F-b* are 4020 ±80 and 4120 ±180 2σ cal BC, respectively (Tab.1). Data obtained from repeated measurements on two aliquots of the same sample, separately treated (170F-a*, 170F-b* and 163F-a*,163F-b*) are consistent. When considering the radiocarbon ages obtained on pre-Mesolithic, Mesolithic (?) and Neolithic burials by Zazzo (2014) (bone, enamel and dentine) and by Gaballo (2009), despite the fact that samples were pre-treated using a different protocol (acetic acid), radiocarbon ages are well comparable with those obtained in this study (Table 1), indicating the effectiveness of the treatment tested in this research (Fig. 4b, Tab. 1).

All these radiocarbon ages (the ones produced in this study and those already published), were treated as a unique dataset by the method of multiple-group calibration (Weninger, 1986; Weninger and Jöris, 2008), with the aim of graphically represent and compare calibrated radiocarbon ages, thus easing ages comparison within the same dataset and between different datasets. The complete dataset of radiocarbon dates on bioapatite shows that ages for pre-Mesolithic bones ranges from 6520 and 4200 cal. years BC, whereas for Mesolithic (?) and Neolithic samples from 4300 and 3610 cal. years BC.

Radiocarbon ages on bioapatite from the human bones of Al Khiday were compared to other datasets which dated: i) periods of humid palaeoenvironmental conditions obtained on fossil shells

(Fig. 4d) indicating the late Quaternary high flown levels of the White Nile (Williams, 2009); ii) events of calcite precipitation forming the pedogenic calcrete horizon found at Al Khiday (Fig. 4d), in which bones were recovered (Dal Sasso et al., in prep – Chapter 5); iii) the archaeological stratigraphy at Al Khiday site (Salvatori et al., 2011) (Fig. 4d).

Radiocarbon ages for pre-Mesolithic samples cover a span of time of more than 2000 years, in all cases resulting much younger than the reference age for this burial phase. A number of pre-Mesolithic graves (16) are clearly cut by Mesolithic pits, the radiocarbon dates of shells contained in dated the pits to 6700-6300 cal. years BC (Salvatori et al., 2011), providing a reference age as a terminus ante quem for the burial phase. The chronological attribution of these pits is in agreement with the chronology established also for other four sites (16D5, 16D4-b, 16D3 and 16D6) in the Al Khiday area (Fig. 4d), located few hundred meters from 16D4 site, producing evidence of Mesolithic and Neolithic settlements, as well as Meroitic and post-Meroitic use of the area (Salvatori et al., 2014). In detail, radiocarbon ages obtained by Salvatori et al. (2011), are referred to: i) shells from the Mesolithic pits at 16D4 site; ii) charcoal from Mesolithic pits at 16D4-b; iii) charcoal and organic sediments from the well-preserved archaeological Mesolithic sequence at 16D5 site and (from 7100 to 6250 cal. years BC) and Neolithic use of the site; iv) shells from the Mesolithic site 16D3; and v) shells from the Neolithic site 16D6. All these data produced a sound chronology for both the Mesolithic period, with a complete sequence dating from 7100 to 6250 cal. years BC, and the Neolithic period, dating from 4550 to 4250 cal. years BC. Moreover, the archaeological and archaeometrical analysis on a large number of potsherds from the well-preserved stratigraphic sequence, revealed important differences in the pottery productions technology over the time, especially in terms of decorative motives and paste composition (Salvatori, 2011; Salvatori, 2012; Dal Sasso et al., 2014-b). These diachronic variations firmly linked to calendric age by radiocarbon dating well-preserved stratigraphic units, from which pottery samples were recovered, were then used as chronological indicator for discriminating different phases within the Mesolithic. Given the consistency of radiocarbon ages obtained from several types of material (suitable for radiocarbon dating), sampled from five archaeological sites and of the results obtained from the archaeological and geomorphological investigations, the chronology established for the Al Khiday area (Fig. 4d) can be considered reliable.

On these bases, the reliability of radiocarbon ages obtained from bioapatite, for this case study, is questionable. In fact, despite the fact that the pre-Mesolithic burial phase precedes the onset of the Mesolithic use of the site and excavation of pits on a stratigraphic base, radiocarbon ages of pre-Mesolithic bones (6520 – 4200 cal years BC) are considerably younger than those of Mesolithic pits, dated to 6700-6300 cal. years BC. Moreover, evidence of erosional processes occurred

between the pre-Mesolithic burial phase and the excavation of Mesolithic pits is attested. Pre-Mesolithic graves are located 10-20 cm under the current surface level, a depth level incompatible with the excavation of a grave. This, coupled with evidence of wind deflation on the surface, suggest that at least 50-70 cm of sediment were eroded since body deposition. However, Mesolithic pits were not affected by such erosion: concentration of coarser archaeological material and removal of the finer fraction of sediments observed at the current surface of pits, resulting from wind deflation, is not consistent with a sediment erosion of 50-70 cm. Therefore, a significant, although not quantifiable, time gap, in which erosional processes took place, has elapsed between body deposition and the excavation of Mesolithic pits. These considerations indicates that radiocarbon ages of pre-Mesolithic bioapatite samples are at least several hundred years younger than what they should be. Given that secondary calcite was completely removed from the bone samples before dating, rejuvenation can only be related to carbonate exchange between bioapatite and the environment. In these samples secondary calcite is intimately associated to bioapatite; micromorphological and histological analysis of bone samples (Dal Sasso et al., 2014-a) proved the occurrence of secondary calcite in channels belonging to the bone vascular system as well as within fractures and microporosity produced by bacterial attack. Micro-Raman spectroscopy imaging revealed the permeation of calcite in the bone tissue, presumably filling nanoporosity between bioapatite crystallite, within the osteon, up to 80-100 µm from the Haverian canal. Moreover, the relationship between the spatial distribution of bioapatite carbonate content and the crystallinity of bioapatite, not considering bone histology, may suggest a poor preservation of biogenic structural carbonate (Dal Sasso et al., in prep – Chapter 4). Occurrence of secondary calcite imply the presence of circulating pore water saturated with respect to calcium carbonate, a condition in which carbonate exchange with bioapatite may be favoured.

Moreover, during diagenesis bones underwent recrystallization (Dal Sasso et al., in prep – Chapter 2), presumably by Ostwald ripening process (Ostwald, 1897), in particular after bioapatite crystallites exposure to pore solutions due to collagen degradation (Collins et al., 2002). Recrystallization may also have favoured the exchange of exogenous carbonate into the bioapatite structure. In this perspective, the acid treatment is not effective in removing the exogenous carbonates incorporated in the bioapatite crystal lattice. In fact, after chemical treatment, the measured increase of crystallinity index (IRSF) and the dissolution of a larger amount of sample with respect to the actual calcite content, was observed. This suggests that the less crystalline and more soluble bone bioapatite fraction was removed together with secondary calcite, whereas the most stable and recrystallized fraction was kept (Nielsen-Marsh and Hedges, 2000-b).

Precipitation of secondary calcite in bone microstructure is driven by pedogenetic processes, active during the Holocene at Al Khiday, that led to the formation and development within sediments of the thick calcrete horizon, the radiocarbon ages of which (Fig. 4c; Dal Sasso et al., in prep – Chapter 5) resulted to be essential in the interpretation of the diagenetic processes of the studied bone. Moreover, since calcrete resulted from a long-lasting process, significantly influenced by changes in climate conditions, available palaeoenvironmental information on the occurrence of humid and dry periods in central Sudan during the Holocene are reported for comparison (Fig. 4d). Periods of high flooding levels of the White Nile are considered good indicators for periods characterized by more humid climate conditions (Williams, 2009). Humid periods (12750-11150, 7750-7050, 5950-5650, about 4350 and 1250-850 cal years BC) were identified by Williams (2009) on the basis of palaeoenvironmental records and of radiocarbon ages (Fig. 4d) of freshwater fossil shells, indicating the occurrence of humid environments along the White Nile, Blue Nile and main Nile river course.

Calcrete horizon formed during a period characterized by a reduced White Nile flow (indicated by the three older radiocarbon dates obtained on calcitic clusters constituting the older part of calcrete nodules, in figure 4c), when a net moisture deficit in the vadose zone and pore water saturated with respect to calcium carbonate promoted calcite precipitation. Subsequently, more humid climate conditions led to partial dissolution and mobilization of calcite, whereas climate changes towards drier conditions caused reprecipitation of calcite in the form of a calcitic matrix cementing soil sediments (less compact with respect to calcitic clusters previously mentioned). Alternation of wet and dry periods caused the partial dissolution and reprecipitation of calcite, leading to a progressive calcite accumulation within the sediments. Radiocarbon ages of about 5950 cal. years BC and about 4250 cal. years BC were obtained on calcitic matrix of calcrete horizon and correspond to two events of calcite mobilization and reprecipitation (Dal Sasso et al., in prep – Chapter 5). Interestingly, these radiocarbon ages cover almost completely the range of radiocarbon ages obtained for pre-Mesolithic bioapatite samples, the majority of them ranging from 6520 and 5450 cal. years BC (Fig. 4b, 4c). This indicates that, as a result of events of calcite mobilization and reprecipitation, structural carbonate of bioapatite significantly exchanged with exogenous carbonate circulating in pore water and later on precipitating as secondary calcite in bone microstructure. Moreover, given that pre-Mesolithic bones experienced both the humid climate periods and presumably were affected by subsequent events of calcite dissolution and precipitation, radiocarbon ages record the combined contribution of ^{14}C activity derived from calcite precipitated during the event at about 5950 cal. years BC and the one at about 4250 cal. years BC. Carbonate exchange for

the enamel apatite samples can be hypothesised too, as enamel is not a closed system with respect to the surrounding environment (Zazzo, 2014).

Assuming that the first event of calcite precipitation within pre-Mesolithic bones occurred during the humid event at about 5950 cal. years BC, a further indication that bones of this burial phase are considerably older may derive from histological analysis (Dal Sasso et al., 2014 – Chapter 1). In fact, textural relationship between alteration features proved that a diachronic sequence of diagenetic events occurred during burial. The first alteration type was bacterial attack, producing non-Wedl microscopical focal destruction (Hackett, 1981); subsequently Mn oxides precipitated within bone micro- and nano-porosity as well as in microporosity produced by bacteria, and finally calcite precipitated. Clear microscopic evidence shows that Mn oxides and calcite precipitation occurred as two distinct events. Mn oxides were identified by XRPD as a mixture of birnessite and todorokite. Mn (II) mobilization within soil sediments is promoted by anoxic conditions, frequently encountered in waterlogged soils. Bones were presumably buried in a humid soil in an oxic-anoxic transition zone, where Mn oxidation and precipitation occurred, possibly enhanced by microbially mediated processes (Tebo et al., 2005). Evidence of skeletons heavily affected by black stains due to Mn oxides is frequently observed in lakeside cemetery or cave contexts (Shahack-Gross et al., 1997, Lòpez-González, 2006; Sereno et al., 2008; Salvatori and Usai, 2008). Occurrence of Mn oxides thus indicates humid environmental condition (hence higher flooding level of the White Nile), probably the most humid encountered by bones recovered from Al Khiday, as Mn oxides were not detected in Neolithic nor in Meroitic bones. Moreover, similar extent of Mn oxides deposition on other archaeological material in the Mesolithic pits was not observed.

Taking into account all the above discussed evidences in a sequence and moving backwards, calcite precipitation (5950 cal. years BC) affected the pre-Mesolithic bones, already permeated by Mn oxides, shortly after the end of the Mesolithic use of the site. The excavation of Mesolithic pits (6700-6300 cal.years BC) cut through some of the graves. Before the Mesolithic period: i) a humid period occurred with very high flow level of the White Nile, during which Mn oxides precipitated within bone microstructure; ii) possibly a dry period occurred, during which wind erosion caused severe erosion of soil sediments between the pre-Mesolithic body deposition and excavation of Mesolithic pit. Moreover bacterial attack of bones, related to an early diagenetic stage and associated to a moderately humid environment (Jans et al., 2004), was extensively detected.

Looking carefully at the available palaeoenvironmental records (Fig. 4d) two humid periods occurred before the Mesolithic occupancy of the site, one ranging from 7750 to 7050 cal. years BC, and the other from 12750 to 11150 cal. years BC, before the Younger Dryas. On the basis of the

above considerations a significant span of time might be assumed to separate the pre-Mesolithic burial phase and the Mesolithic occupation of the Al Khiday area, however a late Pleistocene or early Holocene chronological attribution for this burial phase is just a speculation with evidence gathered so far.

As for Mesolithic (?) and Neolithic samples a similar situation in terms of alteration of carbonate isotopic signature can be hypothesized, however with some uncertainties. Mesolithic (?) samples lack a reliable reference age, since their chronological attribution on the basis of the archaeological stratigraphy is uncertain. Despite this, radiocarbon dating of these samples was tested in order to verify a possible differentiation, in terms of ^{14}C ages, from other burial phases. However, radiocarbon ages obtained on Mesolithic (?) samples (on grave 163 in this study and on grave 9 (Gaballo, 2009) partially overlap with radiocarbon ages of two Neolithic samples from grave 10 (enamel bioapatite by Zazzo (2014) and bone apatite by Gaballo (2009)) (Fig. 4b; Tab. 1). Moreover, radiocarbon ages of both Mesolithic (?) and Neolithic bioapatite samples are 250-650 years younger than the reference age for the Neolithic use of the site (4550-4250 cal years BC). Given that poor assumptions can be made on Mesolithic (?) samples due to their uncertain attribution, Neolithic samples are much more younger than the reference age. This may suggest that, given the poor preservation of bone material, also the structural carbonate of bones belonging to more recent burial phases (for sure the Neolithic one) have been altered by the occurrence of some exogenous carbonate. However a more statistically significant dataset of radiocarbon ages of Neolithic bioapatite samples may confirm or disconfirm this hypothesis.

5. Conclusions

Radiocarbon dating of bioapatite from pre-Mesolithic, Mesolithic and Neolithic bones is not consistent with the age of archaeological burials at Al Khiday. The protocol used in the present study to remove secondary calcite, the effectiveness of which was tested also by FTIR and XRPD analysis, is not responsible of this failure, since analogous dates were obtained by Zazzo (2014) and Gaballo (2009) for bone samples from the same cemetery, although they used different pre-treatment protocols. The rejuvenation of the dates on these bones is proven to be caused by carbonate exchange between bioapatite and the burial environment. Biogenic ^{14}C activity was almost completely overprinted by that of secondary calcite, precipitated within bone micro- and nano-porosity during events of calcite mobilization and precipitation. Diagenetic alterations are mainly driven by environmental and burial conditions. This is a further evidence that changes of climate and palaeoenvironmental conditions over time have to be taken into account when

deciphering the diagenetic history of bones. Results of this research highlight also the great importance of a multidisciplinary approach to the study of the archaeological and palaeoenvironmental contexts; in particular extremely valuable information are provided by the well-defined archaeological context, by the diagenetic study of bone materials and by palaeoenvironmental, geoarchaeological and geomorphological investigations when aiming to assess the reliability of radiocarbon ages obtained on bioapatite sample from a specific archaeological context.

Table 1. Radiocarbon ages of bioapatite samples from 16D4 site

Sample code	Grave number	Burial phase	Sample	%C	^{14}C age	SD	2σ cal BC	2σ cal BP	Reference
170F-a*	170	pre-Mesolithic	Bone apatite	0.66	7596	42	6510-6390	8460-8340	This study
170F-b*	170	pre-Mesolithic	Bone apatite	0.66	7582	49	6520-6360	8470-8310	This study
156F*	156	pre-Mesolithic	Bone apatite	1.20	6963	39	5960-5720	7910-7670	This study
163F-a*	163	Mesolithic (?)	Bone apatite	0.50	5211	39	4100-3940	6050-5890	This study
163F-b*	163	Mesolithic (?)	Bone apatite	0.37	5278	64	4300-3940	6250-5890	This study
-	29	pre-Mesolithic	Enamel apatite	0.87	6940	50	5940-5700	7890-7650	Zazzo (2014)
-	29	pre-Mesolithic	Bone apatite	1.00	7480	45	6480-6200	8430-8150	Zazzo (2014)
-	29	pre-Mesolithic	Bone apatite	0.69	7235	45	6250-5970	8200-7920	Zazzo (2014)
-	18	pre-Mesolithic	Enamel apatite	0.84	6710	50	5720-5520	7670-7470	Zazzo (2014)
-	18	pre-Mesolithic	Dentine + root apatite	0.95	5680	35	4590-4430	6540-6380	Zazzo (2014)
-	18	pre-Mesolithic	Bone apatite	1.19	6010	35	5000-4800	6950-6750	Zazzo (2014)
-	27	pre-Mesolithic	Enamel apatite	0.89	7000	50	6030-5750	7980-7700	Zazzo (2014)
-	10	Neolithic	Enamel apatite	0.84	4950	35	3820-3620	5770-5570	Zazzo (2014)
-	11	pre-Mesolithic	Bone apatite	0.83	6958	55	5990-5710	7940-7660	Gaballo (2009)
-	18	pre-Mesolithic	Bone apatite	2.18	5416	40	4360-4200	6310-6150	Gaballo (2009)
-	14	pre-Mesolithic	Bone apatite	0.15	6198	90	5380-4900	7330-6850	Gaballo (2009)
-	19	pre-Mesolithic	Bone apatite	0.26	6140	65	5290-4890	7240-6840	Gaballo (2009)
-	9	Mesolithic (?)	Bone apatite	0.81	5074	50	4010-3730	5960-5680	Gaballo (2009)
-	10	Neolithic	Bone apatite	0.27	4944	50	3850-3610	5800-5560	Gaballo (2009)

Figure 1: Location of archaeological sites 16D4, 16D4-b and 16D5 at Al Khiday, Khartoum, Sudan (from GOOGLE EARTH, version 7.1.2.041; 15°25'27.80"N, 32°22'11.55"E, alt 106,82 Km, Image Landsat, [11/02/2014]

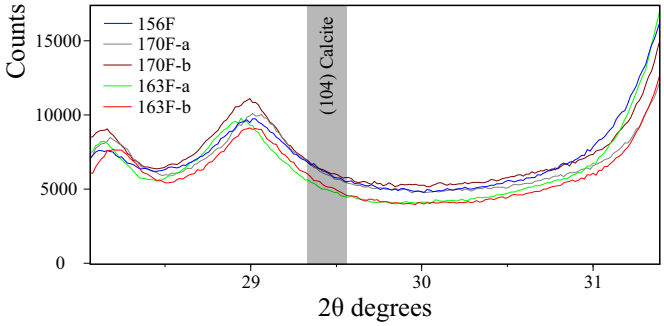

Figure 3. Diffractograms of archaeological samples after treatment in the range 28 - 32 °2θ.

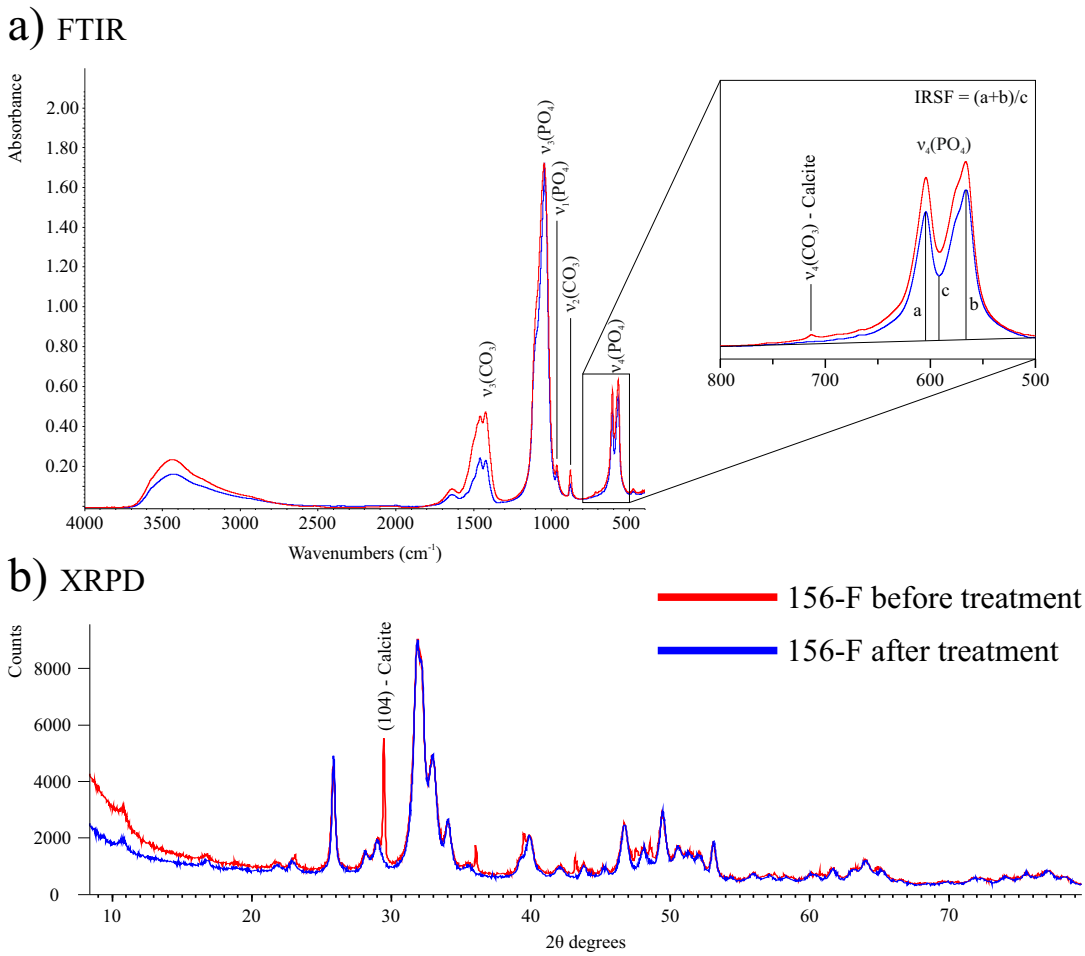

Figure 2. 2a FTIR spectra of archaeological bone (sample 156) before and after acid attack. Attribution of bands to vibrational modes of phosphate and carbonate groups is reported. The method adopted to calculate the IRSF (Weiner and Bar-Yosef, 1990) is also shown. **2b** Diffractogram of archaeological bone before and after acid attack.

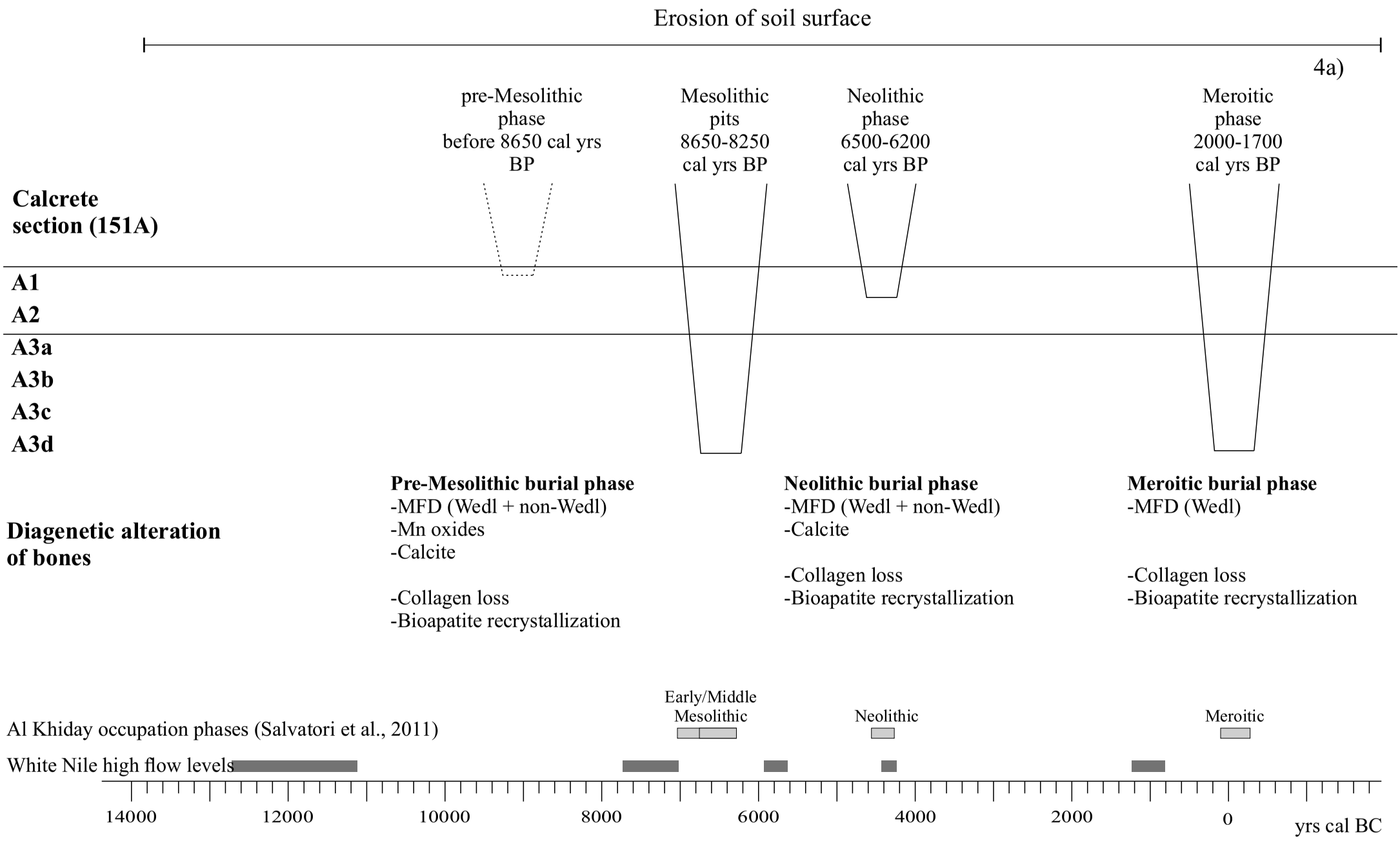
Erosion of soil surface
4a)
pre-Mesolithic phase before 8650 cal yrs BP
Mesolithic pits 8650-8250 cal yrs BP
Neolithic phase 6500-6200 cal yrs BP
Meroitic phase 2000-1700 cal yrs BP
Calcrete section (151A)
A1
A2
A3a
A3b
A3c
A3d
Diagenetic alteration of bones
Pre-Mesolithic burial phase
-MFD (Wedl + non-Wedl)
-Mn oxides
-Calcite
-Collagen loss
-Bioapatite recrystallization
Neolithic burial phase
-MFD (Wedl + non-Wedl)
-Calcite
-Collagen loss
-Bioapatite recrystallization
Meroitic burial phase
-MFD (Wedl)
-Collagen loss
-Bioapatite recrystallization
Al Khiday occupation phases (Salvatori et al., 2011)
Early/Middle Mesolithic
Neolithic
Meroitic
White Nile high flow levels
14000
12000
10000
8000
6000
4000
2000
0
yrs cal BC

Fig. 4

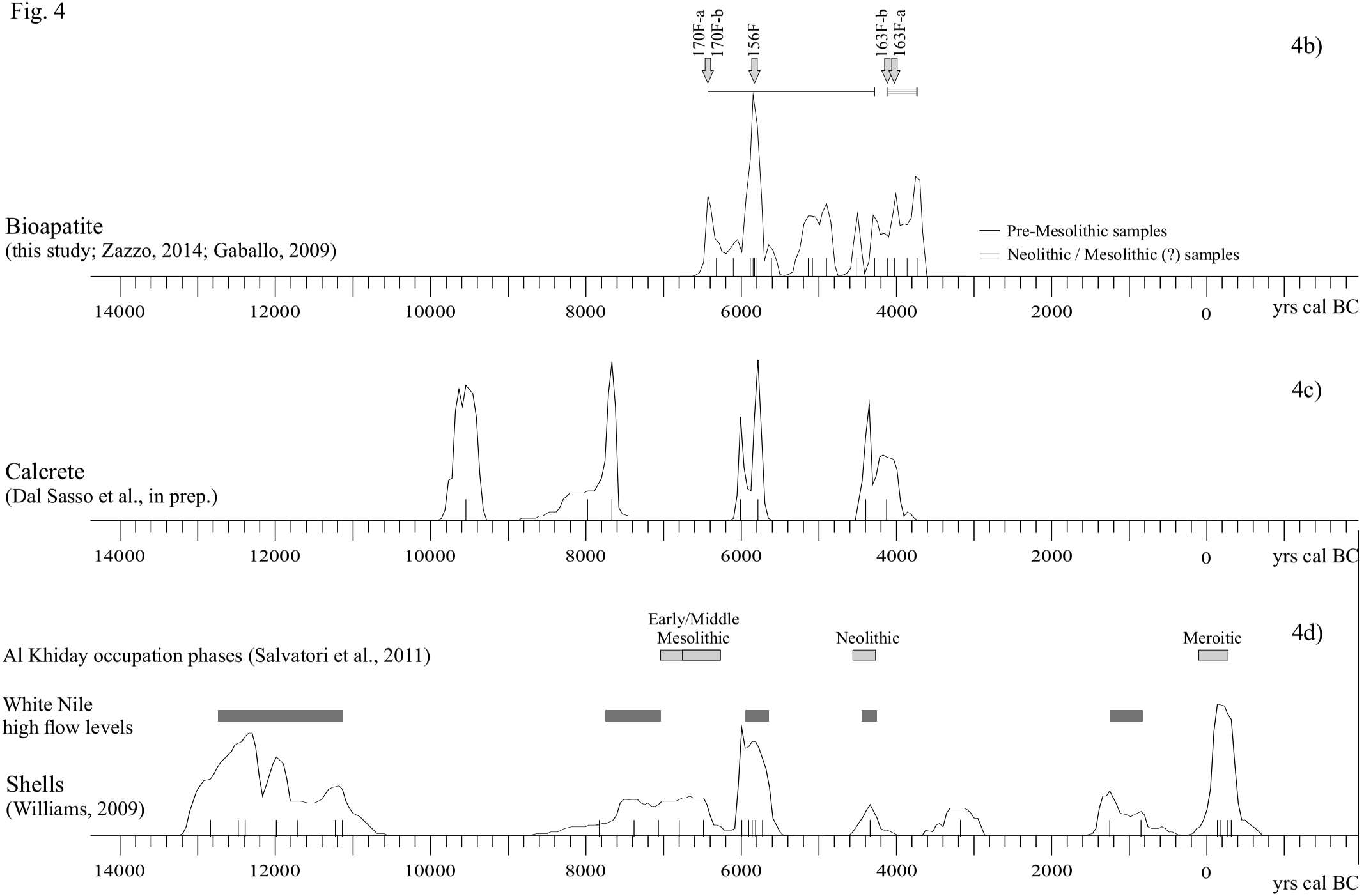
4b)
170F-a
170F-b
156F
163F-b
163F-a
Bioapatite
(this study; Zazzo, 2014; Gaballo, 2009)
Pre-Mesolithic samples
Neolithic / Mesolithic (?) samples
14000
12000
10000
8000
6000
4000
2000
0
yrs cal BC
4c)
Calcrete
(Dal Sasso et al., in prep.)
14000
12000
10000
8000
6000
4000
2000
0
yrs cal BC
4d)
Early/Middle
Mesolithic
Neolithic
Meroitic
Al Khiday occupation phases (Salvatori et al., 2011)
White Nile
high flow levels
Shells
(Williams, 2009)
14000
12000
10000
8000
6000
4000
2000
0
yrs cal BC

CONCLUDING REMARKS

The main aim of this project was to assess the reliability of radiocarbon ages obtained on the bioapatite fraction of bones from the multi-stratified cemetery of 16D4 site (Al Khiday 2, Sudan). In order to achieve this purpose, the diagenetic history of bones was investigated. A multi-analytical approach to the study of bones and their burial environment was carried out to investigate diagenetic alteration of bone in terms of types and extent as well as its dependence on climatic and local burial conditions. The Al Khiday cemetery is a particularly informative case study, since it provided a set of samples suitable to investigate the relationship between diagenesis and changes of environmental/climatic conditions along almost the entire Holocene.

Results produced on the diagenetic study of bone samples proved that:

- bone diagenesis is strongly influenced by changes in environmental and climate conditions. The profound climatic changes, occurring in Central Sudan during the Holocene, determined significant variations over time in environmental and local burial conditions, especially in terms of humidity and amount of circulating pore water. These are the main factors that influenced the occurrence, types and extent of diagenetic alteration (Chapters 1 and 2);
- the changes in climatic and local environmental conditions can produce different types of diagenetic alteration. The detailed textural analysis of the alteration features and their relationship in terms of spatial distribution may highlight a sequence of diagenetic alteration processes, which in turn can be related to specific environmental burial conditions. This provides valuable information on the interpretation of diagenetic history of bones in terms of palaeoenvironmental conditions experienced during burial (Chapter 1);
- the tight relationship between the variation in diagenetic alteration and climatic/environmental changes can be confirmed by the consistency of results obtained on diagenetic parameters by different analytical techniques, namely optical and electron microscopy, Fourier transform infrared spectroscopy, micro-Raman spectroscopy and X-ray powder diffraction (Chapters 1, 2, 3 and 4);
- climatic and local environmental conditions influence the preservation state of bones much more than the age of burial (Chapters 1 and 2); a further evidence of this is provided by the study of pedogenic calcrete horizon and its interaction with archaeological features (Chapter 5);
- a diagenetic study of bones belonging to different burial phases recovered in a multi-stratified cemetery might provide additional constrains to the attribution of graves to a specific burial phase (Chapter 1);

- a multi-analytical approach to the study of bone diagenesis can provide valuable information on different aspects of bone alteration, thus enabling the definition of the diagenetic history of bone material.

As for bioapatite radiocarbon dating, ^{14}C ages obtained for this case study are not reliable. This result was achieved taking into account a large amount of data supplied by the study of bone diagenesis and of burial environment as well as by archaeological, geoarchaeological, geomorphological and palaeoenvironmental investigations. In particular, some aspects have been highlighted by this research:

- bioapatite crystallites in heavily altered bones, in particular when totally deprived of collagen, are presumably exposed to the burial environment. In situations in which carbonate-rich pore fluids circulated within soil sediments, the biogenic ^{14}C activity can be almost completely overprinted by that of exogenous carbonates (Chapters 5 and 6);
- in order to assess the reliability of radiocarbon ages, is essential to identify the source of contaminants which may affect ^{14}C determination. In this case study, secondary calcite, detected within bone micro- and nano-porosity, played a major role in affecting radiocarbon ages of bioapatite. Establishing a model for calcite mobilization and reprecipitation provided a better understanding of the pedogenic/diagenetic processes involved in bioapatite alteration (Chapters 5 and 6);
- as proven by previous studies, bioapatite is not a closed system with respect to the environment, thus carbonate exchange takes place. In extreme cases characterized by poorly preserved bones buried in carbonate-enriched sediments, exogenous carbonate can completely overwhelm the contribution of biogenic carbonate to ^{14}C determination (Chapters 5 and 6);
- a well-defined archaeological site, in terms of a firmly established stratigraphic and chronological sequence, provides primary chronological constrains of burial phases, for which a direct age cannot be assessed (Chapters 6).

The great relevance and potentiality of a multidisciplinary approach to the study of the archaeological and palaeoenvironmental contexts is highlighted in this research. Despite the failure of direct radiocarbon dating methods (on both the organic and mineral fraction of bone), several parameters derived from different disciplines (mineralogical, geochemical, histological, diagenetic, archaeological, geoarchaeological, geomorphological, palaeoenvironmental studies) provided valuable and consistent evidence, the analysis of which resulted in a plausible, although not certain, chronology for the pre-Mesolithic burial phase. Therefore, taking into account evidence produced

by the multi-disciplinary study on archaeological contexts, valuable information is provided not only to assess the reliability of radiocarbon ages, but also to constrain chronological hypothesis that radiocarbon dating cannot verify.

REFERENCES

Achyuthan H. , Flora O., Braida M., Shankar N., Stenni B., 2010. Radiocarbon ages of pedogenic carbonate nodules from Coimbatore region, Tamil Nadu, Journal of the Geological Society of India, 75 (6), 791-798.

Armenteros I., 2009. Diagenesis of carbonate in continental settings. In: Alonso-Zarza A.M., Tanner L.H. (Eds), Developments in Sedimentology, 62, 61-151.

Ascenzi A., Bonucci E., Ostrowski K., Sliwowski A., Dziedzic-Goclawska A., Stachowicz W., Michalik J., 1977. Initial studies on the crystallinity of the mineral fraction and ash content of isolated human and bovine osteons differing in their degree of calcification. Calcified Tissue Research, 23, 7-11.

Asscher Y., Weiner S., Boaretto E., 2011a. Variations in atomic disorder in biogenic carbonate hydroxyapatite using the infrared spectrum grinding curve method. Advanced functional materials, XX, 1-6.

Asscher Y., Regev L.,Weiner S., Boaretto E., 2011b. Atomic disorder in fossil tooth and bone mineral: an FTIR study using the grinding curve method. Archaeoscience, 35, 135-141.

Awonusi A., Morris D.M., Tecklenburg M.M.J., 2007. Carbonate assignment and calibration in the Raman spectrum of apatite. Calcified Tissue International, 81, 46-52.

Balter, V., Saliège J.F., Bocherens H., Person A., 2002. Evidence of physico–chemical and isotopic modifications in archaeological bones during controlled acid etching. Archaeometry, 44 (3), 329-336.

Beasley M.M., Bartelink E.J., Taylor L., Miller R.M., 2014. Comparison of transmission FTIR, ATR, and DRIFT spectra: implications for assessment of bone bioapatite diagenesis. Journal of Archaeological Science, 46, 16-22.

Bell, L.S., 1990. Palaeopathology and diagenesis; an SEM evaluation of structural changes using backscattered electron imaging. Journal of Archaeological Science, 17, 85–102.

Berna, F., Matthews, A., Weiner, S., 2004. Solubilities of bone mineral from archaeological sites: the recrystallization window. Journal of Archaeological Science, 31 (7), 867-882.

Boschian, G., 1997. Sedimentology and soil micromorphology of the Late Pleistocene and Early Holocene deposits of Grotta dell'Edera (Trieste Karst, NE Italy). Geoarchaeology 12, 227–249.

Brady A.L., White C.D., Longstaffe F.J., Southam G., 2008. Investigating intra-bone isotopic variations in bioapatite using IR-laser ablation and micromilling: Implications for identifying diagenesis? Palaeogeography, Palaeoclimatology, Palaeoecology, 266, 190–199.

Bullock, P., Fedoroff, N., Jongerius, A., Stoops, G., Tursina, T., Babel, U., 1985. Handbook for Soil Thin Section Description, Waine Research Publication, Albrighton.

Cailleau G., Braissant O., Verrecchia E. P., 2011. Turning sunlight into stone: the oxalate-carbonate pathway in a tropical tree ecosystem. Biogeosciences, 8, 1755–1767.

Canti, M.G., 2003. Aspects of the chemical and microscopic characteristics of plant ashes found in archaeological soils. Catena 54, 339–361.

Cerling, T.E., 1984. The stable isotopic composition of modern soil carbonate and its relationship to climate. Earth and Planetary Science Letters, 71, 229-240

Child, A.M., 1995. Towards an understanding of the microbial decomposition of archaeological bone in the burial environment. Journal of Archaeological Science, 22, 165-174.

Collins M.J., Nielsen-Marsh C.M., Hiller J., Smith C.I., Roberts J.P., Prigodich R.V., Weiss T.J., CsapoJ.,Millard A.R., Turner-Walker G., 2002. The survival of organic matter in bone: A review. Archaeometry, 44 (3), 383-394.

Cremaschi, M., Salvatori, S., Usai, D., Zerboni, A., 2007. A further tessera to the huge mosaic: studying the ancient settlement pattern of the El Salha region (south-west of Omdurman, Central Sudan). In: Kroeper, K.,Chlodnicki, M., Kobusiewicz, M., (Eds) “Archaeology of the Earliest North-eastern Africa, 39-48, Poznan Archaeological Museum.

Crowley B.E., Wheatley P.V., 2014. To bleach or not to bleach? Comparing treatment methods for isolating biogenic carbonate. Chemical Geology, 381, 234–242.

Dal Sasso G., Maritan L., Usai D., Angelini I., Artioli G., 2014-a. Bone diagenesis at the micro-scale: Bone alteration patterns during multiple burial phases at Al Khiday (Khartoum, Sudan) between the Early Holocene and the II century AD. Palaeogeography, Palaeoclimatology, Palaeoecology, 416, 30-42.

Dal Sasso G., Maritan L., Salvatori S., Mazzoli C., Artioli G., 2014-b. Discriminating pottery production by image analysis: a case study of Mesolithic and Neolithic pottery from Al Khiday (Khartoum, Sudan). Journal of Archaeological Science, 46, 125-143.

Deutz P., Montañez I.P., Monger H.C., Morrison J., 2001. Morphology and isotope heterogeneity of Late Quaternary pedogenic carbonates: Implications for paleosol carbonates as paleoenvironmental proxies. Palaeogeography, Palaeoclimatology, Palaeoecology, 15, 293-317.

Deutz P., Montañez I.P., Monger H.C., 2002. Morphology and Stable and Radiogenic Isotope Composition of Pedogenic Carbonates in Late Quaternary Relict Soils, New Mexico, U.S.A.: An Integrated Record of Pedogenic Overprinting. Journal of Sedimentary Research, 72, 809-822.

Duyckaerts, G., 1959. The infra-red analysis of solid substances: a review. Analyst, 84, 201–214.

Edwards H.G.M., Farwell D.W., de Faria D.L.A., Monteiro A.M.F., Afonso M.C., De Blasis P., Eggers S., 2001. Raman spectroscopic study of 3000-year-old human skeletal remains from a Sambaqui, Santa Catarina, Brazil. Journal of Raman Spectroscopy, 32, 17–22.

Elagib N.A., Mansell M.G., 2000. Recent trends and anomalies in mean seasonal and annual temperatures over Sudan. Journal of Arid Environments, 45, 263–288.

Elliot, J.C., 2002. Calcium phosphate biominerals. In: Kohn, M.J., Rakovan, J., Hughes, J.M. (Eds.), Phosphates: Geochemical, Geobiological and Materials Importance. Reviews in Mineralogy and Geochemistry, 48, 427–453.

Fernández-Jalvo, Y., Andrews, P., Pesquero, D., Smith, C., Marín-Monfort, D., Sánchez, B., Geigl, E., Alonso, A., 2010. Early bone diagenesis in temperate environments Part I: Surface features and histology. Palaeogeography, Palaeoclimatology, Palaeoecology, 288, 62–81.

Gaballo V., 2009. Studio di reperti osteologici provenienti dalla necropoli 16-D-4 (Sudan) attraverso analisi spettroscopiche e spettrochimiche. Unpublished Master thesis in Scienze per i beni culturali, University of Parma.

Garvie-Lok S.J. , Varney T.L., Katzenberg M.A., 2004. Preparation of bone carbonate for stable isotope analysis: the effects of treatment time and acid concentration. Journal of Archaeological Science, 31, 763–776.

Gasse, F., 2000. Hydrological changes in the African tropics since the Last Glacial Maximum, Quaternary Science Review, 19, 189-211.

Geyh M.A., Eitel B., 1998. Radiometric dating of young and old calcrete. Radiocarbon, 40, 795-802.

Gómez-Morales, J., Iafisco, M., Delgado-López, J.M., Sarda, S., Drouet, C., 2013. Progress in the preparation of nanocrystalline apatites and surface characterization: overview of fundamental and applied aspects. Progress in Crystal Growth and Characterization of Materials, 59, 1-46.

Grunenwald A., Keyser C., Sautereau A.M., Crubézy E., Ludes B., Drouet C., 2014. Revisiting carbonate quantification in apatite (bio)minerals: a validated FTIR methodology. Journal of Archaeological Science, 49, 134-141.

Gunasekaran S., Anbalagan G., Pandi S., 2006. Raman and infrared spectra of carbonates of calcite structure. Journal of Raman Spectroscopy, 37, 892-899.

Hackett, C.J., 1981. Microscopical focal destruction (tunnels) in excavated human bones. Medicine Science and the Law, 21, 243–265.

Hassan A.A., Termine J.D., Haynes C., 1977. Mineralogical studies on bone apatite and their implications for radiocarbon dating. Radiocarbon, 19 (3), 364-374.

Haynes C., 1968. Radiocarbon, analysis of inorganic carbon of fossil bone and enamel. Science 161, 687–688.

Hedges, R.E.M., 2002. Bone diagenesis: an overview of the processes. Archaeometry, 44 (3), 319-328.

Hedges, R.E.M., Millard, A.R., Pike, A.W.G., 1995. Measurements and Relationships of Diagenetic Alteration of Bone from Three Archaeological Sites. Journal of Archaeological Science, 22, 201–209.

Hiatt E.E., Pufahl P.K., 2014. Cathodoluminescence petrography of carbonate rocks: a review of applications for understanding diagenesis, reservoir quality, and pore system evolution. In: Coulson, I.M. (Eds), Cathodoluminescence and its application to geoscience, Mineralogical Association of Canada short course 45, Fredericton NB, 75-96.

Hollund, H.I., Ariese F., Fernandes R., Jans M.M.E., Kars H., 2012. Testing an alternative high throughput tool for investigating bone diagenesis: FTIR in attenuated total reflection (ATR) mode. Archaeometry, 55 (3), 507-532.

Jans, M.M.E., Kars,H., Nielsen-Marsh, C.M., Smith, C.I., Nord, A.G., Arthur, P., Earl, N., 2002. In situ preservation of archaeological bone: a histological study within multidisciplinary approach. Archaeometry, 44(3), 343–352.

Jans, M.M.E., Nielsen-Marsh, C.M., Smith, C.I., Collins, M.J., Kars, H., 2004. Characterisation of microbial attack on archaeological bone. Journal of Archaeological Science, 31, 87-95.

Julien, C.M., Massot, M., Poinsignon, C., 2004. Lattice vibrations of manganese oxides Part I. Periodic structures. Spectrochimica Acta Part A, 60, 689-700.

Kazanci M., Roschger P., Paschalis E.P., Klaushofer K., Fratzl P., 2006. Bone osteonal tissue by Raman spectral mapping: orientation-composition. Journal of Structural Biology, 156, 489-496.

King C.L., Tayles N., Gordon K.C., 2011. Re-examining the chemical evaluation of diagenesis in human bone apatite. Journal of Archaeological Science, 38 (9), 2222–2230.

Koch P.L., Tuross N., Fogel M.L., 1997. The Effects of Sample Treatment and Diagenesis on the Isotopic Integrity of Carbonate in Biogenic Hydroxylapatite. Journal of Archaeological Science, 24, 417–429.

Lebon M., Müller K., Bellot-Gurlet L., Paris C., Reiche I., 2011. Application des micro-spectrométries infrarouge et Raman à l'étude des processus diagénétiques altérant les ossements paléolithiques. Archeosciences, revue d'archéométrie, 35, 179-190.

Lebon, M., Reiche, I., Bahain, J-J., Chadefaux, C., Moigne A-M., Fröhlich, F., Sémah, F., Schwarcz, H.P., Falguères, C., 2010. New parameters for the characterization of diagenetic alterations and heat-induced changes of fossil bone mineral using Fourier Transform Infrared Spectrometry. Journal of Archaeological Science, 37, 2265-2276.

Lebon M., Zazzo A, Reiche I., 2014. Screening in situ bone and teeth preservation by ATR-FTIR mapping. Palaeogeography, Palaeoclimatology, Palaeoecology, 416, 110-119.

Lee-Thorp, J.A., 2008. On isotopes and old bones. Archaeometry, 50 (6), 925-950.

LeGeros, R.Z., 1981. Apatites in biological systems. Progress in Crystal Growth and Characterization of Materials, 4, 1-45.

Lòpez-González F., Grandal-d'Anglade A., Vidal-Romanì J.R., 2006. Deciphering bone depositional sequences in caves through the study of manganese coatings. Journal of Archaeological Science, 33, 707-717.

Lutterotti, L., 2010. Total pattern fitting for the combined size-strain-stress-texture determination in thin film diffraction. Nuclear Instruments and Methods in Physics Research, B, 268, 334-340.

Machette M. N., 1985. Calcitic soils of the southwestern United States. Geological Society of America Special Papers, 203, 1-22.

Macklin, M.G., Woodward, J.C., Welsby, D.A., Duller, G.A.T., Williams, F.M., Williams, M.A.J., 2013. Reach-scale river dynamics moderate the impact of rapid Holocene climate change on floodwater farming in the desert Nile. Geology, 41, 695-698.

Morris M.D., Mandair G.S., 2011. Raman assessment of bone quality. Clinical Orthopaedics and Related Research, 469 (8), 2160-2169.

Müller, K., Chadefaux, C., Thomas, N., Reiche, I., 2011. Microbial attack of archaeological bones versus high concentrations of heavy metals in the burial environment. A case study of animal bones from a mediaeval copper workshop in Paris. Palaeogeography, Palaeoclimatology, Palaeoecology, 310, 39-51.

Newman B.D., Campbell A.R., Norman D.I., Ringelberg D.B., 1997. A model for microbially induced precipitation of vadose-zone calcites in fractures at Los Alamos, New Mexico, USA. Geochimica and Cosmochimica Acta, 61 (9), 1783-1792

Nicoll, K., 2004. Recent environmental changes and prehistoric human activity in Egypt and Northern Sudan. Quaternary Science Review, 23, 564-580.

Nielsen-Marsh, C.M., Hedges, R.E.M., 2000. Patterns of diagenesis in bone I: the effects of site environments. Journal of Archaeological Science, 27, 1139-1150.

Nielsen-Marsh C.M., Hedges R.E.M., 2000-b. Patterns of Diagenesis in Bone II: Effects of Acetic Acid Treatment and the Removal of Diagenetic CO_3^{2-}. Journal of Archaeological Science, 27, 1151–1159.

Ostwald, W., 1897. Studien über die Bildung und Umwandlung fester Körper. Zeitschrift für physikalische Chemie, 22, 289-330.

Otto C., de Grauw C.J., Duindam J.J., Sijtsema N.M., Greve J., 1997. Applications of Imaging in Micro-Raman Biomedical Research. Journal of Raman Spectroscopy, 28,143-150.

Paschalis, E. P, Di Carlo E., Betts F., Sherman P., Mendelsohn R., Boskey A. L., 1996. FTIR microspectroscopic analysis of human osteonal bone. Calcified Tissue International, 59, 480-487.

Penel G., Leroy G., Rey C.,Bres E., 1998. MicroRaman Spectral Study of the PO_4 and CO_3 Vibrational Modes in Synthetic and Biological Apatites. Calcified Tissue International, 63, 475-481

Person A., Bocherens H., Saliège J., Paris F., Zeitoun V., Gérard M., 1995. Early diagenetic evolution of bone phosphate: an X-ray diffractometry analysis. Journal of Archaeological Science, 22, 211-221.

Pitre, M.C., Correia, P.M., Mankowski, P.J., Klassen, J., Day, M.J., Lovell, N.C., Currah, R., 2013. Aspects of the chemical and microscopic characteristics of plant ashes found in archaeological soils. Journal of Archaeological Science, 40, 24-29.

Poduska, K.M., Regev, L., Boaretto, E., Addadi, L., Weiner, S., Kronik, L., Curtarolo, S., 2011. Decoupling Local Disorder and Optical Effects in Infrared Spectra: Differentiating Between Calcites with Different Origins. Advanced Materials, 23, 550-554.

Popa, N.C., 1998. The (hkl) Dependence of diffraction-line broadening caused by strain and size for all laue groups in Rietveld refinement. Journal of Applied Crystallography, 31, 176-180.

Potter, M. R., Rossman, G. R., 1979. Mineralogy of manganese dendrites and coatings. American Mineralogist, 64, 1219-1226.

Pucéat E., Reynard B., Lécuyer C., 2004. Can crystallinity be used to determine the degree of chemical alteration of biogenic apatites? Chemical Geology, 205, 83–97.

Regev, L., Poduska, K.M., Addadi, L., Weiner, S., Boaretto, E., 2010. Distinguishing between calcites formed by different mechanisms using infrared spectrometry: archaeological applications. Journal of Archaeological Science, 37 (12), 3022-3029.

Reiche, I., Favre-Quattropani, L.,Vignaud, C., Bocherens, H., Charlet, L., Menu, M., 2003. A multi-analytical study of bone diagenesis: the Neolithic site of Bercy (Paris, France). Measurement Science and Technology, 14, 1608-1619.

Reiche I., Lebon M., Chadefaux C., Müller K., Le Hô A., Gensch M., SchadeU., 2010. Microscale imaging of the preservation state of 5,000-year-old archaeological bones by synchrotron infrared microspectroscopy. Analytical and Bioanalytical Chemistry, 397, 2491-2499.

Reimer, P.J., Bard, E., Bayliss, A., Beck, J.W., Blackwell, P.G., Bronk Ramsey, C., Buck, C.E., Cheng, H., Edwards, R.L., Friedrich, M., Grootes, P.M., Guilderson, T.M., Haflidason, H., Hajdas, I., Hatté, C., Heaton, T.J., Hoffmann, D.L., Hogg, A.G., Hughen, K.A., Kaiser, K.F., Kromer, B., Manning, S.W., Niu, M., Reimer, R.W., Richards, D.A., Scott, E.M., Southon, J.R., Staff, R.A., Turney, C.S.M., Van der Plicht, J., 2013. IntCal13 andMarine13 Radiocarbon Age Calibration Curves 0–50,000 Years Cal. BP. Radiocarbon, 55,1869–1887.

Rey C., Combes C., Drouet C., Grossin D., 2011. Bioactive Ceramics: Physical Chemistry. In: Ducheyne P., Healy K.E., Hutmacher D.W., Grainger D.W., Kirkpatrick C.J. (Eds.), Comprehensive Biomaterials, 1, Elsevier, 187-221.

Richter D.K., Immenhauser A., Neuser R.D., 2008. Electron backscatter diffraction documents randomly orientated c-axes in moonmilk calcite fibres: evidence for biologically induced precipitation. Sedimentology, 55 (3), 487-497.

Rink W.J., Schwarcz, H.P., 1995. Tests for Diagenesis in Tooth Enamel: ESR Dating Signals and Carbonate Contents. Journal of Archaeological Science, 22 (2), 251–255.

Roche, D., Ségalen, L., Balan, E., Delattre, S., 2010. Preservation assessment of Miocene-Pliocene tooth enamel from Tugen Hills (Kenian Rift Valley) through FTIR, chemical and stable-isotope analyses. Journal of Archaeological Science, 37, 1690-1699.

Salesse K.,Dufour E. Lebon M., Wurster C., Castex D., Bruzek J., Zazzo A., 2014. Variability of bone preservation in a confined environment: The case of the catacomb of Sts Peter and Marcellinus (Rome, Italy). Palaeogeography, Palaeoclimatology, Palaeoecology, 416, 43-54.

Saliège, J.-F., Person, A., Paris, F., 1995. Preservation of $^{12}C/^{13}C$ original ratio and ^{14}C dating of the mineral fraction of human bones from Saharan tombs. Niger. Journal of Archaeological Science 22, 301–312.

Salvatori S., Usai D.(eds), 2008. A Neolithic cemetery in the Northern Dongola Reach (Sudan): Excavation at Site R12. Sudan Archaeological Research Society Publication.

Salvatori, S., Usai, D., 2009. El Salha Project 2005: New Khartoum Mesolithic sites from central Sudan. Kush, 19, 87-96.

Salvatori, S., Usai, D., Zerboni, A., 2011. Mesolithic site formation and palaeoenvironment along the White Nile (Central Sudan). African Archaeological Review, 28, 177-211.

Salvatori, S., 2012. Disclosing archaeological complexity of the Khartoum Mesolithic. New data at the site and regional level. African Archaeological Review, 29, 399-472.

Salvatori S., Usai D., Abdelrahman M.F., Di Matteo A., Iacumin P., Linseele V., Magzoub M.K., 2014. Archaeological evidence at Al Khiday. New insight on the prehistory and History of Central Sudan. In: Anderson J.R., Welsby D.A. (Eds), Proceedings of the 12th International Conference of Nubian Studies, Peeters Publishers, Leuven, Belgium.

Salvo, L., Cloetens, P., Maire, E., Zabler, S., Blandin, J. J., Buffière, J. Y., Josserond, C., 2003. X-ray micro-tomography an attractive characterisation technique in materials science. Nuclear Instruments and Methods in Physics Research Section B: Beam Interactions with Materials and Atoms, 200, 273-286.

Scherrer, P., 1918. Bestimmung der Größe und der inneren Struktur von Kolloidteilchenmittels Röntgenstrahlen Nachrichten von der Gesellschaft der Wissenschaften zu Göttingen, Mathematisch-Physikalische Klasse, 2, 98-100.

Sereno P.C., Garcea E.A.A., Jousse H., Stojanowski C.M., Saliége J.F., Maga A., Ide O.A., Knudson K.J., Mercuri A.M., Stafford T.W., Kaye T.G., Giraudi C., N'siala I.M., Cocca E., Moots H.M., Dutheil D.B., Stivers J.P. 2008. Lakeside Cemeteries in the Sahara: 5000 Years of Holocene Population and Environmental Change. PlosOne, 3 (8), 1-22.

Shahack-Gross R., Bar Yosef O., Weiner S., 1997. Black-Coloured Bones in Hayonim Cave, Israel: Differentiating Between Burning and Oxide Staining. Journal of Archaeological Science, 24, 439–446.

Smith, C.I., Nielsen-Marsh, C.M., Jans, M.M.E., Collins, M.J., 2007. Bone diagenesis in the European Holocene I: patterns and mechanisms. Journal of Archaeological Science, 34, 1485-1493.

Smith G.D., Clark R.J.H., 2004. Raman microscopy in archaeological science. Journal of Archaeological Science, 31, 1137-1160.

Sponheimer, M., Lee-Thorp, J.A., 1999. Alteration of enamel carbonate environments during fossilization. Journal of Archaeological Science, 26, 143-150.

Stoops, G., 2003. Guidelines for analysis and description of soil and regolith thin sections. Soil Science Society of America, Madison, WI.

Stoops, G., Marcellino, V., Mees, F., 2010. Interpretation of micromorphological features of soil and regoliths. Elsevier, Amsterdam.

Sudarsanan, K., Young., R.A:, 1969. Significant precision in crystal structural details: Holly Springs hydroxyapatite. Acta Crystallographica B, 25, 1534–1543.

Surovell T.A., Stiner, M.C., 2001. Standardizing infra-red measures of bone mineral crystallinity: an experimental approach. Journal of Archaeological Science, 28, 633-642.

Tebo, B.M., Johnson, H.A., McCarthy, J.K., Templeton, A.S., 2005. Geomicrobiology of manganese(II) oxidation. Trends in Microbiology, 13 (9), 421-428.

Termine, J.D., Posner, A.S., 1966. Infra-red determination of percentage of crystallinity in apatitic calcium phosphates. Nature, 211, 268-270.

Terrasi F., De Cesare N., D'OnofrioA., Lubritto C., Marzaioli F., Passariello I., Rogalla D., Sabbarese C., Borriello G., Casa G., Palmieri A., 2008. High precision ^{14}C AMS at CIRCE. Nuclear Instruments and Methods in Physics Research B, 266, 2221–2224.

Thomas D.B., Ewan Fordyce R., Frew R.D., Gordon, K.C. 2007. A rapid, non-destructive method of detecting diagenetic alteration in fossil bone using Raman spectroscopy. Journal of Raman Spectroscopy, 38, 1533-1537.

Thompson,T.J.U., Islam, M., Piduru, K., Marcel, A., 2011. An investigation into the internal and external variables acting on crystallinity index using Fourier Transform Infrared Spectroscopy on unaltered and burned bone. Palaeogeography, Palaeoclimatology, Palaeoecology, 299, 168–174.

Timlin J.A., Carden A., Morris M.D., 1999 Chemical Microstructure of Cortical Bone Probed by Raman Transects. Applied Spectroscopy,53 (11)1429-1435.

Trueman, C.N.G., Behrensmeyer, A.K., Tuross, N., Weiner, S., 2004. Mineralogical and compositional changes in bones exposed on soil surface in Amboseli National Park, Kenya: diagenetic mechanisms and the role of sediment pore fluids. Journal of Archaeological Science, 31, 721-739.

Turner-Walker, G., Syversen, U., 2002. Quantifying histological changes in archaeological bones using BSE-SEM image analysis. Archaeometry, 44 (3), 461–468.

Ungár, T., Tichy, G., Gubicza, J., Hellmig, R.J., 2005. Correlation between subgrains and coherently scattering domains. Powder Diffraction, 20 (4), 366-375.

Usai D., 2003. The Is.I.A.O. El Salha project. Kush, 18, 173-182.

Usai D., Salvatori S., 2002. The Is.I.A.O. El Salha archaeological project. Sudan & Nubia, 6, 67-72.

Usai D., Salvatori S., 2005. The IsIAO archaeological project in the El Salha area (Omdurman South, Sudan): results and perspectives. Africa, 60 (3-4), 474-493.

Usai D., Salvatori, S. 2007. The oldest representation of a Nile boat. Antiquity, 81, 314.

Usai D. Salvatori S. Iacumin P. Di Matteo A. Jakob T. Zerboni A., 2010. .Excavating a unique pre-Mesolithic cemetery in Central Sudan. Antiquity,84, 323.

VašinováGaliová M., NývltováFišáková M., Kynický J., Prokeš L., Neff H., Mason A.Z., Gadas P., Košler J., Kanický V., 2013. Elemental mapping in fossil tooth root section of Ursus arctos by laser ablation inductively coupled plasma mass spectrometry (LA-ICP-MS). Talanta, 105, 235-243

Vogel J.C., Geyh M.A., 2008.Radiometric dating of hillslope calcrete in the Negev Desert, Israel. South African Journal of Science, 104, 11-12.

Wang, Y., McDonald, E., Amundson, R., McFadden, L., Chadwick, O., 1996. An isotopic study of soils in chronological sequences of alluvial deposits, Providence Mountains, California. Geological Society of America Bulletin, 108, 379-391.

Weiner, S., 2010. Biological materials: bones and teeth. In: Weiner, S., Microarchaeology: beyond the visible archaeological record, Cambridge University press, 99-134.

Weiner, S., Bar-Yosef, O., 1990. State of preservation of bones from prehistoric sites in the Near East: a survey. Journal of Archaeological Science, 17, 187-196.

Weiner, S., Traub, W., 1992. Bone structure: from ångstroms to microns. The FASEB Journal, 6, 879–885.

Weiner, S., Wagner, H.D., 1998. The material bone: Structure-mechanical function relations, Annual Review of Materials Science, 28, 271-298.

Weninger, B. and Jöris, O., 2008. A 14C age calibration curve for the last 60 ka: the Greenland-Hulu U/Th timescale and its impact on understanding the Middle to Upper Paleolithic transition in Western Eurasia. Journal of Human Evolution, 55, 772-781.

Weninger, B., 1986. High-precision calibration of archaeological radiocarbon dates. Acta Interdisciplinaria Archaeologica, IV, 11-53. Nitra.

Williams, M.A.J., 2009. Late Pleistocene and Holocene environments in the Nile basin. Global and planetary change, 69, 1-15.

Williams, M.A.J., Adamson, D., 1980. Late Quaternary depositional history of the Blue and White Nile rivers in central Sudan. In Williams, M.A.J., Faure, H., (Eds.), The Sahara and the Nile: Quaternary environments and prehistoric occupation in northern Africa, 281–304. Rotterdam: Balkema.

Williams, M.A.J., Jacobsen, G.E., 2009. A wetter climate in the desert of northern Sudan 9900-7600 years ago, Sahara, 22, 7-14.

Williams M.A.J., Usai D., Salvatori S., Williams F.M., Zerboni A., Maritan L., submitted. Late Quaternary environments and prehistoric occupation in the lower White Nile valley, central Sudan. Quaternary Science Reviews.

Wopenka, B., Pasteris, J.D., 2005. A mineralogical perspective on the apatite in bone Materials Science and Engineering, 25 (2), 131-143.

Wright P., 2007. Calcrete. In: Nash D.J., McLaren S.J. (Eds), Geochemical Sediments and Landscapes, Wiley-Blackwell, 10-45.

Young, A., 1993. The Rietveld Method. IUCr, Oxford Science Publications.

Zazzo A., Saliège J.F., 2011. Radiocarbon dating of biological apatites: A review. Palaeogeography, Palaeoclimatology, Palaeoecology, 310, 52-61.

Zazzo A., 2014. Bone and enamel carbonate diagenesis: a radiocarbon prospective. Palaeogeography, Palaeoclimatology, Palaeoecology, 416, 168-178.

Cherkinsky A., 2009. Can We Get a Good Radiocarbon Age from "Bad Bone"? Determining the Reliability of Radiocarbon Age from Bioapatite. Radiocarbon, 51, 647-655.

Zerboni, A., 2011. Micromorphology reveals in situ Mesolithic living floors and archaeological features in multiphase sites in Central Sudan. Geoarchaeology: An International Journal, 26, 365-391.

Zerboni, A., 2013. Early Holocene palaeoclimate in North Africa: an overview, in: Shirai, N. (eds.), Neolithisation of Northeastern Africa, Studies in Early Near Eastern Production, Subsistence, and Environment, Berlin, ex oriente, 16, 65-82.

APPENDIX I

Plan of the 16D4 archaeological site

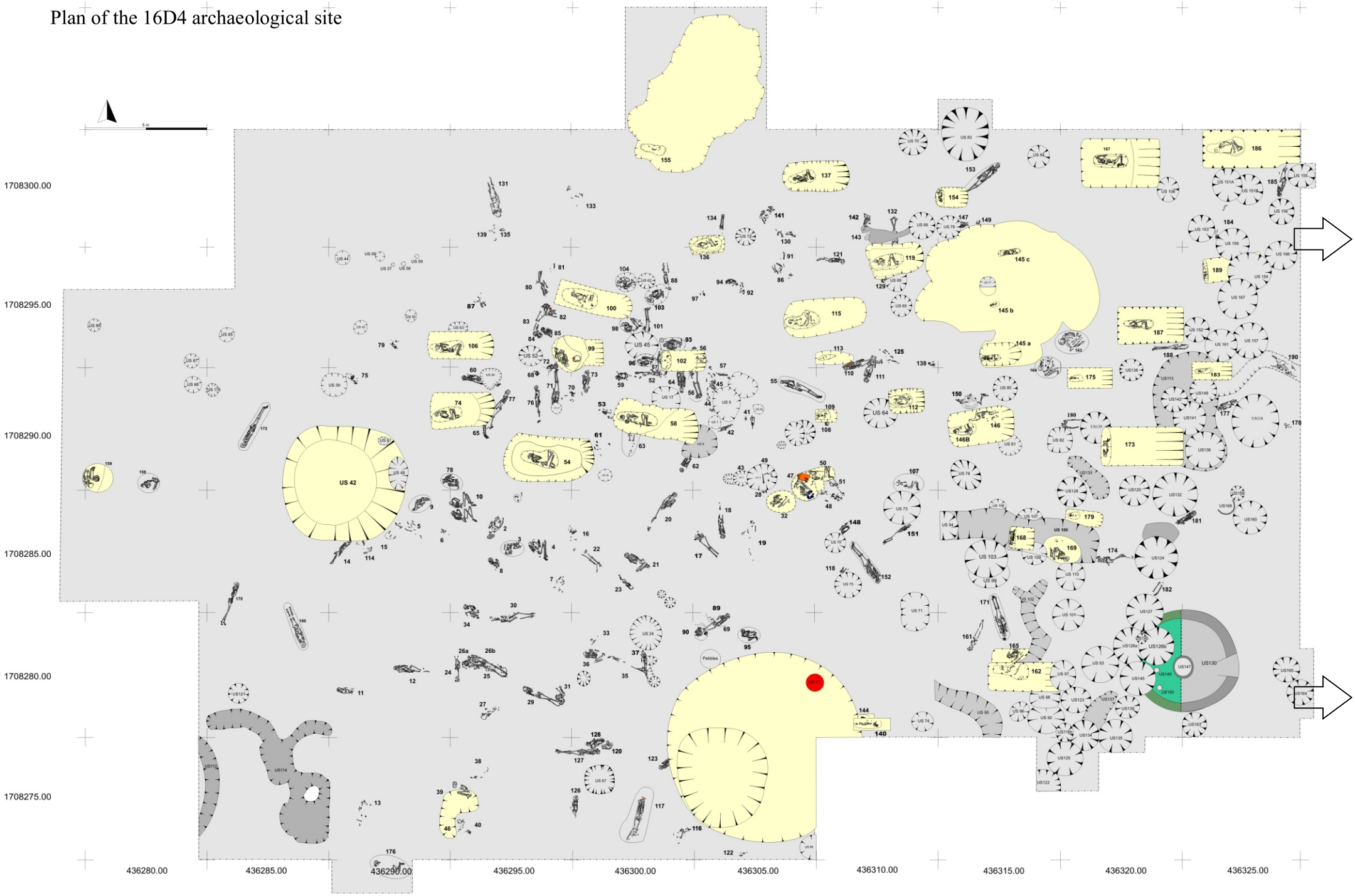

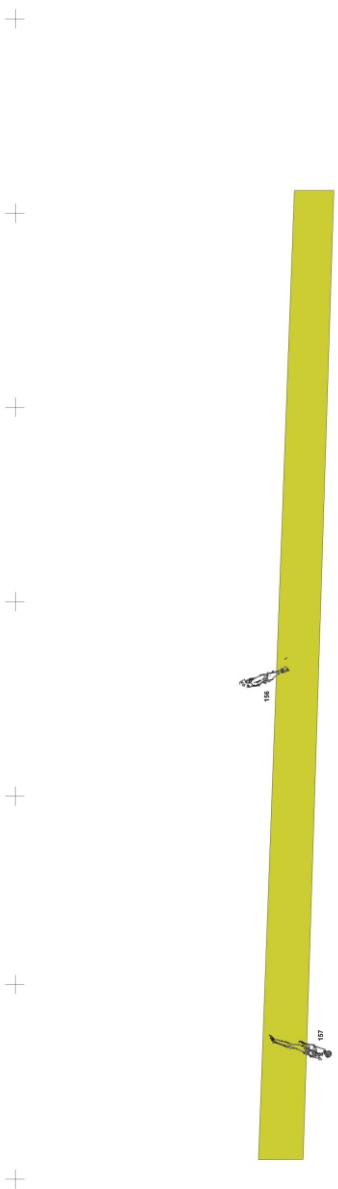
156
157

Plan of the 16D4 archaeological site (only graves)

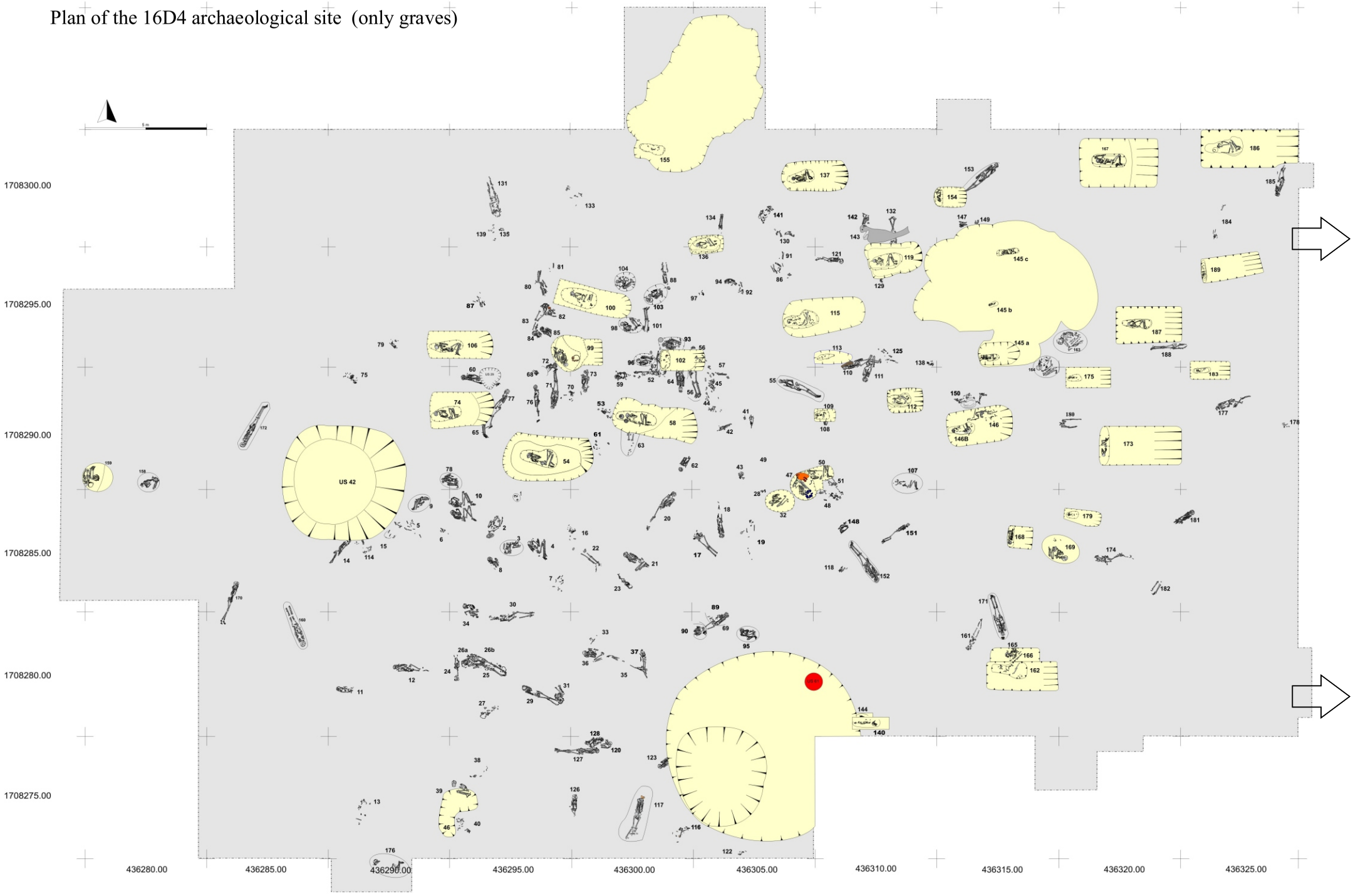

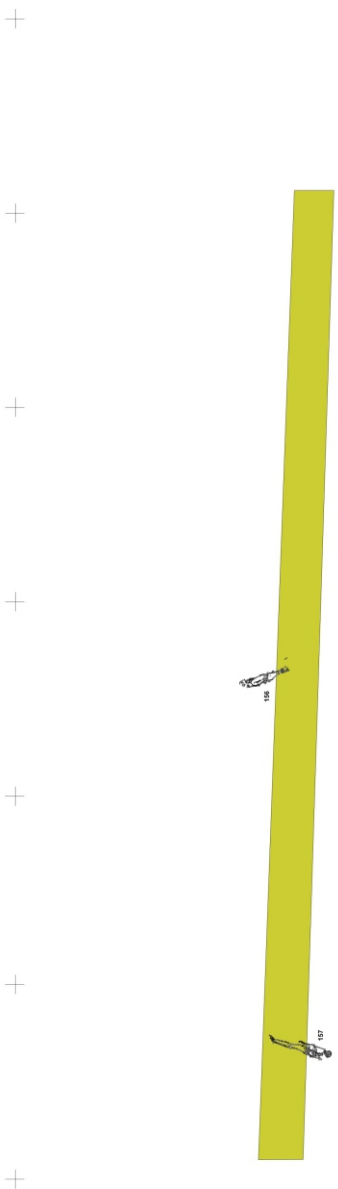
156
157

Acknowledgements

I would like to express my sincere gratitude to Prof. Gilberto Artioli, Dr. Lara Maritan and Dr. Ivana Angelini for their scientific and patient guidance through the doctoral years as well as for their enthusiasm and commitment in this research project.

I am particularly grateful to Dr. Donatella Usai and Dr. Sandro Salvatori, directors of El Salha Archaeological Project, for the precious collaboration and fruitful discussion that led to the accomplishment of this research.

I particularly wish to thank Dr. Andrea Zerboni, Dr. Matthieu Lebon, Dr. Ina Reiche, Dr. Elisabetta Boaretto and Dr. Maria Chiara Dalconi for their contributions as well as for the discussion of results that undoubtedly improved the quality of this work.

I wish to thank Prof. Filippo Terrasi Dr. Fabio Marzaioli (Centre for Isotopic Research on Cultural and Environmental heritage - CIRCE) for their scientific and analytical support for ^{14}C-AMS dating.

I would like to thank Prof. Pier Luigi Zanonato and Dr. Luca Nodari for providing the access to the FTIR spectrometer at the Department of Chemical Sciences (University of Padova).

I wish to thank the following people from the Department of Geosciences (University of Padova) for their valuable support during the lab analyses: Leonardo Tauro, Dr. Elena Masiero, Dr. Federico Zorzi, Dr. Luca Peruzzo, Sandra Boesso, Stefano Castelli, Dr. Aurelio Giaretta.

I would like to thank all team members involved in the El Salha Archaeological Project, in particular Dr. Tina Jackob for her help for bonr sampling.

I wish to thank the National Corporation for Antiquities and Museums, Khartoum (Sudan), in particular the General Director Abdelrahman Ali Mohamed for authorizing the study of archaeological bones. I thank Centro Studi Sudanesi e sub-Sahariani (CSSeS) and Ministero degli Affari Esteri (MAE) of the Italian Government for funding the archaeological research.